STRUCTURAL HEALTH MONITORING AND BRIDGE CONDITION ASSESSMENT

By

Feng Xiao

RECOMMENDED:

Dr. Gang S. Chen

Dr. Yongtao Dong

Dr. Yujiang Xiang

Dr. J. Leroy Hulsey
Advisory Committee Chair

Dr. J. Leroy Hulsey
Chair, Department of Civil and Environmental Engineering

APPROVED:

Dr. Doug Goering
Dean, College of Engineering and Mines

Dr. John C. Eichelberger
Dean of the Graduate School

27 July 2016
Date

STRUCTURAL HEALTH MONITORING AND BRIDGE CONDITION ASSESSMENT

A

DISSERTATION

Presented to the Faculty

of the University of Alaska Fairbanks

in Partial Fulfillment of the Requirements

for the Degree of

DOCTOR OF PHILOSOPHY

By

Feng Xiao, B.S., M.Sc.

Fairbanks, Alaska

August 2016

Abstract

This research is mainly in the field of structural identification and model calibration, optimal sensor placement, and structural health monitoring application for large-scale structures. The ultimate goal of this study is to identify the structure behavior and evaluate the health condition by using structural health monitoring system. To achieve this goal, this research firstly established two fiber optic structural health monitoring systems for a two-span truss bridge and a five-span steel girder bridge. Secondly, this research examined the empirical mode decomposition (EMD) method's application by using the portable accelerometer system for a long steel girder bridge, and identified the accelerometer number requirements for comprehensively record bridge modal frequencies and damping. Thirdly, it developed a multi-direction model updating method which can update the bridge model by using static and dynamic measurement. Finally, this research studied the optimal static strain sensor placement and established a new method for model parameter identification and damage detection.

Table of Contents

Page

Signature Page i

Title Page iii

Abstract v

Table of Contents vii

List of Figures xi

List of Tables xv

Acknowledgements xvii

Chapter 1 Introduction 1

1.1 Background 1

1.2 Objectives 3

1.3 References 5

Chapter 2 Structural Health Monitoring of the Klehini River Bridge 9

2.1 Abstract 9

2.2 Introduction 10

2.2 Bridge Description 11

2.3 Development of the Structural Health Monitoring System 15

2.3.1 Moving-Load Analysis 15

2.3.2 Modal Analysis 19

2.3.3 Local Finite Element Analysis 21

2.3.4 Crack Gauge 25

2.4 Results and Discussions 26

2.4.1 Preliminary Sensor Layout 26

2.4.2 Types of Monitoring 28

2.4.3 Equipment 29

2.4.4 Power Supply and Internet for Remote Monitoring 31

2.4.5 Installation of SHM and Integration of the System 32

2.5 Conclusions and Future Work 32

2.6 Acknowledgments 34

2.7 References 34

Chapter 3 Ambient Loading and Modal Parameters for the Chulitna River Bridge 37

3.1 Abstract 37

3.2 Introduction 38

3.3 Bridge Description 42

3.4 Dynamic Test Description 43

3.5 Spectrum Analysis 46

3.6 Empirical Mode Analysis and Parameter Evaluations 49

3.7 Discussion and Theoretical Consideration 58

3.8 Conclusions 61

3.9 Acknowledgments 63

3.10 References 63

Chapter 4 Multi-direction Bridge Model Updating using Static and Dynamic Measurement 67

4.1 Abstract 67

4.2 Introduction 68

4.3 Bridge Description 69

4.4 Static and Dynamic Test 71

4.5 Multi-direction Model Updating 75

4.5.1 Simple Accuracy Test 75

4.5.2 Group Directional Members and Select Objective Functions 77

4.5.3 Bridge Longitudinal Direction Behavior 78

4.5.4 Model Updating in Longitudinal Direction 81

4.5.5 Bridge Transversal Direction Behavior 83

4.5.6 Model Updating in Transversal Direction 90

4.5.7 Updated Finite Element Model 94

4.6 Conclusions 97

4.7 References 97

Chapter 5 Optimal Static Strain Sensor Placement for Bridge Model Parameter Identification by using Numerical Optimization Method 101

5.1 Abstract 101

5.2 Introduction 102

5.3 Numerical Optimization Method for Model Parameter Identification 104

5.3.1 Two Member Truss 104

5.3.2 Structure Stiffness Matrix 105

5.3.3 Displacement and Loads 105

5.3.4 Model Updating by Using Numerical Optimization 107

5.4 Optimal Sensor Placement based on Numerical Optimization 110

5.4.1 Eight Member Truss 111

5.4.2 Sensor Number and Layout Optimization 111

5.4.3 Sensor Number Influence on the Speed of Numerical Optimization 112

5.5 Numerical Optimization in Damage Detection 115

5.6 Numerical Optimization Model Updating for Large Scale Structure 116

5.6.1 Klehini River Bridge 117

5.6.2 Model Parameter Identification for Klehini River Bridge..... 118

5.7 Conclusions 121

5.8 References 122

Chapter 6 Conclusions and Future Work 125

List of Figures

Page

Figure 2.1: Klehini River Bridge 12

Figure 2.2: Bridge Dimension 13

Figure 2.3: Examples of Conditions 14

Figure 2.4: Global Finite Element Model 16

Figure 2.5: Partly Buried Expansion Bearing 17

Figure 2.6: Preliminary Strain Sensor Layout 19

Figure 2.7: Mode Shapes and Natural Periods 20

Figure 2.8: Preliminary Accelerometer Sensor Layout 21

Figure 2.9: Moment Diagram 22

Figure 2.10: Girder-to-Column Connection 23

Figure 2.11: Moment-Rotation L1 Connection 24

Figure 2.12: L1 Hot Spot Strain 25

Figure 2.13: Inspection Location Diagram 26

Figure 2.14: Preliminary Crack Gauge Layout 26

Figure 2.15: Preliminary Sensor Layout on Trusses 27

Figure 2.16: System Configuration 30

Figure 2.17: SHM System in NEMA Enclosure 31

Figure 3.1: Chulitna River Bridge 43

Figure 3.2: Portable Accelerometer on One Measure Point 44

Figure 3.3: Portable Accelerometer Location and Number 45

Figure 3.4: Dynamic Test 46

Figure 3.5: Time History (a) and FFT of a Typical Measured Acceleration Signal in the Vertical Direction at the Middle of Span 3 (Point 12) (b) 47

Figure 3.6: Time History (a) and FFT of a Typical Measured Acceleration Signal in the Vertical Direction at the Middle of Span 1 (Point 9) (b) 48

Figure 3.7: Decomposed Components of a Measured Acceleration Signal in the Vertical Direction at the Middle of Span 3 (Point 12) 54

Figure 3.8: Power Spectrum of the Decomposed Components (c1: Top; c2: Bottom) of a Measured Acceleration Signal in the Vertical Direction at the Middle of Span 3 (Point 12) 54

Figure 3.9: Decomposed Components of a Measured Acceleration Signal in the Vertical Direction at the Middle of Span 1 (Point 9) 55

Figure 3.10: Power Spectrum of the Decomposed Components (c1: Top; c2: Middle; c3: Bottom) of a Measured Acceleration Signal in the Vertical Direction at the Middle of Span 1 (Point 9) . 56

Figure 3.11: Characteristic Plots of the Decomposed Signals Corresponding to Two Specific Frequencies in the Vertical Direction at the Middle of Span 3 (Point 12) 57

Figure 3.12: Characteristic Plots of the Decomposed Signals Corresponding to Three Specific Frequencies in the Vertical Direction at the Middle of Span 1 (Point 9) 58

Figure 3.13: First Longitudinal Mode of Vibration from the FEM analysis, 1.367 Hz..... 59

Figure 3.14: Second Longitudinal Mode of Vibration from the FEM Analysis, 2.044 Hz 60

Figure 3.15: Second Mode of Vertical Vibration from the FEM Analysis for 3.348 Hz 60

Figure 3.16: Fourth Mode of Vibration in the Vertical Direction from the FEM Result, 4.249 Hz 60

Figure 4.1: Elevation and Plan View of Chulitna River Bridge 70

Figure 4.2: Current Picture of the Chulitna River Bridge..... 71

Figure 4.3: Fiber-Optic Structural Health Monitoring System 72

Figure 4.4: Bridge Health Monitoring System Sensor Summery 73

Figure 4.5: Using Portable Data Acquisition System on the Chulitna River Bridge..... 74

Figure 4.6: Locations Where the Influence of Mesh Refinement was Checked (see Table 4.1).. 77

Figure 4.7: Strain Sensor at the Cross Section of Mid-span 3 79

Figure 4.8: Stress Compression in Longitudinal Members before Modification 80

Figure 4.9: Plan View: Bearings that are Not Contact with Masonry Plates..... 83

Figure 4.10: Strain Sensor (Red) and Displacement Sensor (Green) at the Cross Section of Pier 3 84

Figure 4.11: Strain Sensor (Red) and Displacement Sensor (Green) at the Cross Section of Pier 5 84

Figure 4.12: Vertical Movement at 5 Unconnected Bearing Supports..... 85

Figure 4.13: Stress Comparison in Cross-Frames before Model updating in Transversal Direction 89

Figure 4.14: Stress Comparison in Cross-Frames after Model Updating in Transversal Direction 91

Figure 4.15: Three Trucks Positioned on Span 3, Southbound 93

Figure 4.16: Multi-direction Model Updating Flowchart 94

Figure 4.17: Objective with Model Development 96

Figure 5.1: Two-member Truss with Notation 105

Figure 5.2: Functions of Iteration for Newton Method..... 109

Figure 5.3: Functions of Iteration by Steepest Decent Method 110

Figure 5.4: Eight-member Truss with Notation 111

Figure 5.5: Two Sensors Model Parameter Identification 113

Figure 5.6: Eight Sensors Model Parameter Identification..... 114

Figure 5.7: Truss Structure Sensor Layout 115

Figure 5.8: Functions of Iteration for Damage Detection..... 116

Figure 5.9: Klehini River Bridge 117

Figure 5.10: Crack on Truss Member 118

Figure 5.11: Location of Damaged Member..... 118

Figure 5.12: Separated Structure by Using Displacement Sensor 119

Figure 5.13: Separated Structure..... 119

Figure 5.14: Member 2 Cross Section Area Identification by Using Newton Method 121

List of Tables

Page

Table 2.1: Summary Number of Sensors 28

Table 3.1: Comparison of Natural Frequencies between the FFT Method and EMD Method 56

Table 3.2: Comparison Natural Frequencies between Field Measurements and FEM Results.... 59

Table 4.1: Simple Accuracy Comparison between the Initial and the Refined Model..... 76

Table 4.2: FEM Using Revised Variables 82

Table 4.3: Natural Frequency Differences after Model Revisions for Longitudinal Behavior 82

Table 4.4: Difference in Flange Stress (%) after Model Revisions for Longitudinal Behavior ... 83

Table 4.5: Difference in Lower Chord Stress (%) after Model Revisions..... 83

Table 4.6: Two Trucks at Pier 3, before Transverse Modifications 88

Table 4.7: Two Trucks at Pier 5 Stress Results before Transverse Updating..... 88

Table 4.8: Two Trucks at Pier 3 Stress Results after Model Modifications (psi)..... 90

Table 4.9: Two Trucks at Pier 5 Stress Results after Model Modifications (psi)..... 90

Table 4.10: Percent Difference between FEM and Experimental Flange Stresses Mid-Span 3... 92

Table 4.11: Percent Difference between FEM and Experimental 92

Table 4.12: Year 2012 Natural Frequency Difference; Calibrated FEM..... 93

Table 5.1: Newton Method with the Backtracking Line Search..... 109

Table 5.2: Sensor Layout with Numerical Optimization 112

Acknowledgements

I would like to thank my advisor, Professor J. Leroy Hulsey, for his endless support and guidance of my research throughout my Ph.D. study. He is my ultimate role model as a researcher, advisor, and lecturer. His dedication to teaching is sincerely appreciated.

I would also like to thank my committee members, Dr. Gang Sheng, Dr. Yujiang Xiang, and Dr. Yongtao Dong. Their advice was invaluable in finalizing the research effort. Their support is greatly appreciated.

The study in this dissertation was sponsored and supported by the Alaska University Transportation Center (AUTC) and the Alaska Department of Transportation & Public Facilities. Their financial support is greatly appreciated.

I thank my parents for their encouragement for continuing my study and support during all of the challenges I have faced.

Chapter 1 Introduction

1.1 Background

Many existing structures in-service are deficient because of long-term fatigue, design or construction problems, etc. Over two hundred million trips are taken daily across deficient bridges in America's 102 largest metropolitan regions. In total, one in nine of America's bridge are rated as structurally deficient, while the average age of the nation's 607,380 bridges is currently 42 years. The Federal Highway Administration (FHWA) estimates that to eliminate the nation's bridge deficient backlog by 2028, there is a need to invest $ 20.5 billion annually (ASCE, 2013). Due to the economic boom, a huge number of large-scale and complex civil structures such as long-span bridges, high-rise buildings, and large-space structures have been constructed in China during the past twenty years. However, according to other countries' experiences, enormous cost and effort will be required for maintenance of these structures and for safeguarding them from damage in the next twenty years (Chang et al., 2009).

American Association of State Highway and Transportation Officials indicated the nondestructive load testing classified as static load tests and dynamic load tests. A static load test is conducted using stationary loads to avoid bridge vibration. A dynamic load test excited vibration in the bridge. Dynamic tests may be performed to measure modes of vibration, frequencies, dynamic load allowance, and to obtain load history and stress ranges for fatigue evaluation (AASHTO, 2011).

Structural health monitoring (SHM) systems are being deployed to collect static or dynamic response. Typically, sensors are classified into traditional foil-strain gages, fiber optic sensors, and wireless sensors based on data transfer difference. The foil-strain gage takes advantage of the

physical property of electrical conductance. The fiber optic sensor can measure data by using light reflection, the sensor made by fiber optic so it solve the problem of corrosion, and data can transfer longer distance compared with foil-strain gage. Wireless sensor can apply for large scale structure, and simply the sensor layout. (Karbhari, Ansari, 2009).

The main SHM is to identify the "as-is" structural condition which includes the damage, fatigue, load distribution, load rating, etc. That condition may be different from "as-built" structural condition which comes from the structural design. Normally, an "as-built" condition numerical model was built based on the construction draw. And a structural health monitoring system installed on the real structure to measure the structural static and dynamic response. The measured result from SHM system will different with the model's analytical results. The model updating by using manually or automatically method can modify the "as-built" model to an "as-is" model. The structural safety condition could be evaluate based on the "as-is" model (AASHTO, 2011).

To predict the structure status, structural health monitoring (SHM) requires information on the dynamic properties of structures, usually including natural frequencies and damping ratios. Dynamic tests can identify the natural frequencies and associated damping ratios, and it can validate the finite element modeling (FEM). Experimental modal analysis has been widely used to evaluate the behavior of civil engineering structures. This analysis is typically done by extracting structural modal parameters such as natural frequencies, damping ratios, and mode shapes from vibration measurements (Farrar and James 1997; Caicedo et al., 2004; Conte, 2008; Siringoringo and Fujino, 2008).

Updating the model requires designing a SHM system to capture the structural response which can correctly evaluate the "as-is" model's accuracy. The limited number of dynamic sensors can identify the structural dynamic behavior, and it can qualify the overall stiffness of structure in the

global level. However, the global dynamic behavior is not sensitive to the local problem. Bakir et al. (2007) indicated that changes in natural frequencies cannot or hardly provide the spatial information about structural damage. On the other hand, local damages can be successfully detected and qualified based on using strain and displacement sensors (Sanayei et al., 2012), but the sensor number will be increased. The research also indicated the model's accuracy can be qualified by combining the static and dynamic measurement (Schlune et al., 2009, Jung and Kim, 2013, Xiao et al., 2015), and it could evaluate the model's accuracy on a local and global level.

A critical step in model calibration, whether it be manual tuning or using optimization techniques, is defining an error function to assess the quality of the match between the analytical and measured data (Sanayei et al., 2012). The location and parameters for comparing the analytical and measured data could be optimized. In order to reduce the cost of the structural health monitoring system, the optimal sensor placement is also required to be studied at the stage of sensor layout.

1.2 Objectives

The ultimate goal of this study is to identify the structure behavior and evaluate the health condition by using an optimal structural health monitoring system. To achieve this goal, the objectives are as follows:

1. To establish two fiber optical structural systems for a truss bridge, and a steel girder bridge.
2. To examine the EMD method's application by using the portable accelerometer system for a long steel girder bridge under the ambient free-decay truck loading.
3. To identify the accelerometer number requirements for comprehensively recording bridge modal frequencies and damping ratios.

4. To develop a new approach for bridge model updating by using the static and dynamic measurement from the structural health monitoring system.

5. To identify the optimal strain sensor placement and examine the structural response.

6. To establish a new method which can apply the automatic model parameter identification for a real bridge.

Chapter 2 describes a methodology to develop the bridge health monitoring system which can be suitable for Alaska's remote locations and harsh weather. A three-dimensional finite element model was built by using SAP2000. Subsequently, a moving-load analysis was performed to determine the bridge critical sections. Determined critical sections combined with field inspections can identify the SHM system layout which includes a preferred sensor layout, system integrator, and instrumentation. Various sensors were used in evaluating bridge performance and monitoring environmental conditions.

In Chapter 3, a bridge finite element model, field dynamic test of the "Ambient vibrational response (AVR)", and structural health monitoring system (SHMS) are used to analyze, evaluate, and monitor the structural performance. In the field dynamic test, fifteen portable accelerometers were placed on centerline along the bridge length to record the structural response, and an ambient free-decay response was used to evaluate the dynamic properties of the bridge structure. Natural frequencies and modal damping ratios were identified and characterized using the Hilbert-Huang transform and fast Fourier transform methods. This chapter has been accepted by the journal named Advances in Structural Engineering as Xiao et al. (2016).

In Chapter 4, a multi-direction bridge model updating method based on the static and dynamic test. A fiber optics structural health monitoring system was installed on a bridge, and 73 fiber optic sensors captured the static and dynamic data at the local-level. A portable accelerometer system

was used to record an ambient loading test. 15 force-balanced accelerometers were placed along the bridge center to record the bridge global behavior. The original bridge finite element model was built according to the construction drawings. The bridge model was updating by using multi-level test data. A new multi-direction model updating approach was established to separate the model updating into several stages based on the member's direction. In each stage, the uni-direction members were updated in a local-global level. This chapter has been published in Applied Physics Research as Xiao et al. (2015).

In Chapter 5, a method to identify optimal strain sensor placement for examining structural response is presented. Based on applied static forces, and optimal placement to obtain measured strains, the structural stiffness parameters can be identified. Change in a cross sectional area can be determined and used to minimize the difference between analytical and measured strains. These strain differences are evaluated by comparing measured with numerical. This approach is used to identify the optimal sensor placement. The objective of this research is to identify the minimum number of static strain sensors and the optimal sensor layout needed to conduct a parametric model identification. This research includes automatic model parameter identification, optimal static strain sensor placement, damage detection, and the method's application for a real bridge.

Finally, Chapter 6 summarized the key achievements and findings of this dissertation and discusses potential future work for the research of structural health monitoring

1.3 References

AASHTO, (2011), The Manual for Bridge Evaluation.

ASCE, (2013), 2005 Report Card for America's infrastructure.

Bakir, P. G., Reynders, E., Roeck, G. D., (2007), Sensitivity-based finite element model updating using constrained optimization with a trust region algorithm, Journal of Sound and Vibration, 305, pp. 211-225.

Caicedo, J. M., Dyke, S. J., Johnson, E. A., (2004), Natural excitation technique and Eigen system realization algorithm for phase I of the IASC-ASCE benchmark problem: Simulated data, J. Eng. Mech., 130(1), 49–60.

Chang, S. P., Yee, J. Y., Lee, J., (2009), Necessity of the bridge health monitoring system to mitigate natural and man-made disasters, Structure and Infrastructure Engineering, 5(3), pp. 173-197.

Conte, J. P., (2008), Dynamic testing of Alfred Zampa Memorial Bridge, J. Struct. Eng., 134(6), 1006–1015.

Farrar, C. R., James, G. H., III. (1997). System identification from ambient vibration measurements on a bridge, J. Sound and Vibration, 205(1), 1–18.

Jung, D. S., Kim, C. Y., (2013), Finite element model updating of a simply supported shewed PSC I-girder bridge using hybrid genetic algorithm, KSCE Journal of Civil Engineering,17(3), pp. 518-529.

Karbhari, V. M., Ansari, F., (2009), Structural health monitoring of civil Infrastructure systems, Woodhead Publishing Limited, UK.

Sanayei, M., Phelps, J. E., Sipple, J. D., Bell, E. S., Brenner, B. R., (2012), Instrumentation, nondestructive testing, and finite element model updating for bridge evaluation using strain measurement, Journal of Bridge Engineering, Vol. 17, No. 1.

Schlune, H., Plos, M., Gylltoft, K., (2009), Improved bridge evaluation though finite element model updating using static and dynamic measurements, Engineering Structure, 31, pp. 1477-1485.

Siringoringo, D. M., Fujino, Y. (2008), System identification of suspension bridge from ambient vibration response, Engineering Structure, 30(2), pp. 462–477.

Xiao, F., Hulsey, J. L., Chen, G. S., (2015), Multi-direction bridge model updating using static and dynamic measurement, Applied Physics Research, Vol. 7, No. 1.

Xiao, F., Chen, G. S., Hulsey, J. L., Dolan, J. D., Dong, Y., (2016), Ambient Loading and Model Parameters for the Chulitna River Bridge, Advances in Structural Engineering, Vol. 19, No. 4.

Chapter 2 Structural Health Monitoring of the Klehini River Bridge[1]

2.1 Abstract

This paper describes a methodology used to evaluate the structural condition of a bridge in a remote area of Alaska in the United States. The objective was to develop a structural health monitoring (SHM) program to improve bridge safety and asset management. The idea is to evaluate the structural integrity and serviceability of the bridge and gather information by monitoring its structural response (strains, accelerations, mode shapes, and natural frequency) to help to determine if the structure is undergoing change. A three-dimensional element model using SAP2000 was prepared to simulate the bridge. Subsequently, a moving-load analysis was performed using the finite element model to determine the critical sections of the bridge. Results of a modal analysis and field inspections were used to establish a bridge SHM system, including a preferred sensor layout, system integrator, and instrumentation suitable for Alaska's remote locations and harsh weather. Various sensors were used in evaluating bridge performance to measure and monitor structural and environmental conditions. The SHM system provides reliable information on the structural health of the bridge. As a new safety and management tool, this system will complement traditional bridge inspection methods, provide early warning if strain levels become too high, and help with asset management of the bridge.

[1] This chapter has been accepted by journal, and will be published as Xiao, F., Hulsey J. L., Chen, S. G., Structural health monitoring of the Klehini River Bridge, To be published in Journal of Vibration Engineering & Technologies, Vol. 4, No. 4, 2016.

2.2 Introduction

Bridges in Alaska are routinely subjected to extremely cold temperatures. In some locations, there can be excessively deep snow, strong winds, and even seismic events. Bridges in these harsh conditions are often located in remote areas. Maintenance, rehabilitation, and replacement of these bridges in a cost-effective manner depend on reliable inspection and condition assessment. Inspections of these bridges are both costly and time-consuming. Compared with other states in the nation, bridge monitoring in Alaska is needed more and is more challenging due to harsh weather conditions and issues related to the remote locations of many of the state's bridges. For example, power is not always available at a remote bridge site, and this causes special challenges in data retrieval and reliable data communication from the site.

Though structural health monitoring (SHM) has become a much-discussed topic (Karbhari and Ansari, 2010; Phares et al., 2005), it has not yet been widely implemented. Bridge SHM can be used to provide early warnings about bridge safety and to monitor the structural condition and changes in condition in real time (by monitoring strain, acceleration, displacement, temperature, and displacements). Other uses include providing valuable data for engineers who are preparing asset management plans.

Rapid advances in bridge evaluation technologies have occurred recently (Whelan et al., 2008; Whelan and Janoyan, 2009; Stein, 2005; Hemphill, 2004; Miyashita and Nagai, 2010; Dong et al., 2011). If properly implemented, SHM can aid in several aspects of bridge management, such as reducing inspection costs while improving inspection quality, prioritizing repair/maintenance schedules, increasing the accuracy of deterioration estimations, and assisting with decision-making processes. However, challenges exist in integration and interpretation of the information from sensor networks. Additional difficulties arise when monitoring bridges in remote, cold regions

such as Alaska, because a harsh environment affects the reliability and durability of SHM equipment and sensors, power supplies, and data communication tools.

The overall objective of this study was to establish a SHM system based on available knowledge and technologies related to bridges in cold, harsh environments and to provide guidelines for implementation of an SHM program. We proposed to instrument the Klehini River Bridge to monitor its structural response to active traffic loading and evaluate its structural condition in real time, reasoning that such development and implementation would greatly enhance the ability of the Alaska Department of Transportation and Public Facilities (ADOT&PF) Bridge Section to safely manage the bridge during its service life.

2.2 Bridge Description

The Klehini River Bridge is located at the Porcupine Crossing Road at Mile 26.3 Haines Highway in Alaska. The bridge structure is made of two-span riveted steel parker trusses (see Fig. 2.1). The total length of the bridge is 74 meters (243 feet). The dimensions of the Klehini River Bridge are shown in Fig. 2.2. The superstructure consists of various box sections with inverted channel sections riveted to two steel plates. The timber deck is supported by a series of timber girders connected to transverse I-beams. Both spans rest on a central concrete abutment and the side banks.

Figure 2.1: Klehini River Bridge

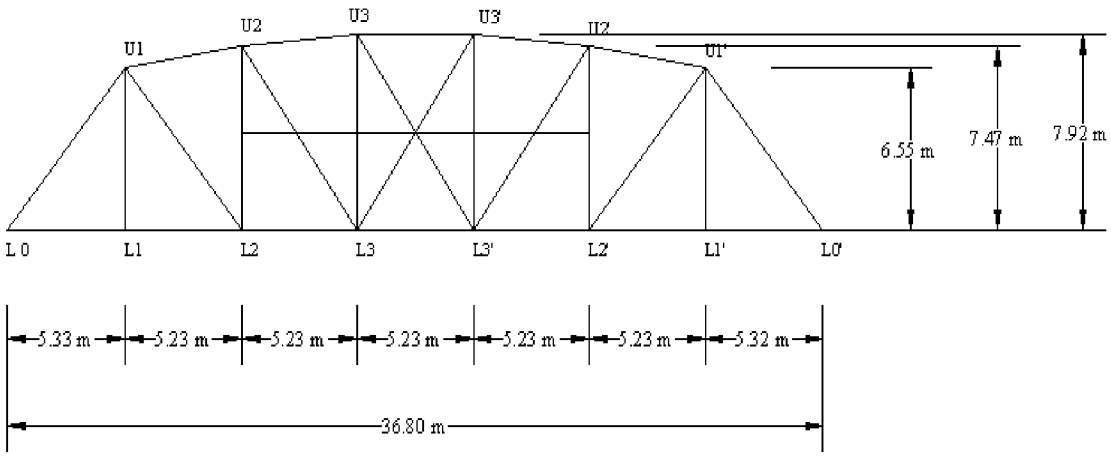

(a) Elevation view

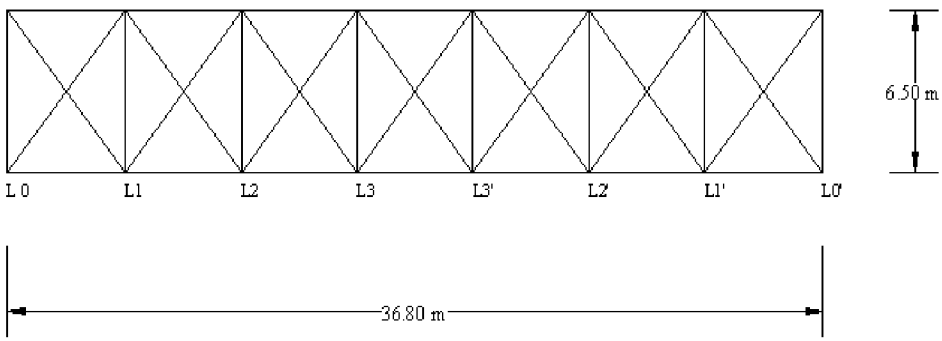

(b) Plan view

Figure 2.2: Bridge Dimension

The truss structure, which originally spanned the Mendenhall River in Juneau, was known as the Mendenhall River Bridge. In 1969 and 1971, the trusses were partially disassembled, shipped to Haines, and installed at their current location.

The bridge's poor superstructure condition rating is based on observed damages to the steel trusses, thought to have been caused by disassembly at the Mendenhall River, shipping, installation

at the Klehini River, or a combination of these activities during the 1969 and 1971 period. The truss damage has been noted on a 1974 inspection. Recent ADOT&PF inspections (ADOT&PF, 2008; ADOT&PF, 2010) reported damage to several structural members, including torn gusset plates, cracking at rivet holes, damaged or missing lateral bracing, and damaged sway bracing. Examples of these conditions are shown in Fig. 2.3. The ADOT&PF also identified weld repairs at several locations of the structural elements. Gouges, flame cut holes, bullet holes, and tack welds for cracks on the truss members were noted as great concerns related to potential degradation.

a. Torn Gusset Plate

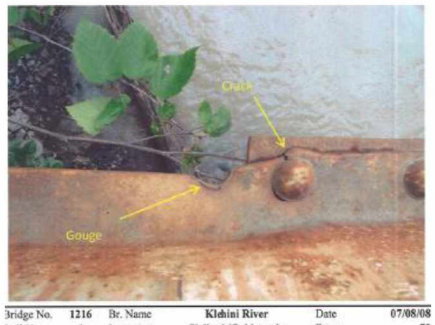

b. Cracking at a Rivet Hole

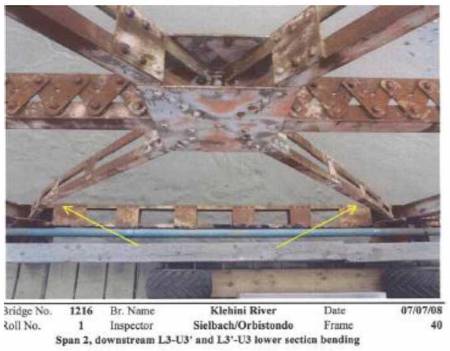

c. Bent Truss Members

d. Bent Lower Sway Bracing

Figure 2.3: Examples of Conditions

The Klehini River Bridge serves as the only access route to this region, and is a vital link to several small communities in the area. The ADOT&PF is tasked with inspecting and managing the bridge until it is replaced. To accomplish this, the ADOT&PF Bridge Section performs annual hands-on inspections supplemented with non-destructive evaluation (NDE), using magnetic particle and ultrasonic examination on previously identified deformations, defects, or welded repairs. These inspections have only provided temporary condition evaluations at known defective areas. To ensure safe operation of this bridge, a footprint of the bridge's response to active traffic is needed, as is the capability for more frequent detection of changes in current defective areas.

2.3 Development of the Structural Health Monitoring System

This study addresses specific issues associated with the bridge in question: torn gusset plates, cracks at rivet holes, damaged or missing lateral bracing, damaged sway bracing, and the soundness of identified weld repairs on structural elements at several locations. The proposed plan includes accelerometers for extracting modal characteristics and local diagnostic monitoring using strain and crack gauges.

Since damage and deterioration exist at many locations on the bridge, it was impractical to install sensors at all the locations. Therefore, an optimized sensor layout for the bridge was prepared based on the results of a moving-load analysis, a modal analysis, and the latest inspection reports.

2.3.1 Moving-Load Analysis

Three-dimensional (3-D) linear elastic finite element global models of the Klehini River Bridge were prepared using SAP2000 (Fig. 2.4), a finite element analysis computer program. The model represents the structure in its current as-built configuration. The truss members, girders, stringer,

and floor beams were modeled by 3-D frame elements that have three translational degrees of freedom (DOF) and three rotational DOF at each node. The deck was modeled by shell elements.

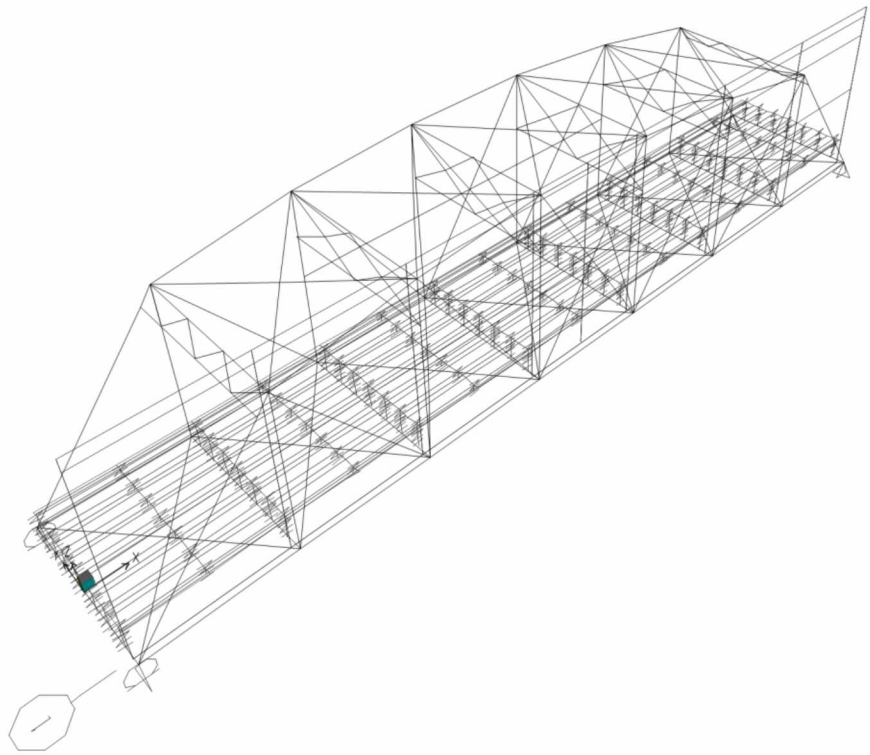

Figure 2.4: Global Finite Element Model

Most finite element global models for truss structures use single DOF elements for the members, that is, hinged ends. However, in this structure, the member end connections are rusty and the connections are semi-rigid. In order to estimate a worst-condition influence of the end conditions on the critical members, three finite element models (Model-1, Model-2, and Model-3) were developed. In finite element Model-1, truss connections were considered hinges. In finite element Model-2, the truss member connections were rigid. In finite element Model-3, the truss member connections were hinges, but the abutment support (Fig. 2.5) had rusted (oxidized) and

soil buildup was present. These conditions were considered in the model. A worst support condition, where expansion bearings were not free to rotate, was treated as a fixed bearing.

Figure 2.5: Partly Buried Expansion Bearing

Bridge bearings were modeled using rigid elements to connect the superstructure and pier to simulate the actual behavior. The fixed bearing behavior at a pier was modeled by simply releasing the rotational DOF in the vertical bending plane of the bridge. For Model-1 and Model-2, the expansion bearing behavior at the abutment was modeled by assigning roller restraints in the longitudinal direction and hinge restraints in the transverse direction at the bearings. In other words, the DOF allowed are the longitudinal translation and the vertical bending rotation. For Model-3, the expansion bearing behavior at the abutment was modeled using fixed bearing behavior, which approximates poor support conditions.

The results from a moving-load analysis were evaluated based on Model-1, Model-2, and Model-3. Using the moving-load analysis in SAP2000, the finite element global models were used to determine the critical section of the bridge. The vehicle class was defined to contain three types of vehicles: HL-93K, HL-93M, and HL-93S. The Klehini River Bridge has only one traffic lane. Therefore, the vehicles were moved in both directions along one lane of the bridge. The program was used to evaluate maximum and minimum response throughout the structure as a function of vehicle type and location.

The strain gauges are used to provide a stress history of the members. A stress history is used to assess if the members are overstressed and if any bending stresses occur in these members. The strain diagrams for the different models provide a priority arrangement for the strain gauges.

Peak compression strain and peak tensile strain are essential to monitoring member response. Sections having both large tension and compression also need to be monitored, in that failure stress is significantly lower than other types of stress. Peak compression strain appears on the end of the top chord. Peak tensile strain appears at the middle of the lower chord. Peak compression-tensile appears at the outside of the diagonals. A preliminary strain sensor layout is shown in Fig. 2.6.

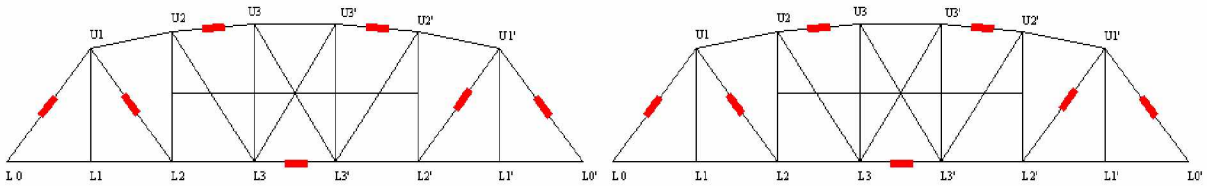

(a) Elevation view

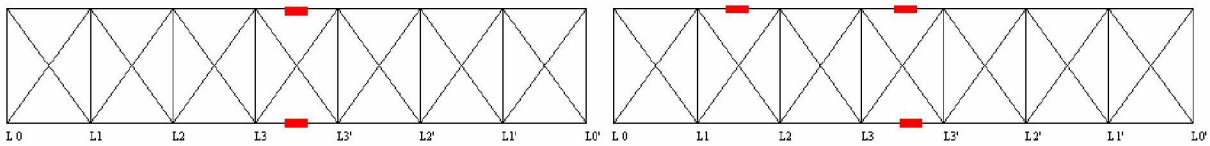

(b) Plan view

Figure 2.6: Preliminary Strain Sensor Layout

2.3.2 Modal Analysis

Modal analysis can be used to determine the actual stiffness of the Klehini River Bridge. Stiffness matrices are dominated by higher modes, and flexibility matrices are dominated by lower modes. So the actual stiffness of a bridge can be identified by adjusting the stiffness matrices until the finite element model's higher modes are equal to the measured modes. In order to measure higher modes and determine the natural frequencies, an accelerometer sensor plan should be chosen based on the initial finite element modal analysis results. The positions of accelerometers depend on the lower mode shapes in longitudinal, transverse, vertical, and rotational directions.

In a finite element modal analysis, natural frequencies, mode vectors, and mass participation factors are determined by the Ritz vector method. The mass participation factor for a mode provides a measure of how important the mode is for computing the response to the acceleration loads in each of the three global directions. In building design, there is a rule of thumb that the

accumulated modal mass participation factor in every direction is over 90%. An analysis of the bridge specified a need for 120 modes to achieve this percentage.

The accelerometer sensor plan follows standard procedures for the acquisition of the dynamic properties (or signature) of the structure. Lower modes and corresponding frequencies were measured by accelerometers. From the modal analysis, lower natural periods and mode shapes for four directions were successfully identified (Fig. 2.7). Because of the limited number of accelerometers, the accelerometers were fixed at the best positions to measure the first three modes and corresponding frequencies. A finite element modal analysis was used to predict the mode shapes. These conditions provide a guideline for the placement of accelerometers.

(a) 1st bending: 0.1240 s

(b) 2nd bending: 0.0716 s

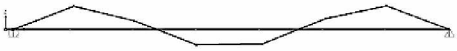

(c) 3rd bending: 0. 0534 s

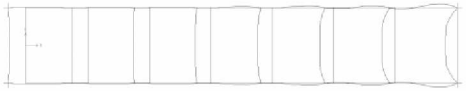

(d) 1st longitudinal: 0.1962 s

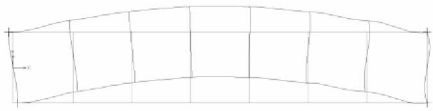

(e) 1st transverse: 0.1852 s

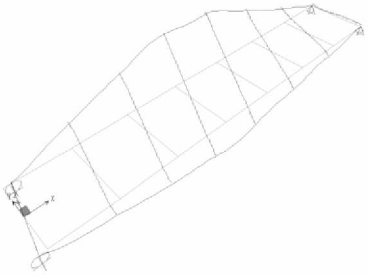

(f) 1st torsion: 0.0874 s

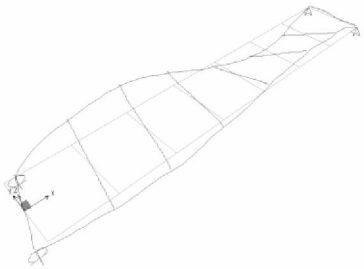

(g) 2nd torsion: 0.0473 s

Figure 2.7: Mode Shapes and Natural Periods

According to the modal analysis results, accelerometers were placed at the bridge deck level (bottom chords of the trusses) along the length of the bridge (see Fig. 2.8) to measure the natural frequencies and mode shapes of the bridge structure. The resulting information can also be used for monitoring the global condition of the bridge and for mode identification.

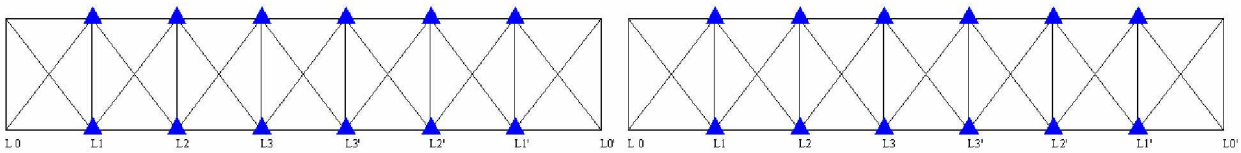

Figure 2.8: Preliminary Accelerometer Sensor Layout

2.3.3 Local Finite Element Analysis

Historically, steel portal frames were designed assuming that beam-to-column joints are ideally pinned or fully rigid. This approach simplified analysis and structural design processes, but at the expense of not obtaining a detailed understanding of joint behavior, which is semi-rigid in reality. In frame analysis, joint rotational behavior should be considered. This is usually done by using the moment-rotation curve. In this research, a local finite element model (substructure) was built to determine the rotational stiffness of a selected section.

Moving-load analysis revealed large bending moments in the girder-to-column section (Fig. 2.9). Therefore, it was essential to determine the rotational stiffness of the girder-to-column section and update the global model local stiffness.

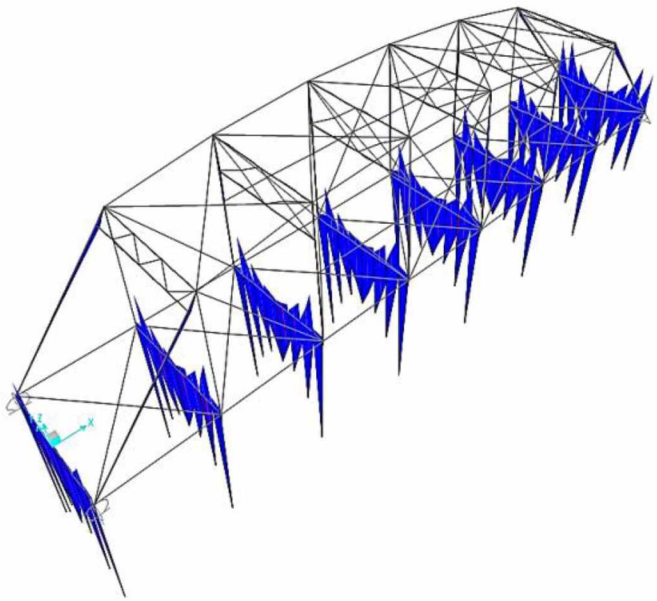

Figure 2.9: Moment Diagram

The girder-to-column connection (see Fig. 2.10) consists of angle cleats riveted to the flange of the members. A local riveted bridge connection model was developed using ABAQUS (substructure scheme). The refined connection model, which consists of an assembly of a lower chord truss and a vertical column, was modeled as fixed. The remaining girder was modeled as a cantilever. The connection consists of four angles, each riveted to the girder web and column flange. All of the elements were modeled by using 8-noded brick elements with full integration. A Young's modulus of 200 GPa, Poisson's ratio of 0.3, and linear elastic behavior were assumed for the finite element analysis. Two equal and opposite point loads separated by some distance (a couple) were applied at the end of the girder. The loading introduced a pure moment on the girder. Part of the girder was assumed as a rigid body to reduce the influence of girder bending, so the calculated rotation was essentially at the connection only. The magnitude of the force was increased in steps in order to investigate the moment-rotation behavior of the connection.

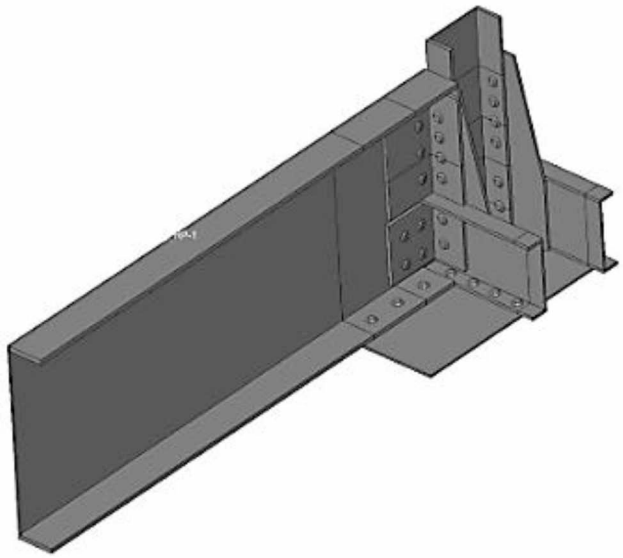

Figure 2.10: Girder-to-Column Connection

The moment-rotation behavior of the connection is shown in Fig. 2.11. The effect of friction was taken into account in the finite element model by defining a coefficient of friction of 0.3 between the surfaces in contact. The moment can transfer to this connection by updating the general model rotational stiffness. In that case, the connection's behavior can be identified when different kinds of vehicles cross the bridge.

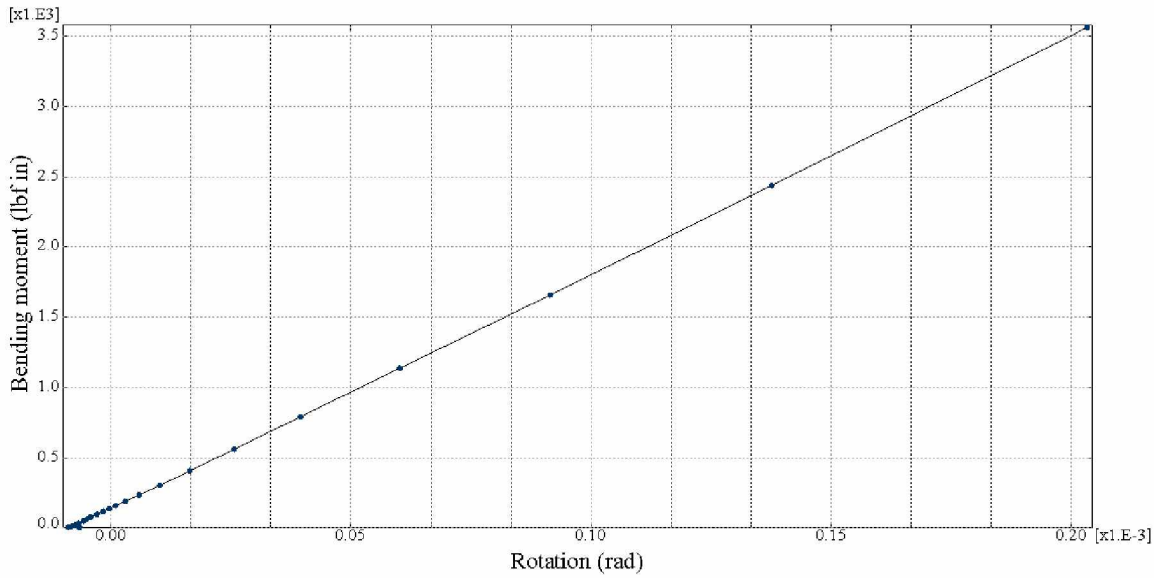

Figure 2.11: Moment-Rotation L1 Connection

The finite element local model (substructure) was used to evaluate the L1 connection's rotational stiffness. The hot-spot strain picture can be obtained from the finite element analysis results (Fig. 2.12).

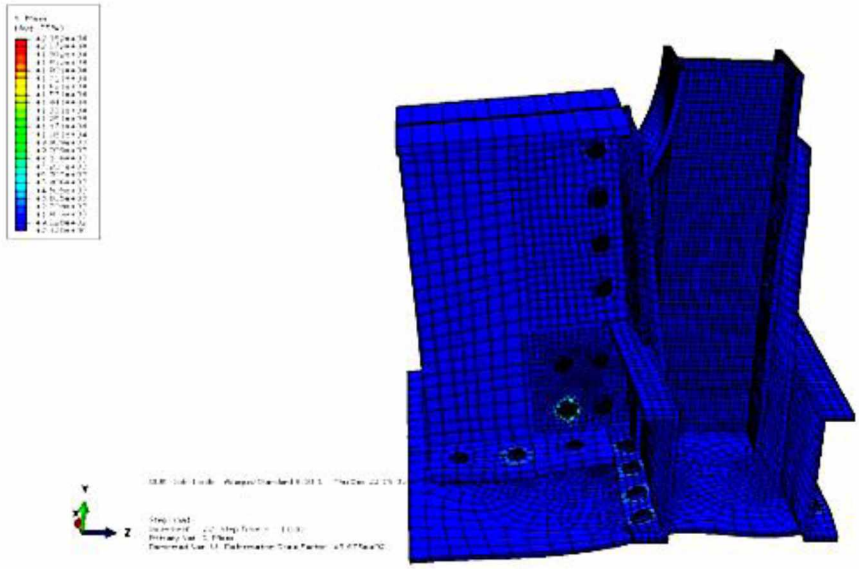

Figure 2.12: L1 Hot Spot Strain

The hot-spot strain shows no obvious strain in the outside gusset plate. The fatigue damage should begin in the inside gusset plate. In the fracture critical bridge inspection reports 2008 and 2010 (AKDOT, 2008; AKDOT, 2010), no crack is observed in the inside gusset plate. So cracks at the outside gusset plate were due to other types of load damage. Those kinds of cracks can be imitated by the local finite element model so that the severity of the cracks and their possible influence on deformation of the connection can be determined.

2.3.4 Crack Gauge

Crack gauges will show movement and progression of cracking at sensor locations. Crack gauges are also able to track the number of loading cycles, which can be used to help establish the remaining service life.

According to a 2011 report by QA Services, Inc. (On System Bridge Inspection, 2011), 19 cracks were identified as locations NDE 1 through NDE 19 (Fig. 2.13). In a 2012 field inspection, a new crack was found and identified as location NDE 20, which was selected to monitor crack propagation. The preliminary crack gauge layout is shown in Fig. 2.14.

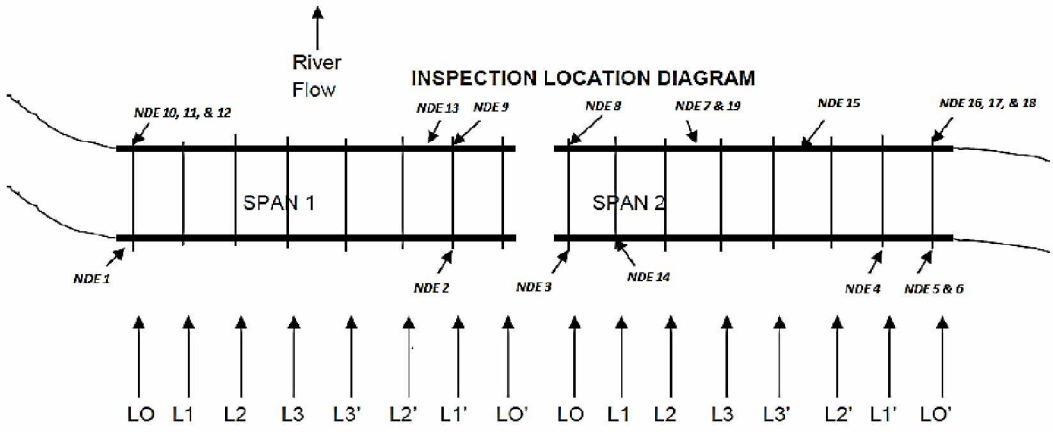

Figure 2.13: Inspection Location Diagram

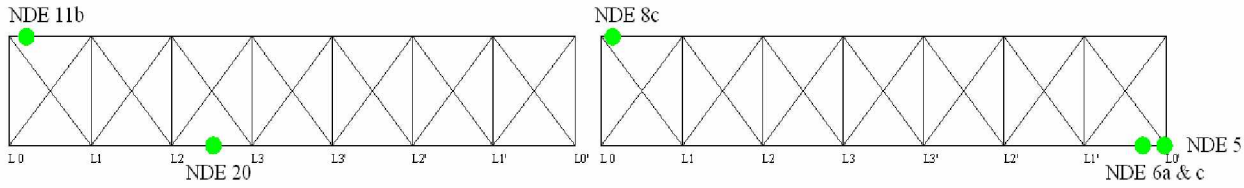

Figure 2.14: Preliminary Crack Gauge Layout

2.4 Results and Discussions

2.4.1 Preliminary Sensor Layout

A preliminary sensor layout (including accelerometers, strain, and temperature sensors, and crack gauges) is shown in Fig. 2.15. An installation of 56 sensors was proposed for monitoring the

Klehini River Bridge. However, since this study aimed to monitor gradual degradation of the bridge, the sensor arrangement does not cover all the cracks but provides information about changes in the load path when cracks gradually increase in length. The design of the bridge structure allows for the use of a minimal number of temperature compensation sensors. In this case, four temperature sensors were separated in each truss. Preliminary structural analysis showed that the diagonal members of the trusses are fracture-critical members. For this reason, a strain sensor should be placed to monitor each fracture-critical member, resulting in eight sensors. The main load path in the lower chord members should also be monitored, especially those where weld-repaired lower chords exist. Strain sensors were located near the middle points of each truss for an additional four sensors, and one sensor was added for a weld repair on the lower chord truss. Sixteen strain sensors were allocated for monitoring the top chords of each truss.

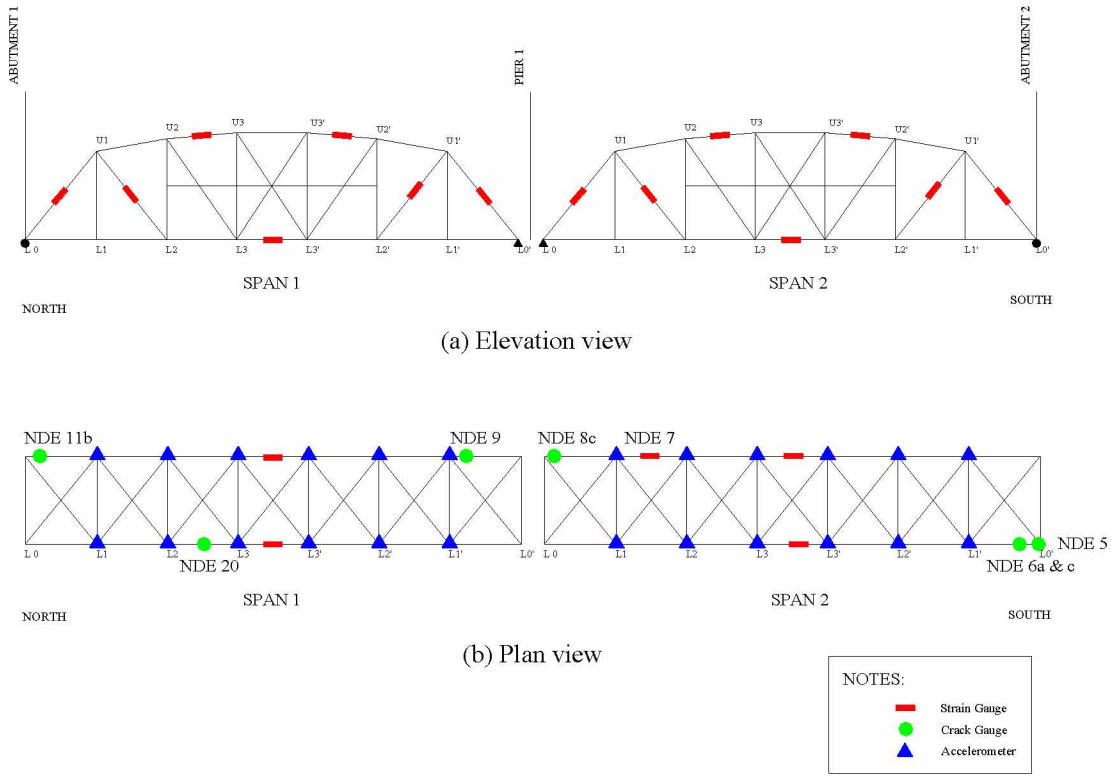

Figure 2.15: Preliminary Sensor Layout on Trusses

Because of poor conditions around the bridge supports, including oxidation and soil buildup, expansion bearing supports were selected to monitor rotation with tilt meters. If the expansion bearing supports are not free to rotate as they should, the bridge may exhibit twist. Finally, an additional seven crack sensors were selected for locations near specific defects in gusset plates and channel flanges to monitor crack activity. The following table is a brief summary of the number and locations of these sensors.

Table 2.1: Summary Number of Sensors

Sensor and Locations	**Number of Sensors**
Strain Sensors on the Top Chord Members	16
Strain Sensors on the Diagonal Members	8
Strain Sensors on the Lower Chord Members	5
Crack Sensors	7
Portable Accelerometers	12
Tilt Meter (at expansion supports)	4
Temperature Sensors	4
Total	56

The objective of this sensor plan was to develop an optimum number and type of sensors that can be used to monitor structural health and to develop an understanding of the primary causes of damage. Final placement of the sensors may change slightly due to physical space constrictions.

2.4.2 Types of Monitoring

Dynamic monitoring: The accelerometer sensor plan follows standard procedures for the acquisition of dynamic properties of the structure. Accelerometers were placed at the bridge deck

level (lower chords of the trusses) along the length of the bridge to provide the natural periods and mode shapes of the bridge structure. This information can be used for monitoring the global condition of the bridge; it can also be used to calibrate and validate structural analysis models. A more accurate computer model allows for increased confidence in the structural evaluation and future analysis for repair or design.

Stress monitoring: ADOT&PF's annual fracture critical inspections of the Klehini River Bridge have found torn gusset plates and cracked rivet holes on the primary trusses, as well as damaged sway and lateral bracing members. Strain gauges were placed at selected truss members. The strain gauges provide a stress history of the members to assess if they are being overstressed.

Deformation/crack monitoring: Crack gauges can show movement and progression of cracking at sensor locations. Also, crack gauges can track the number of loading cycles for establishing remaining service life. Analysis of both strain gauge and crack gauge data can be used in ascertaining the cause of cracks at rivet holes.

2.4.3 Equipment

We selected fiber-optic sensors because this technology is stable over long periods and is ideal for use in a SHM system (Grivas and Garlock, 2003, Pines and Atkan, 2002). Fiber-optic sensors can be connected in series. Fusion splices are preferred to minimize loss. Armored cable, cable in conduit, or other similar types of protection are often used to minimize damage to sensors caused by animals, people, and weather. Optical fiber sensor data are carried through optical leads and routed to the optical interrogator unit at the site via a multiplexer (Fig. 2.16). Optical data are converted to electrical signals at the interrogator and fed into the local computer (the controller

and data-acquisition module). Data from the local computer are transmitted to the Internet via satellite, since hard-wire Internet is not available at the study site.

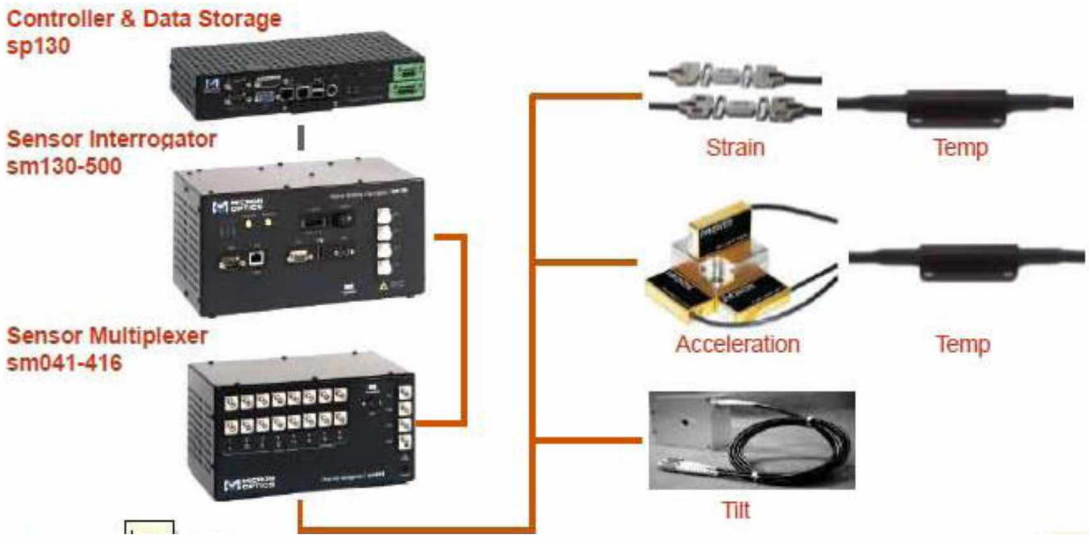

Figure 2.16: System Configuration

The optical system should be housed inside a NEMA enclosure with controlled temperature and humidity (Fig. 2.17). The required conditions and the necessary temperature and humidity controls will be explored before a final system is chosen. The NEMA enclosure should have a NEMA 4 or 4X rating with interior insulation, and a door-operated light fixture, heater, and fan with thermostat controls. The enclosure should have at least five openings for electrical, Internet (satellite or DSL), and fiber connections. A disconnect and a fuse block are needed too. Approximately 8 cubic feet of interior space is required to host the optical system.

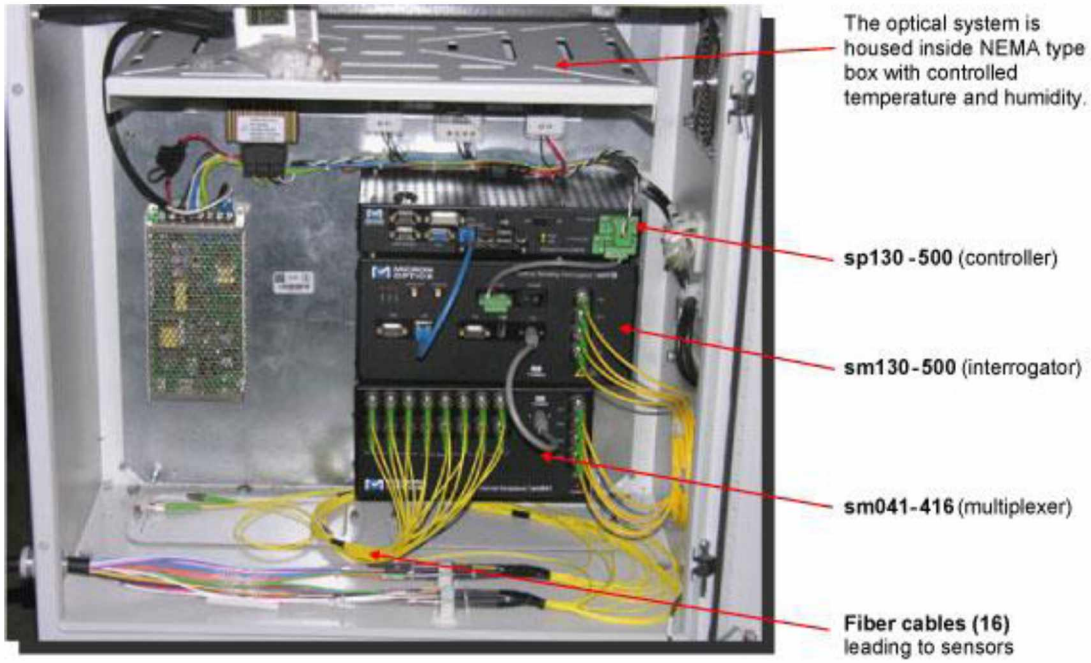

Figure 2.17: SHM System in NEMA Enclosure

2.4.4 Power Supply and Internet for Remote Monitoring

At the Klehini River Bridge, the power supply for the SHM system will be obtained from a nearby utility pole through a transformer. An active power line is at the site, and a pole with a meter is installed at the bridge. The research team verified that sufficient power is available to run the SHM and power the sensors. At other remote sites, power supply equipment such as batteries, charger controllers, wind turbines, and solar panels may be necessary choices.

Since no cell service is available at the Klehini River Bridge crossing, the SHM system needs to be integrated with the Internet for remote monitoring. A land telephone line operated by Alaska Power and Telephone (AP&T) crosses the bridge. Per our conversation with AP&T, DSL Internet service with 4 Mbps speed through the phone line should be available when the sensors are installed (currently, the fastest speed at the bridge is 512 Kbps).

2.4.5 Installation of SHM and Integration of the System

A work plan will be developed for a telecom contractor to install fiber-optic sensors on the bridge. Armored cable, cable in conduit, or other similar types of protection shield the sensors from weather exposure. The optical fiber sensor data are carried through optical leads and routed to the optical interrogator unit at the site. Optical data are converted to electrical signals at the interrogator, and the data are fed into the local computer (the controller and data-acquisition module). Data from the local computer are transmitted to a remote computer via DSL Internet.

2.5 Conclusions and Future Work

This paper has presented the design method for developing a structural health monitoring system that can be used in cold, remote areas. A fiber-optic sensor system was selected for use in an extremely cold climate. A SAP2000 global finite element model was prepared based on as-built conditions. A moving-load analysis based on the American Association of State Highway and Transportation Officials (AASHTO) 2007 (AASHTO, 2007) was used to determine the calculated states of stress and strain in fracture-critical members. Strain gauges were placed on those critical members to ensure that the live load would not exceed stress-and-strain limits during actual traffic conditions. From the modal analysis, the lowest mode shapes and natural periods in vertical, transverse, longitudinal, and rotational direction were found based on the mass participation factor. The mode shapes indicated the best position to place the accelerometers. After field measurement of mode shapes and natural periods, the field dynamic results will be calibrated with the finite element results to identify the accuracy of the finite element model. A local finite model (substructure) was developed using ABAQUS to determine the rotational stiffness of one connection. The preliminary layout of crack gauges was based on recent inspection reports and

field inspections. Cracks were classified as three kinds: cracks at the end of lower chord lower flanges, cracks at the mid-span outside gusset plates, and weld repair at the end-span gusset plates. The selection of cracks for monitoring was based on movement possibilities at the expansion bearings.

Based on the recent inspection reports of the bridge provided by ADOT&PF, a second finite element global model including the detected degradation/defects on the bridge will be created to relate the "current in use" condition. It is proposed that this model is prepared in ABAQUS. The modified model will be calibrated from field static and dynamic testing to represent the actual bridge condition and will be used to predict the response of the bridge during active traffic loading. Several local (substructure) finite element models will be built to simulate the cracks and the semi-rigid connection. The local (substructure) finite element model can be connected with the global model by using reference points that enhance the accuracy of the finite element model. Mode identification will be performed by comparing the numerical dynamic results with field measurements. The finite element model will be modified in the future based on model identification results.

The modified finite element model can help researchers check the influence of local damage on global behaviors and the influence of different kinds of traffic loads on local damage. This information is essential in predicting the future behavior of a bridge. With an accurate finite element model, load rating can be conducted based on the guidance of the Manual for Bridge Evaluation (AASHTO, 2011). Load rating results can show the condition of each bridge member and give the bridge owner guidance for repair or replacement of the bridge.

2.6 Acknowledgments

This study was sponsored and supported by the Alaska University Transportation Center (AUTC) Grant Number 510015 and the Alaska Department of Transportation and Public Facilities. Their financial support is greatly appreciated.

2.7 References

AASHTO LRFD Bridge Design Specifications, (2007), American Association of State Highway and Transportation Officials.

AASHTO Manual for Bridge Evaluation, (2011), American Association of State Highway and Transportation Official.

Alaska Department of Transportation and Public Facilities, (2008), Fracture Critical Inspection Report – Bridge Number 1216: Klehni River Bridge.

Alaska Department of Transportation and Public Facilities, (2010), Fracture Critical Inspection Report – Bridge Number 1216: Klehni River Bridge.

Dong, Y., Liu, H., Song, R., (2011), Bridge Structural Health Monitoring and Deterioration Detection – Synthesis of Knowledge and Technology, Report INE/AUTC 309036, University of Alaska Fairbanks.

Grivas, D. A., Garlock, M., (2003), Sensing systems for bridges: An assessment of the state-of-the-art, In: Mahmoud, K. M. (Ed.), Proceedings of the Second New York City Bridge Conference. New York: A.A. Balkema, pp. 269–284.

Hemphill, D., (2004), Structural Health Monitoring System for the East 12th Bridge, Iowa State University.

Karbhari, V. M., Ansari F., (2010), Structural health monitoring of civil infrastructure systems, the European Workshop on Structural Health Monitoring, 5th edition.

Miyashita, T., Nagai, M., (2010), Development of sensor node and analytical framework for vibration-based structural health monitoring of existing bridges, 5th World Conf. on Structural Control & Monitoring, Tokyo.

On System Bridge Inspection, (2011), Klehini-BN 1216, State Project 80803 Report, QA Services, Inc.

Phares, B. M., Wipf, T. J., Greimann, L. F., Lee Y., (2005), Health Monitoring of Bridge Structures and Components Using Smart Structure Technology, Vols. 1 & 2, Iowa State University.

Pines, D., Aktan, A. E., (2002), Status of SHM of long-span bridges in the United States. Progress in Structural Engineering and Materials, vol. 4, no. 4, pp. 372–380.

Stein, P., (2005), Utilization of Handheld Field Testing System for Improvements of Bridge Load Rating Values in PONTIS, Iowa State University.

Whelan, M. J., Fuchs, M. P., Gangone, M. V., Janoyan, K. D., (2008), Development of a Wireless Bridge Monitoring System for Condition Assessment Using Hybrid Techniques, Clarkson University.

Whelan, M. J., Janoyan, K. D., (2009), Wireless Network for Monitoring of Geo-Structural Systems, Clarkson University.

Chapter 3 Ambient Loading and Modal Parameters for the Chulitna River Bridge[2]

3.1 Abstract

The Chulitna River Bridge is a 790-ft five girder, five-span steel bridge on the Parks Highway between Fairbanks and Anchorage, Alaska. This bridge was built in 1970 and widened in 1993. Under the no-live load condition, five support bearings are not in contact. Heavily-loaded trucks often travel across this bridge to the oil fields in Prudhoe Bay, Alaska. A virtual finite element modeling (FEM), dynamic field testing of the "Ambient vibrational response (AVR)", and structural health monitoring system (SHMS) are used to analyze, evaluate and monitor the structural performance. As the first stage of the research, this paper presents results from the dynamic testing and evaluation of the structural responses of the bridge. In the dynamic field testing, fifteen portable accelerometers were placed on centerline along the bridge length to record the structural response, and an ambient free-decay response was used to evaluate the dynamic properties of the bridge structure. Natural frequencies and modal damping ratios were identified and characterized using Hilbert-Huang transform and fast Fourier transform methods. Compared with conventional approaches, this study demonstrates that (1) the Hilbert-Huang method was found to be effective and suitable for modal parameter identification of a long steel girder bridge by using ambient truck loading; (2) The nonlinear damping were, for the first time, identified based on Hilbert-Huang Transform's amplitude-time slope; (3) modal frequencies are very sensitive to sensor location so their position should be optimized.

[2] Published as Xiao, F., Chen, S. G., Hulsey J. L., Dolan, J. D., Dong, Y., Ambient loading and modal parameters for the Chulitna River Bridge, Advances in Structural Engineering, Vol. 19, No. 4, 2016.

Keywords: Bridge vibration and monitoring, Bridge structural dynamics, Bridge structural system identification, Structural health monitoring.

3.2 Introduction

Twenty-six percent of the nearly 600,000 bridges in the United States were identified as structurally deficient or functionally obsolete by the U.S. Department of Transportation. While a structurally deficient bridge may not necessarily be unsafe, it may be closed or restricted to light vehicles, typically because of deteriorated structural components that lower the bridge rating. The same U.S. Department of Transportation report classified about 27% of the 1200 bridges in Alaska as being structurally deficient and functionally obsolete. Due to Alaska's harsh environment and heavily loaded trucks on the state's highways, it is important for the Alaska Department of Transportation and Public Facilities (ADOT&PF) to have the capability of monitoring the condition of the state's bridge structures.

Accurate prediction of bridge status and structural health monitoring (SHM) require information on the dynamic properties of bridges, usually including natural frequencies and damping ratios. Dynamic tests were conducted on the Chulitna River Bridge to identify its natural frequencies and associated damping ratios. These values were used to validate the finite element modeling (FEM) and analysis of the bridge.

A benchmark study on modal identification of the bridge and correlation with FEM results was conducted. Experimental modal analysis has been widely used to evaluate the behavior of civil engineering structures. This analysis is typically done by extracting structural modal parameters such as natural frequencies, damping ratios, and mode shapes from vibration measurements. In the classical experimental modal analysis, frequency response functions or impulse response functions

in the time domain are usually the bases for system identification; they produce accurate estimates of modal parameters for further use in SHM (Mukhopadhyay et al., 2015). However, it is very difficult in dynamic field tests of bridges to obtain frequency response functions and impulse response functions in the time domain, as typically only the structure dynamic response output can be measured in field tests. System identification methods based on response-only measurements have received increasing attention.

Output-only system identification methods can be classified into two main groups: frequency domain methods and time domain methods. Frequency domain methods include the peak picking method and frequency domain decomposition technique based on the response of auto/cross-spectral densities. Time domain output-only system identification methods include the Ibrahim time domain method (Ibrahim and Mikukcik, 1977) and the least-squares complex exponential method (Brown et al., 1979). Many efforts have been made to identify bridge dynamics using these methods (Farrar and James, 1997; Caicedo et al., 2004; Conte, 2008; Siringoringo and Fujino, 2008).

The approach taken in this study reliably estimated the dynamic properties of the bridge by using its ambient free-decay response signal. Theoretical consideration and FEM analysis of the natural modes are given. Measurements were taken for the ambient free-decay response of the bridge, and the spectrum analysis was conducted. The conventional spectrum results of the fast Fourier transform (FFT) were used to give a preliminary evaluation of the bridge's vibration properties in the context of a linear system of natural modes. The frequency domain approach based on the Fourier transform has drawbacks such as leakage (aliasing), requiring large amounts of data or tests for averaging. Moreover, the FFT is commonly accurate for calculating the

frequency content of a stationary signal. Therefore, when applied to a nonstationary signal, FFT provides the average characteristics of the signal over time and spreads its local behavior globally.

Generally, the Hilbert-Huang transform (HHT) method is superior to the FFT method in identifying modal damping ratios of a structure with closely spaced modes of vibration (Chen et al., 2004). The HHT-based approach can single out some natural frequencies of a structure from mixed frequency content in recordings that also contain the time-dependent excitation and noise frequencies. Results show, however, that damping ratios are given by the HHT method (Yang and Lei 1999) are lower than ratios are given by the FFT method. The FFT-based method overestimates the modal damping ratios (Xu et al., 2003). In addition to employing conventional approaches to identify system response, we adopted the empirical mode decomposition (EMD) method (Huang et al., 1999; Yang et al., 2004) to enhance the characteristics of the test signal and to improve identification. EMD is a method of decomposing a nonlinear and nonstationary signal into a series of zero-mean amplitude-modulation frequency-modulation (AM-FM) components that represent the characteristic time scale of the observation. EMD generates the adaptive basis intrinsic mode functions (IMFs) from the signal. The advantage of this method is that it does not require the limitations of linearity required by the Fourier transform and its extension. Accurate natural frequencies and damping ratios are the essential standards for modal updating. The enhanced approach provides accurate dynamic parameters for any monitored bridges. These parameters can evaluate the safety of a bridge. Crakes, rust, etc., have limited influence on bridge dynamic behavior, so accurate dynamic parameters can give a valid warning signal and assists bridge researchers in understanding bridge performance. Comparing field measurements with FEM dynamic parameters can indicate the accuracy of the FEM.

Chen et al. (2004) examined the EMD method for a suspension bridge by using wind load. The results show that the EMD method produced reliable natural frequencies and damping ratios; however, this conclusion was based on Typhoon Victor only. More field studies of the EMD method in other loading conditions before a general conclusion is reached. In this study, the EMD method is examined using the portable accelerometer data of a long steel girder bridge under ambient free-decay truck loading.

The damping is usually considered to be a more sensitive index than frequency and modal shape for health monitoring of a structure (Wang and Li, 2013; Gonzalez et al., 2012; Curadelli et al. 2008). In some situations, damping-based detection has the advantages than other modal parameters detection as many damages such as cracks in structures are not well undetectable by using changes in natural frequencies or modal shapes. In general, it is admitted that increasing the crack severity directly increases the damping factor, whereas the changes in frequencies and modal shapes are complicated for the crack increases (Bovsunovsky, 2004; Modena et al., 1999). Several studies used EMD method to identify the structure linear damping based on amplitude-time slope (Shi et al., 2012; Wang and Chen, 2014; Chen et al., 2004). Shi et al. 2012 identified high-rise building's linear damping from free and ambient vibration. Wang et al. 2014 found linear damping based on a steel frame model under ambient vibration. Chen et al. 2004 identified the suspension bridge linear damping by using wind load. Many structures have linear type damping, but exist studies haven't identified the nonlinear damping based on the amplitude-time slope. This research first identified the nonlinear damping by using this method.

3.3 Bridge Description

The Chulitna River Bridge, built in 1970, is located at Historic Mile Post 132.7 on the Parks Highway which is the most direct route connecting Anchorage with Fairbanks. Heavily loaded vehicles of up to 410,000 pounds regularly travel on this route to and from the North Slope oil fields. The original bridge was a 790-foot-long five-span continuous girder structure with two exterior steel plate girders, 3 sub-stringers, and a cast-in-place concrete deck of 34 feet width. In 1993, the bridge deck width was increased to 42 feet 2 inches by replacing the original cast-in-place deck with precast concrete deck panels. To accommodate the increased loads, the two original exterior plate girders were strengthened, three new longitudinal steel trusses were installed using the original stringers as top chords, and steel bracing was added to the piers (Fig. 3.1a). There are five roller bearings at each pier and there are not or partially connected with the supports at pier 3 and pier 5. Those disconnections are caused by the reconstruction of the bridge. Figure 3.1(b) shows the gap between one roller bearing and support, and this bridge may exist nonlinear behavior. A series of dynamic field tests was conducted on the Chulitna River Bridge to identify the modal properties of the bridge.

a. Bridge overview

b. Disconnection between roller bearing and supports

Figure 3.1: Chulitna River Bridge

3.4 Dynamic Test Description

A portable data acquisition system was used to collect dynamic data. The system is composed of portable uniaxial accelerometers, an integrator, a laptop, and cables. The portable accelerometers are EpiSensor ES-U2 Force Balance accelerometers with user-selectable full-scale recording ranges of ±4g, ±2g, ±1g, ±1/2g or ±1/4g and a bandwidth from DC to 200 Hz (Fig. 3.2).

In a weak motion, the weight of the instrument and the friction between the sensor and floor ensure accurate reproduction of ground motion (Episensor User Guide, 2011).

Figure 3.2: Portable Accelerometer on One Measure Point

Fifteen accelerometers were put on the surface of the concrete deck. The accelerometers were positioned above each pier and at mid-spans. For the longer spans 2, 3 and 4, additional sensors were added to provide more data collection points (Figure 3.3). Accelerometers were placed on one straight line along the mid-width of the bridge deck. Three trial measurements were made in the vertical, transverse and longitudinal directions. For transverse measurements, the accelerometers were pointed in the downstream direction; for longitudinal trials, the accelerometers in the north direction.

Prior to recording the acceleration, the system was zeroed and tested for continuity and background noise. For each test, a 30 ft boom truck was used to excite the bridge. The truck crossed the bridge from the north end to the south end of the upstream lane at a speed of 45 mph (Fig. 3.4).

The wind effect during the dynamic test can be neglected. The bridge was closed to other traffic until the vibration totally damped out.

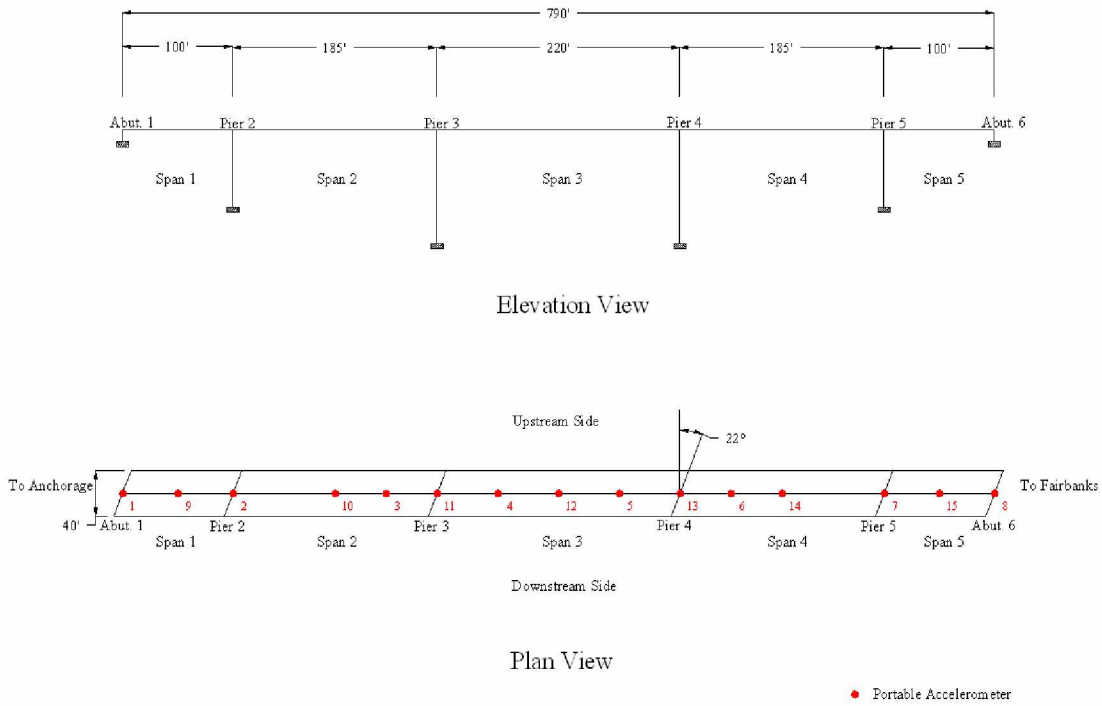

Figure 3.3: Portable Accelerometer Location and Number

Figure 3.4: Dynamic Test

3.5 Spectrum Analysis

From the tests, it was found that the analyzed modal parameters are sensitive to sensor locations due to the mode shape of the vibration taking place. In some locations, the magnitudes of vibration were too small to offer reliable specific modal information or the vibration was too weak to be identified. As such, optimization of sensor locations are necessary, otherwise multiple point measurements are needed in practice to guarantee reliable, robust and effective measurements.

In the following text, only the two most sensitive data locations -- the ones with the largest response—were included for processing. Figure 3.3 shows that Points 9 and 12 are at the center of the short end span and the long central span of the bridge which could be two of the most sensitive locations. Figure 3.5 shows a measured acceleration signal and its FFT for a typical measured acceleration signal in the vertical direction in the middle of Span 3 (Point 12). Figure 3.5(b) shows that there are multiple peaks, with f_1 = 1.500 Hz, f_2 = 2.846 Hz, and f_3 = 3.224 Hz being dominate. A measured vertical acceleration signal at the middle of Span 1 (Point 9) and its FFT are shown in Figure 3.6. Note the multiple peaks in Figure 3.6(b), with dominant frequencies at f_{1a} = 2.190 Hz,

f_{2a} = 2.846 Hz, and f_{3a} = 4.586 Hz. Theoretically, both Points 9 and 12 consist of similar and consistent modal information. Actually, the results for Point 9 show a very small peak signal of 1.500 Hz, whereas the results for Point 12 show very small peaks of 2.190 Hz and 4.586 Hz. As such, even though Points 12 and 9 are relatively the most sensitive, the monitoring based on Point 12 alone or Point 9 alone is not enough. The weak signals render the reliability of system identification. Results for the remaining points in Figure 3.3 are far weaker than the results for Points 9 and 12.

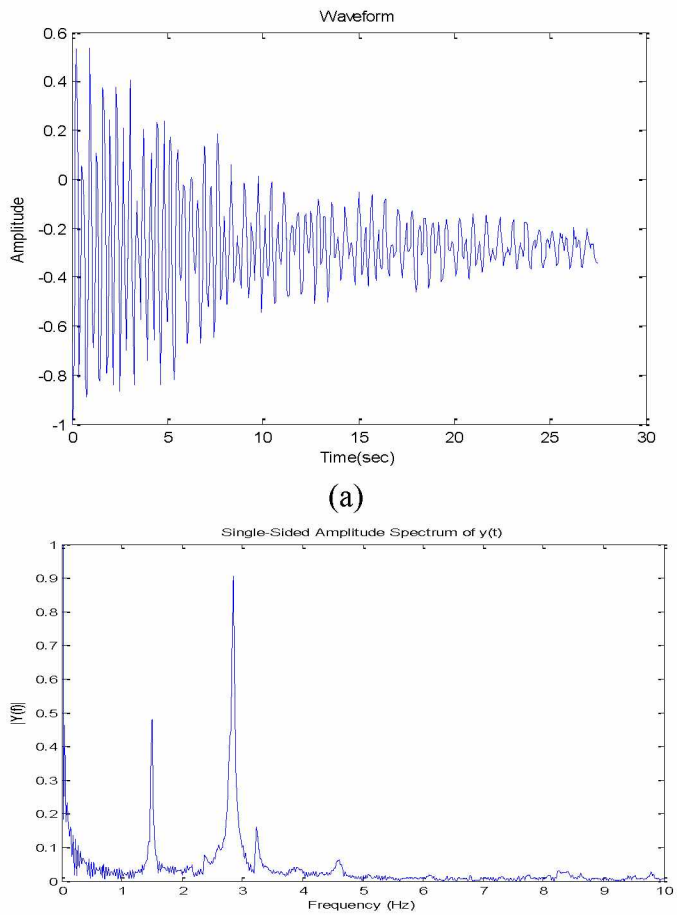

(b)

Figure 3.5: Time History (a) and FFT of a Typical Measured Acceleration Signal in the Vertical Direction at the Middle of Span 3 (Point 12) (b)

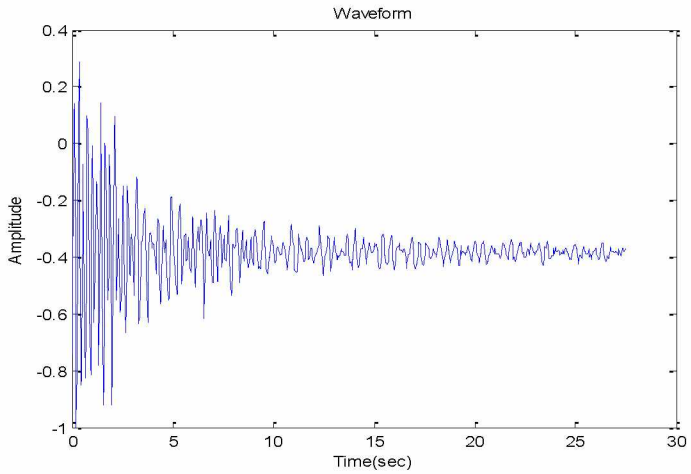

(a)

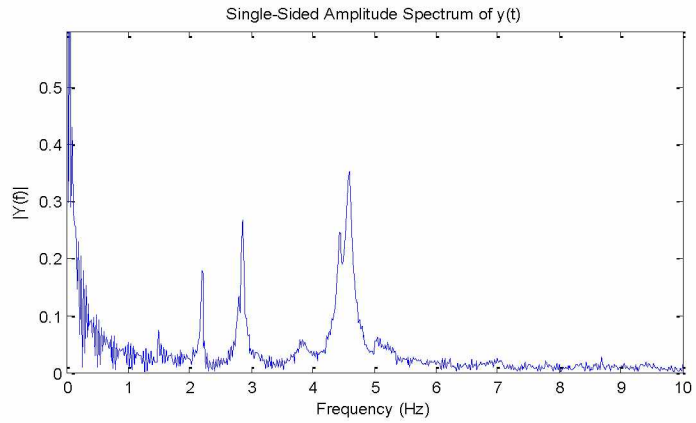

(b)

Figure 3.6: Time History (a) and FFT of a Typical Measured Acceleration Signal in the Vertical Direction at the Middle of Span 1 (Point 9) (b)

These results suggest that the dominant components, with specific frequencies of f_1 = 1.500 Hz, f_{1a} = 2.190 Hz, f_2 = 2.846Hz, and f_{3a} = 4.586 Hz, can be used as the characteristic quantity or index for integrity monitoring or bridge ambient response investigations. To make use of a dominant component for future analysis, the component must be extracted from the original test signal. Filtering techniques can be implemented to extract this component from the original signal.

However, in this study, the EMD method, with its applicability to complex problems is used to extract the specific signal and to identify the system parameters.

3.6 Empirical Mode Analysis and Parameter Evaluations

In order to decompose the signal being characterized in the time-frequency expression of the signal in Figures 3.5 and 3.6, the empirical mode decomposition (EMD) method, instead of filtering was used. . The fundamental formulations for EMD method are presented in the following and the process was programmed using MATLAB. The EMD method decomposes a nonlinear and nonstationary signal into a series of zero-mean AM-FM components that represent the characteristic time scale of the observation. A multi-component AM-FM model for a nonlinear and nonstationary signal, $x(t)$, can be represented as

$$x(t) = \sum_{j=1}^{n} a_j(t)\cos[\varphi_j(t)] \tag{3.1}$$

where $a_j(t)$ and $\varphi_j(t)$ represent the instantaneous amplitude and the instantaneous phase of the jth component, and n is the number of components. In the EMD approach, decomposition is done by iteratively conducting a sifting process. The zero-mean AM-FM components are called IMFs, which must satisfy the following requirements: (1) The number of extreme and the number of zero crossings in the IMF must be equal or differ at most by one; (2) at any point, the mean value of the envelopes defined by the local maxima and local minima must be zero. In short, the signal is locally symmetric around the time axis. The sifting process to find IMFs for the signal $x(t)$ is as the following.

At first, find positions and amplitudes of all local maxima and all local minima in the input signal $x(t)$. Then create an upper envelope using cubic spline interpolation of the local maxima and a lower envelope using cubic spline interpolation of the local minima. Calculate the mean of the upper and lower envelopes which is defined as $m_1(t)$. Subtract the envelope mean signal, $m_1(t)$, from the original input signal,

$$h(t) = x(t) - m_1(t). \tag{3.2}$$

Check whether $h(t)$ meets the requirements to be an IMF. If not, treat $h(t)$ as new data and repeat the previous process. Then set

$$h_{11}(t) = h_1(t) - m_{11}(t) \tag{3.3}$$

Repeat this sifting procedure k times until $h_{1k}(t)$ is an IMF; this is designated as the first IMF.

$$c_1(t) = h_{1k}(t) \tag{3.4}$$

The next step is to subtract $c_1(t)$ from the input signal and define the remainder, $r_1(t)$, as the first residual. Since the residual, $r_1(t)$, still contains information related to longer period

components, it is treated as a new data stream and Step (1) is repeated for the new signal. This procedure can be repeated *j* times to generate *j* residuals, $r_j(t)$, resulting in

$$\begin{cases} r_1(t) - c_2(t) = r_2(t) \\ \vdots \\ r_{n-1}(t) - c_n(t) = r_n(t) \end{cases} \tag{3.5}$$

The sifting process is stopped when either of two criteria is met: (1) the component, $c_n(t)$, or the residual, $r_n(t)$, becomes so small as to be considered inconsequential, or (2) the residual, $r_n(t)$, becomes a monotonic function from which an IMF cannot be extracted. By summing Equations (4) and (5), we obtain the objective IMF,

$$x(t) = \sum_{i=1}^{n} c_{imf\,i}(t) + r_n(t). \tag{3.6}$$

In other words, the original signal can now be represented as the sum of a set of IMFs plus a residual. Next, the Hilbert transform is applied to all IMFs, $c_j(t)$, in Equation (6) to derive model parameters including frequency and damping,

$$H[c_j(t)] = \frac{1}{\pi} \int_{-\infty}^{\infty} \frac{c_j(t)}{t-\tau} d\tau. \tag{3.7}$$

The Hilbert transform, $H[c_j(t)]$, and $c_j(t)$ form a complex signal, $Z_j(t)$, where

$$Z_j(t) = c_j(t) + iH[c_j(t)] = a(t)e^{i\varphi(t)}. \tag{3.8}$$

Then the envelop of each IMF can be given by

$$a_j(t) = \sqrt{[c_j(t)]^2 + \{H[c_j(t)]\}^2}\ , \quad \varphi_j(t) = \arctan\{H[c_j(t)]/c_j(t)\} \tag{3.9}$$

in which $a_j(t)$, the instantaneous amplitude of $x(t)$, reflects how the energy of $x(t)$ varies with time. The term $\varphi_j(t)$ is the instantaneous phase of $x(t)$. The instantaneous frequency, $\omega(t)$, is defined as the time derivative of the instantaneous phase $\varphi(t)$ as follows:

$$\omega(t) = \frac{d\varphi(t)}{dt}. \tag{3.10}$$

Then the original signal $x(t)$ can be expressed as

$$x(t) = \sum_{j=1}^{n} a_j(t) \exp\left[i\int \omega_j(t)dt\right]. \tag{3.11}$$

Theoretically, the measured acceleration response of the $\ddot{w}$ can be approximately decomposed by the EMD as follows:

$$\ddot{w}(t) = \sum_{j=1}^{k} \ddot{w}_j(t) + \sum_{i=1}^{n-k} c_i(t) + r_n(t) \tag{3.12}$$

where $\ddot{w}_j(t)$ is the *j*th modal acceleration response and $c_i(t)$ is the *i*th IMF:

$$\begin{aligned} \omega_j(t) &= \omega_{dj} t - \theta_j \\ \ln a_{ij} &= -\varsigma_j \omega_j t + \ln r_{ij} \end{aligned} \tag{3.13}$$

Thus, the damped natural frequency ω_{dj} can be obtained from the slope of the phase angle plot in $\omega_j(t)$ versus *t*, and ς_j can be obtained from the slope of the plot in $\ln a_{ij}$ versus *t*. The linear least-squares method can be used to fit the plots of $\ln a_{ij}$ vs. time and $\omega_j(t)$ vs. time.

In the next step, signal decomposition and parameter identification are illustrated by using a typical measured acceleration signal, as shown in Figures 3.5 and 3.6. The decomposed components of a measured acceleration signal at Point 12 are shown in Figure 3.7, which indicates that the magnitude of c1 and c2 is much higher than the rest of the components. To characterize the decomposed signal, the power spectrum of the decomposed signal is calculated as shown in Figure 3.8, where the decomposed component c1 has a specific frequency of 2.830 Hz and the decomposed component c2 has a specific frequency of 1.510 Hz. This characterization is consistent with the analysis described above. We next focus on c1 and c2 to identify the corresponding characteristic parameters.

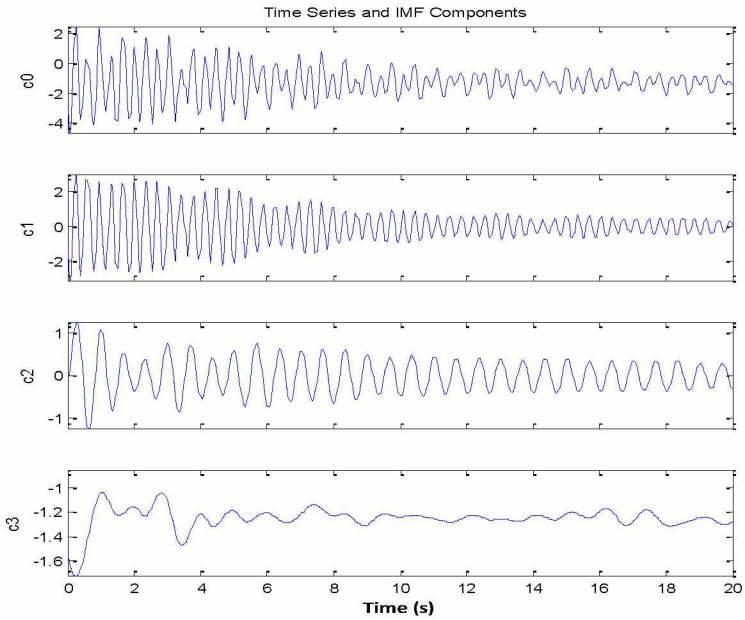

Figure 3.7: Decomposed Components of a Measured Acceleration Signal in the Vertical Direction at the Middle of Span 3 (Point 12)

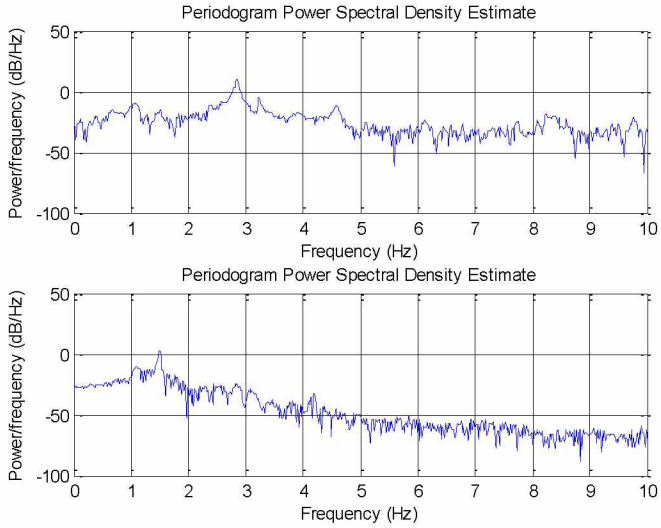

Figure 3.8: Power Spectrum of the Decomposed Components (c1: Top; c2: Bottom) of a Measured Acceleration Signal in the Vertical Direction at the Middle of Span 3 (Point 12)

Figure 3.9 shows the decomposed components of a measured acceleration signal at Point 9, which indicate that the magnitude of c1, c2, and c3 are much higher than the rest of the components. To characterize the decomposed signal, the power spectrum of the decomposed signal is calculated as shown in Figure 3.10, where the decomposed component c1 has a specific frequency of 4.620 Hz, the decomposed component c2 has a specific frequency of 2.820 Hz, and c3 has a specific frequency of 2.230 Hz. This characterization is consistent with the analysis described above. Components c1, c2, and c3 are used to identify the corresponding characteristic parameters. Table 3.1 shows the relation of natural frequencies calculated by the two methods.

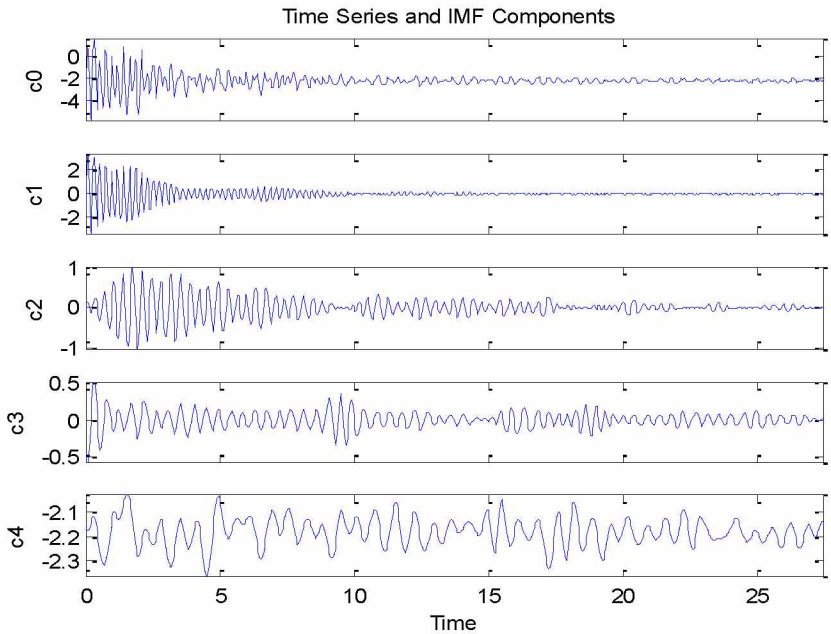

Figure 3.9: Decomposed Components of a Measured Acceleration Signal in the Vertical Direction at the Middle of Span 1 (Point 9)

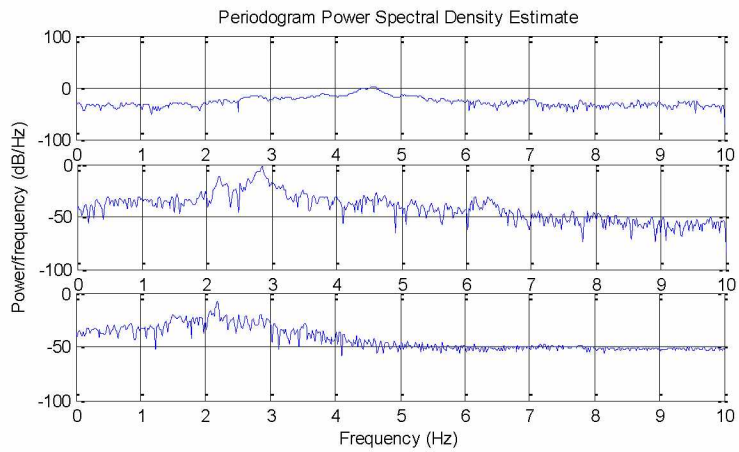

Figure 3.10: Power Spectrum of the Decomposed Components (c1: Top; c2: Middle; c3: Bottom) of a Measured Acceleration Signal in the Vertical Direction at the Middle of Span 1 (Point 9)

Table 3.1: Comparison of Natural Frequencies between the FFT Method and EMD Method

Number	FFT Method	EMD Method	Difference
1	1.500 Hz	1.510 Hz	-0.7%
2	2.190 Hz	2.230 Hz	-1.8%
3	2.846 Hz	2.820 Hz	0.9%
4	4.586 Hz	4.620 Hz	-0.7%

The characteristic plots of the decomposed signals corresponding to two specific frequencies in the vertical direction in the middle of Span 3 (Point 12) are shown in Figure 3.11. The damping coefficients can be identified as $\xi_1 = 0.0070$ and $\xi_2 = 0.0057$. To identify nonlinear damping, we can assume a power law nonlinear damping with a couple of unknown parameters for an oscillator, then figure out its decay envelop; then the EMD based damping decay curve can be used to identify the unknown parameters through least square or optimization methods.

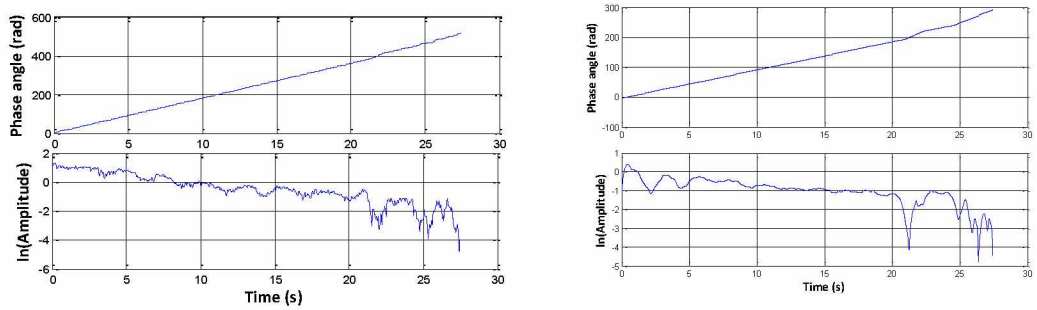

Figure 3.11: Characteristic Plots of the Decomposed Signals Corresponding to Two Specific Frequencies in the Vertical Direction at the Middle of Span 3 (Point 12)

The characteristic plots of the decomposed signals corresponding to three specific frequencies in the vertical direction in the middle of Span 1 (Point 9) are shown in Figure 3.12. The damping coefficients can be identified as $\xi_{1a} = 0.014$, $\xi_{2a} = 0.0071$, and $\xi_{3a} = 0.0060$.

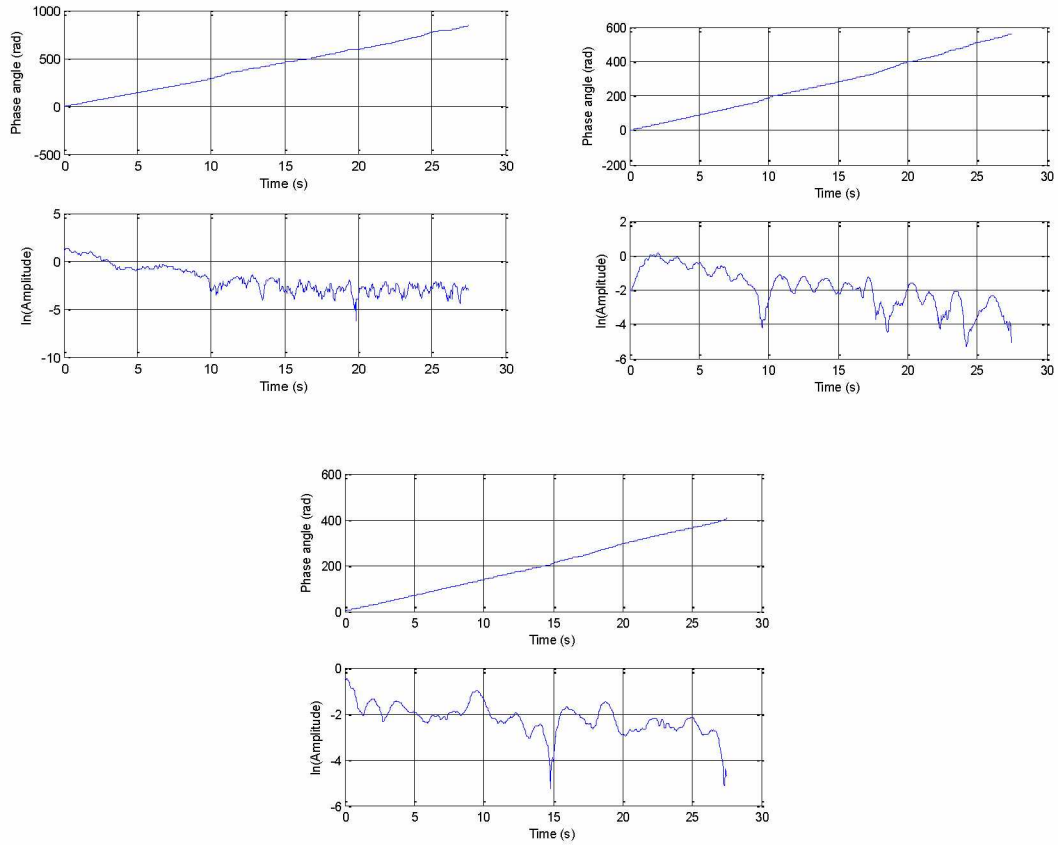

Figure 3.12: Characteristic Plots of the Decomposed Signals Corresponding to Three Specific Frequencies in the Vertical Direction at the Middle of Span 1 (Point 9)

3.7 Discussion and Theoretical Consideration

The measured results were correlated with the FEM results (Table 3.2) to gain some understanding of the bridge performance. According to the mass participation ratio is higher in longitudinal direction, the 1.500 Hz and 2.190 Hz frequencies belong to the longitudinal modes of vibration. The correlations between field measurements and the FEM results are shown in Table 3.2.

Table 3.2: Comparison Natural Frequencies between Field Measurements and FEM Results

Mode	Field Measurement	FEM Result	Error
Longitudinal Mode 1	1.500 Hz	1.367 Hz	8.9%
Longitudinal Mode 2	2.190 Hz	2.044 Hz	6.7%
Vertical Mode 1	2.846 Hz	2.756 Hz	3.2%
Vertical Mode 2	3.224 Hz	3.348 Hz	-3.8%
Vertical Mode 3	4.586 Hz	4.249 Hz	7.3%

The locations of these points to be compared are shown in Figure 3.3. The FFT peak frequency of 1.500 Hz is higher at Point 12 (Fig. 3.5[b]) Point 9 (Fig. 3.6[b]). This correlates to the first longitudinal mode from the FEM results, which shows obvious movement in Span 3 (Fig. 3.13).

Figure 3.13: First Longitudinal Mode of Vibration from the FEM analysis, 1.367 Hz

The measured frequency 2.190 Hz is the second longitudinal mode's frequency. There is no 2.190 Hz peak in Figure 3.5(b); however, the peak shows in Figure 3.6(b), which means that minimal movement occurs at Point 12 in Span 3 and obvious vibration at Point 9 in Span 1. The second longitudinal mode from the FEM result is shown in Figure 3.14. This mode of vibration correlates well with the measured result which shows a larger magnitude of movement at Point 9than at Point 12.

Figure 3.14: Second Longitudinal Mode of Vibration from the FEM Analysis, 2.044 Hz

According to the FEM analysis, in the second mode of vertical vibration, minimal vibration occurs in Spans 1 and 5 (Figure 3.15), which results in no indication of the natural frequency of the 3.224 Hz FFT peak at Point 9 in Span 1 (Fig. 3.6[b]) and only a weak indication of 3.224 Hz at Point 12 in Span 3 (Fig. 3.5[b]). .

Figure 3.15: Second Mode of Vertical Vibration from the FEM Analysis for 3.348 Hz

The fourth mode of vertical vibration determined using the FEM analysis is shown in Figure 3.16. Obvious deflections occur due to vibration in Spans 1 and 5, and no obvious deflection occurs in Span 3. From the field measurement results at Point 12 (see Fig. 3.5[b]) and Point 9 (Fig. 3.6[b]), this vertical vibration mode has a frequency of 4.586 Hz. The field measurement results show a peak only at Point 9 in Span 1 (Fig. 3.6[b]) but a minimal movement of Point 12 in Span 3 in the mode.

Figure 3.16: Fourth Mode of Vibration in the Vertical Direction from the FEM Result, 4.249 Hz

The damping coefficients were identified using the slope of the amplitude-time plot. Compared with the typical linear damping case in structure (Shi et al., 2012; Wang and Chen, 2014; Chen et al., 2004), the amplitude-time slopes in Figures 3.11 and 3.12 show nonlinear damping exists in this bridge. For our case, some mode exhibit linear damping, some appear nonlinear damping, which may suggest that some specific modal damping is relevant to some kind of damage. These nonlinear behaviors are necessary for understanding long-term behavior, an important feature in SHM.

This study demonstrated that multiple sensors are required to comprehensively record the bridge response for efficiently identifying modal frequencies and damping related with the different modes of vibration. . If the sensor locations are not optimally determined ahead of time or an insufficient number of sensors are used, significant information required for characterization of the structural performance will be lost due to weak signals. This conclusion conflicts with previous claims that just one acceleration sensor is required for output-only frequency and damping identification (Lin et al., 2011). Most likely, one sensor would be unable to identify all of the modes of vibration due to being located at a node of vibration or due to the weak signal associated with a location that has minimal motion.

3.8 Conclusions

This study investigated the dynamic behavior of the Chulitna River Bridge by using ambient free-decay response. By using frequency spectrum analyzes, several modes of vibration were characterized with resonance frequencies of 1.500 Hz, 2.190 Hz, 2.846 Hz, 3.224 Hz, and 4.586

Hz. The frequencies of 2.846 Hz, 3.224 Hz, and 4.586 Hz are vertical vibration mode frequencies. The frequencies of 1.500 Hz and 2.190 Hz are bridge longitudinal mode frequencies.

A finite element model was developed to simulate the virtual response of the bridge. Calculated frequency values using this model compared well with the measured results.

Based on portable accelerometer data, empirical mode decomposition, and the Hilbert transform were used to identify the modal parameters including the damping coefficients of the steel girder Chulitna Bridge under ambient free-decay truck loading. This approach was first examined by using the portable accelerometer data of a long steel girder bridge under ambient free-decay truck loading. Compared with conventional approaches, the Hilbert-Huang method was found to be effective and suitable for modal parameter identification of Chulitna River Bridge.

This research firstly identified the bridge nonlinear damping behavior based on the nonlinear slope of amplitude-time by using Empirical mode decomposition and the Hilbert transform method. The nonlinear amplitude-time slope demonstrates the nonlinear behavior exist in this bridge. The identified damping is a sensitive index for structural health monitoring.

We demonstrated that multiple sensors are required to comprehensively record modal frequencies and damping. Multiple sensors are necessary to efficiently and effectively identify pertinent information about the bridge prior to conducting field testing so that the sensor locations can be optimized into groups to provide measurements of significant value. Improperly located sensors or an insufficient number of sensors may result in the loss of significant information due to weak instrument signals. This conclusion conflicts with previous claims that just one acceleration sensor is required for output-only frequency and damping identification.

This research identified the dynamic behavior of the bridge. In next stage of the research, the bridge finite element model was updated based on the ambient test results and real-time monitoring

data. The updated bridge model was used to calculate the load rating, and evaluate the safety of this bridge.

3.9 Acknowledgments

Support of this research by the Alaska University Transportation Center, Grant No. 510015, is gratefully acknowledged. We wish to acknowledge the support of the Alaska Department of Transportation and Public Facilities, University of Alaska Fairbanks, University of Alaska Anchorage, and Alaska Native Science and Engineering Program.

3.10 References

Bovsunovsky, A., (2004), The mechanisms of energy dissipation in the nonpropagating fatigue cracks in metallic materials, Engineering Fracture Mechanics, 71(16-17), 2271-2281.

Brown, D. L., Allemang, R. J., Zimmerman, R. D., Mergeay, M., (1979), Parameter estimation techniques for modal analysis, SAE Paper No. 790221, SAE Transactions, 88, 828–846.

Caicedo, J. M., Dyke, S. J., Johnson, E. A., (2004), Natural excitation technique and eigensystem realization algorithm for phase I of the IASC-ASCE benchmark problem: Simulated data, J. Eng. Mech., 130(1), 49–60.

Chen, J., Xu, Y. L., Zhang, R. C., (2004), Modal parameter identification of Tsing Ma suspension bridge under Typhoon Victor: EMD-HT method., J. Wind Engineering and Industrial Aerodynamic, 92, 805–827.

Conte, J. P., (2008), Dynamic testing of Alfred Zampa Memorial Bridge, J. Struct. Eng., 134(6), 1006–1015.

Curadelli, R.O., Riera, J.D., Ambrosini, D., Amani, M.G., (2008), Damage detection by means of structural damping identification, Engineering Structures, 30(2008), 3497-3504.

EpiSensor User Guide, (2011), EpiSensor ES-U2 Uniaxial Force Balance Accelerometer User Guide, Kinemetrics, Inc.

Farrar, C. R., James, G. H., III., (1997), System identification from ambient vibration measurements on a bridge, J. Sound and Vibration, 205(1), 1–18.

Gonzalez, A., Obrien, E.J., McGetrick, P.J., (2012), Identification of damping in a bridge using a moving instrumented vehicle, Journal of Sound and Vibration, 331 (2012), 4115-4131.

Huang, N. E., Shen, Z., Long, S. R., (1999), A new view of non-linear water waves: The Hilbert spectrum, Annual Review of Fluid Mechanics, 31, 417–457.

Ibrahim, S. R., Mikulcik, E. C., (1977), Method for the direct identification of vibration parameters from the free responses, Shock and Vibration Bulletin, 47(4), 183–198.

Lin, C. W., Chiou, D.J., Huang, P.C., (2011), Structural system identification for vibration bridges using the Hilbert-Huang transform, Journal of Vibration and Control December 14, 2011.

Modena, C., Sonda, D., D.Zonta., (1999), Damage localization in reinforced concrete structures by using damping measurements, Proceedings of the International Conference on Damage Assessment of Structures, Dublin, Ireland, 132–141.

Mukhopadhyay T, Dey T K, Chowdhury R, Chakrabarti A, (2015), Structural damage identification using response surface based multi-objective optimization: A comparative study, Arabian Journal for Science and Engineering 40(4) 1027-1044.

Shi, W.X., Shang, J.Z., Lu, X.L., (2012), Modal identification of Shanghai World Financial Center both from free and ambient vibration response, Engineering Structures, 36(2012), 14-26.

Siringoringo, D. M., Fujino, Y., (2008), System identification of suspension bridge from ambient vibration response, Engineering Structures, 30(2), 462–477.

Wang, Y.F., Li, X.R., (2013), Nonlinear damping of FRP-confined damaged reinforced concrete columns, Engineering Structures, 57(2013), 289-295.

Wang, Z.C., Chen, G., (2014), Analytical mode decomposition with Hilbert transform for modal parameter identification of buildings under ambient vibration." Engineering Structures, 59(2014), 173-184.

Xu, Y. L., Chen, S. W., Zhang, R. C., (2003), Modal identification of Di Wang Building under Typhoon York using the Hilbert–Huang transform method, The Structural Design of Tall and Special Buildings, 12(1), 21–47.

Yang, J. N., Lei, Y., (1999), Identification of natural frequencies and damping ratios of linear structures via Hilbert transform and empirical mode decomposition, International Conference on Intelligent Systems and Control, IASTED/Acta Press, Anaheim, CA, 310–315.

Yang, J. N., Lei, Y., Lin, S., Huang, N., (2004), Hilbert-Huang based approach for structural damage detection." J. Engineering Mechanics, 130, 85–95.

Chapter 4 Multi-direction Bridge Model Updating using Static and Dynamic Measurement [3]

4.1 Abstract

This research presents a multi-direction bridge finite element model updating method based on static and dynamic tests. A fiber optics structural health monitoring system was installed on the bridge site and 73 fiber optic sensors captured the static and dynamic data at the local-level. A portable accelerometer system was used to record the ambient loading test and 15 force-balanced accelerometers were placed along bridge center to record the bridge global behavior. The original model was built according to the construction drawings. The bridge model was updating by using multi-level test data. A new multi-direction model updating approach was established to separate the model updating into several stages based on the member's direction. In each stage, the uni-direction members were updating in local-global level. This study found the multi-direction model updating can reduce the number of objective functions and variables in each stage and bridge model updating in the uni-direction has limited influence on the other directions. It is necessary to update a steel girder bridge's finite element model in the multi-direction in order to ensure the model's accuracy.

Keywords: Bridge model updating, Structural health monitoring, Fiber optic

[3] Published as Xiao, F., Hulsey, J. L., and Chen, S. G., Multi-direction Bridge Model Updating using Static and Dynamic Measurement, Applied Physics Research, Vol. 7, No. 1, 2015.

4.2 Introduction

Consider that the current approach to structural health monitoring can be divided into two distinct areas: (1) using the structural dynamic properties to detect structural behavior at the global level based on the dynamic parameters (Bedon and Morassi,2014; Goulet et al., 2013; Caglayan et al., 2012; Liu et al., 2014; Dan et al., 2014), and (2) using several sensors to quantify the condition of the local components of the bridge structure based on the static measurements (Sanayei et al., 2012). Both approaches have advantages and limitations. Dynamic parameters give information about the global response of structures and, therefore, are not very sensitive to local phenomena. On the other hand, static measurements, such as strains and displacements, are more sensitive to the response in their vicinity and, therefore, they better suited to determine local defects (Perea et al., 2013).

Model updating at the global-local level will overcome the weakness of only using one type of measurement and combined global-local performance will assist in evaluating the bridge behavior accurately, however, it will also enhance the number of objective functions which are the difference between the measurements and the analyzed results. In this case, more variables will be selected in order to make the objective functions coverage. A large number of objective functions and variables will take longer for the mathematical operation. In order to solve this problem, a new bridge finite model updating strategy required to establish in order to control the number of functions and simplify the process of model updating.

This research effort is focused on developing an optimization technique for calibrating a finite element model against experimental data in local-global level. A new multi-direction model updating method has been developed in this paper. This approach will enable control the number of objective functions and simplified the process of model updating.

Compared with existing global-local bridge model updating (Schlun et al., 2009; Jung and Kim, 2013), this approach used bridge members' direction to group bridge components. Girder, Stringer, and Deck etc. are the longitudinal members and cross frame, roller supports are the transversal members. Each direction members were updated in the global-local level independently. The advantage of this approach is it separates model updating into several stages and in each stage, the objective functions and variables are reduced.

The study results indicated updating uni-direction member can only enhance the accuracy in this direction and it have a very low influence on the accuracy of other direction members. The overall accuracy of bridge model is contributed by both longitudinal members and transversal members.

4.3 Bridge Description

The Chulitna River Bridge was built in 1970 on a 22-degree skew. It is 790-feet long with five spans of 100, 185, 220, 185, and 100 feet (Fig. 4.1). The superstructure was a 34-foot-wide by 6¾-inch-thick cast-in-place concrete deck supported by two exterior continuous longitudinal variable depth girders and three interior stringers. The girder stringers are spaced at 7 feet on center. The interior stringers are supported by cross frames that are carried by the exterior girders.

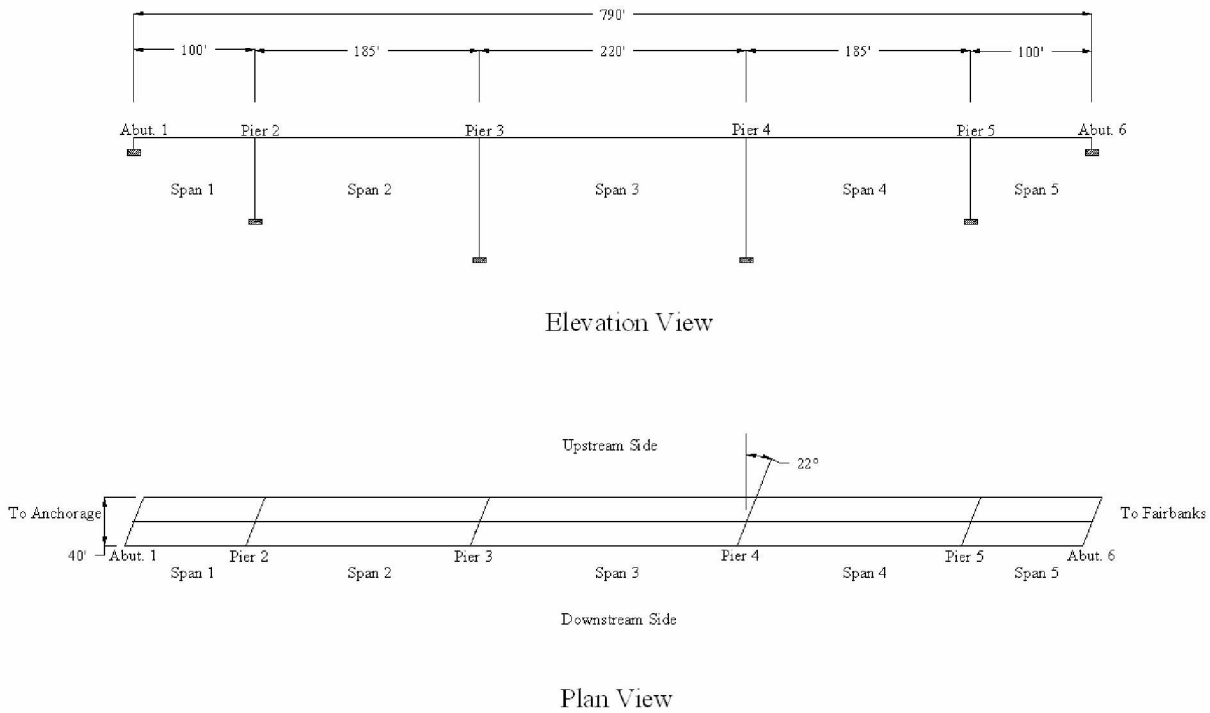

Figure 4.1: Elevation and Plan View of Chulitna River Bridge

In 1993, the bridge deck was widened and made of precast concrete deck panels. The increased load was accounted for by strengthening the variable depth exterior girders and converting the W21x44 interior stringers to an interior truss girder; the W21x44 stringer became the upper chord of the truss (Fig. 4.2).

Figure 4.2: Current Picture of the Chulitna River Bridge

4.4 Static and Dynamic Test

The research team developed a structural health monitoring system (SHMS) that could be used to monitor Alaska bridges, instrument the bridge, calibrate the system, and load test the structure. In addition to monitoring the bridge response to traffic, the research team was to develop and calibrate a FEM that would provide a reliable bridge behavioral response to traffic AASHTO loading and special permitted vehicles. The paper provides the experimental data obtained from two different field-evaluation systems: local and global.

Localized response data are obtained through the use fiber-optic sensors such as strain gauges, displacement sensors, tilt meters, etc. at specific locations. In an attempt to understand and evaluate the response of the Chulitna River Bridge to traffic loads. The global field monitoring is an ambient acceleration study that attempts to identify natural frequencies of the structure once it is excited.

Horizontal, vertical, and transverse frequencies were measured by 15 portable accelerometers distributed across the top deck of the structure.

There are various methods and sensors that may be used to evaluate the discrete locations (local-level monitoring) to evaluate long-term response of the structural elements. This may be accomplished by measuring at the discrete points, temperature, acceleration, strain, and deflection. Although there are various sensors available for measuring strains, etc., not all perform well over the long term. Thus, in this study, the researchers selected a Fiber-optic structural health monitoring system (Fig. 4.3) for the purpose of insuring that drift would be minimized over time.

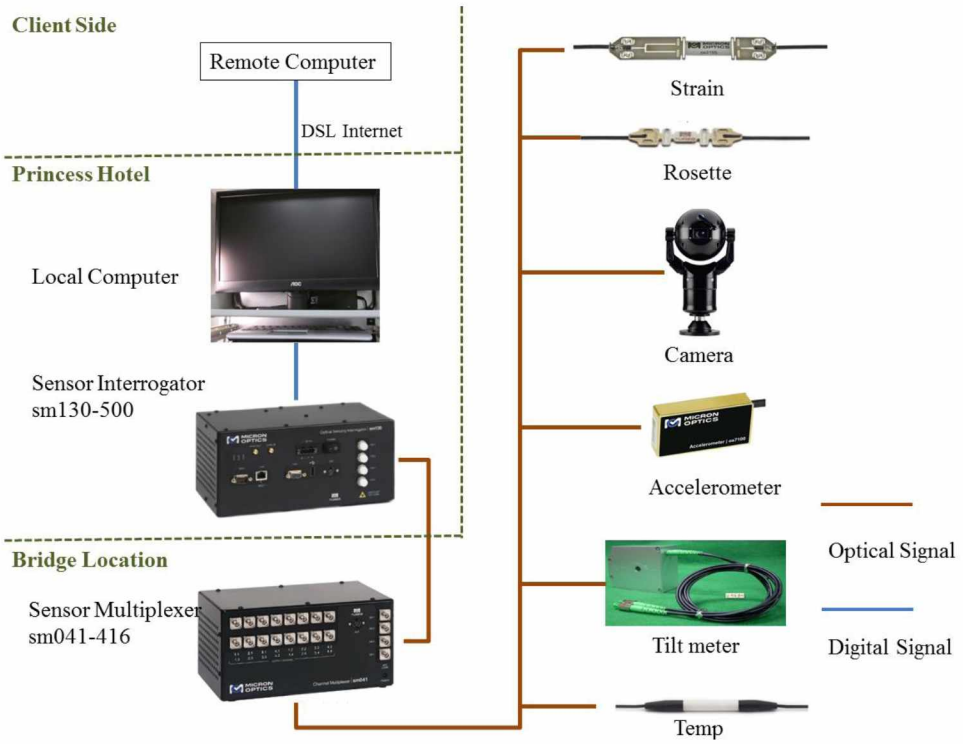

Figure 4.3: Fiber-Optic Structural Health Monitoring System

Fiber optic sensors have been shown to provide stable long-term real-time monitoring for bridge structures. In this research, the Chulitna River Bridge was instrumented to evaluate the local-level behavior. There are a total of 73 sensors (strain gages, accelerometers, temperature sensors, rosettes, and tilt meters) at locations that were selected to evaluate the local-level structural health of this structure. (Fig. 4.4) The long-term monitoring can indicate the change of local components with time.

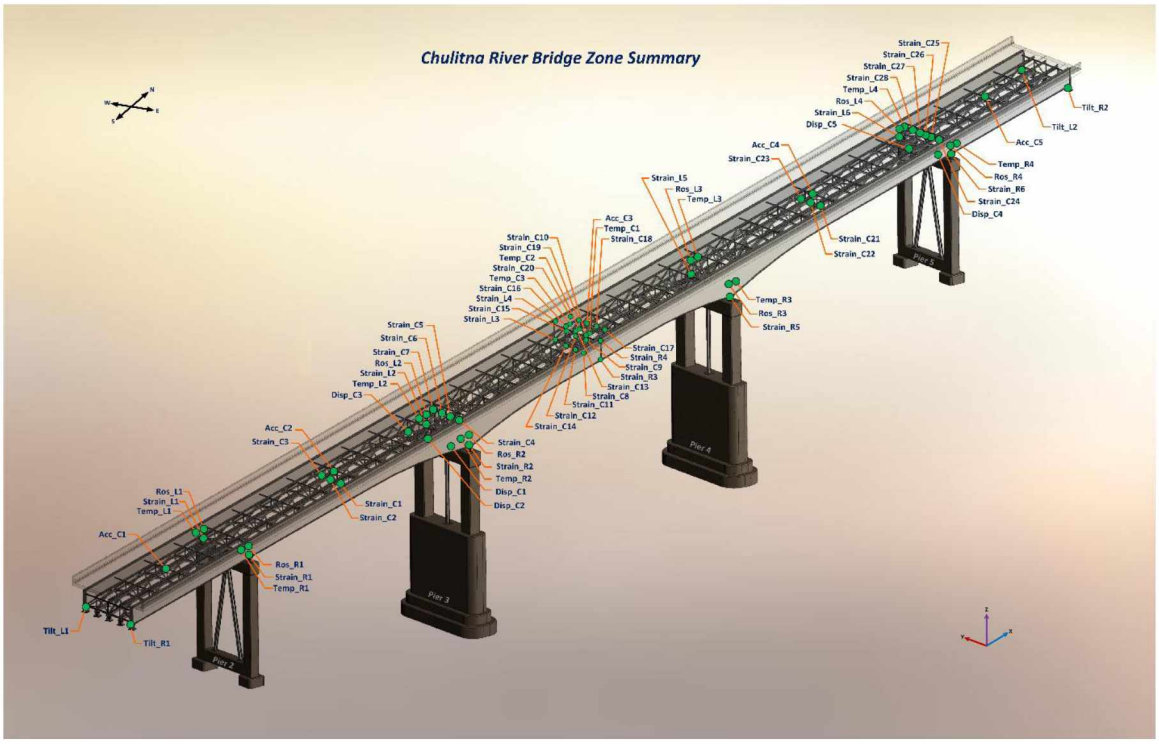

Figure 4.4: Bridge Health Monitoring System Sensor Summery

Consider a "Piezoelectric force" balanced portable data acquisition system, see Fig. 4.5. It is a movable system that enables the engineer to record accelerations at several places along the bridge. The data is digital format in this study and it was used to identify dynamic behavior at the global-

level. The recorded data was used to find natural frequencies, damping, mode shapes and identify possible nonlinear behavior. The resulting data is essential information for calibrating and updating the global-level performance of a virtual model of the bridge. In this study, the researcher has calibrated the virtual model using finite elements to approximate behavior of the structure.

Figure 4.5: Using Portable Data Acquisition System on the Chulitna River Bridge

Earlier research by the author has shown that the errors between natural frequencies' evaluated from field measurements versus those calculated using an initial finite element model of this bridge is up to 10% (Table 4.1), (Xiao et al., 2014). These results are a global-level comparison. However, a comparison between strain values evaluated using the field measured strains (using fiber optic sensors) and the initial finite element values at mid-span was in error by as much as 150% (Hulsey and Xiao, 2013).

4.5 Multi-direction Model Updating

In this research, an enhanced approach for updating the virtual bridge model was developed. The idea is that this model will represent the structural response when subjected to load conditions typically expected in the field. The virtual model (FEM) for this bridge will be calibrated to reduce errors in global-local evaluation so that the virtual model may more accurately be calibrated and updated and it accurately represents the behavior and condition of the structure. Combined the global and the local evaluation, it will introduce more variables to be adjusted and it will involve more objective functions to be solved. It is a challenge to make the objective functions coverage when there are a large number of variables. This section shows the multi-direction global-local model updating approach which can solve this problem and simply the model calibration for large complicated bridge structure.

4.5.1 Simple Accuracy Test

Before model changes were made, simple accuracy tests were performed on the bridge initial finite element model. That is, the number of elements (original mesh) was increased in an effort to evaluate the results for a newly refined mesh. This test was conducted to ensure that it would converge to provide a reasonable estimate of the structural response. The desired level of accuracy was set at 2%. Subsequently, the mesh size was reduced to half its current size to determine if the resulting displacements and forces would change significantly or if the change was small enough to be considered acceptable. Multiple locations on the bridge were checked. These locations were ones of critical interest to the project (i.e., high tension, large displacement, etc.). Nine sections were considered when checking the strains and stresses. These nine sections are located in different spans and sides of the bridge. Four longitudinal displacements on different sides of the abutments

were selected for checking. We refined the mesh for the FEM to half its current size in both lines and areas. In Table 4.1, the error shows the difference between the initial model and the refined model. This comparison is based on three trucks that were stopped and positioned so that the front axles were 369 feet from the south abutment (Abutment 1); the three trucks were in the middle of Span 3.

The locations that are presented in Table 4.1 are illustrated in Figure 4.6. Table 4.1 indicates that the error between the two models is low. Ignoring the sign, the largest error is 1.04%, which is within the acceptable the level of accuracy. In general, the fine mesh used in the initial model should give sufficiently accurate results.

Table 4.1: Simple Accuracy Comparison between the Initial and the Refined Model

	Locations		Number	Initial Model	Refined Model	Error (%)
Force (lbs)	Mid-Span 2 Lower Chord	East	1	-25,388	-25,476	-0.35
		Middle	2	-25,739	-25,858	-0.46
		West	3	-26,612	-26,673	-0.23
	Mid-Span 3 Lower Chord	East	4	80,867	81,199	-0.41
		Middle	5	83,554	83,893	-0.41
		West	6	81,238	81,584	-0.43
	Mid-Span 4 Lower Chord	East	7	-26,447	-26,562	-0.43
		Middle	8	-25,474	-25,624	-0.59
		West	9	-25,546	-25,625	-0.31
Displacement Long. Dir. (mm)	Abutment 1 Roller Support	East	10	-2.81	-2.84	-1.04
		West	11	-2.82	-2.84	-0.66
	Abutment 2 Roller Support	East	12	-2.21	-2.23	-0.92
		West	13	-2.21	-2.21	-0.12

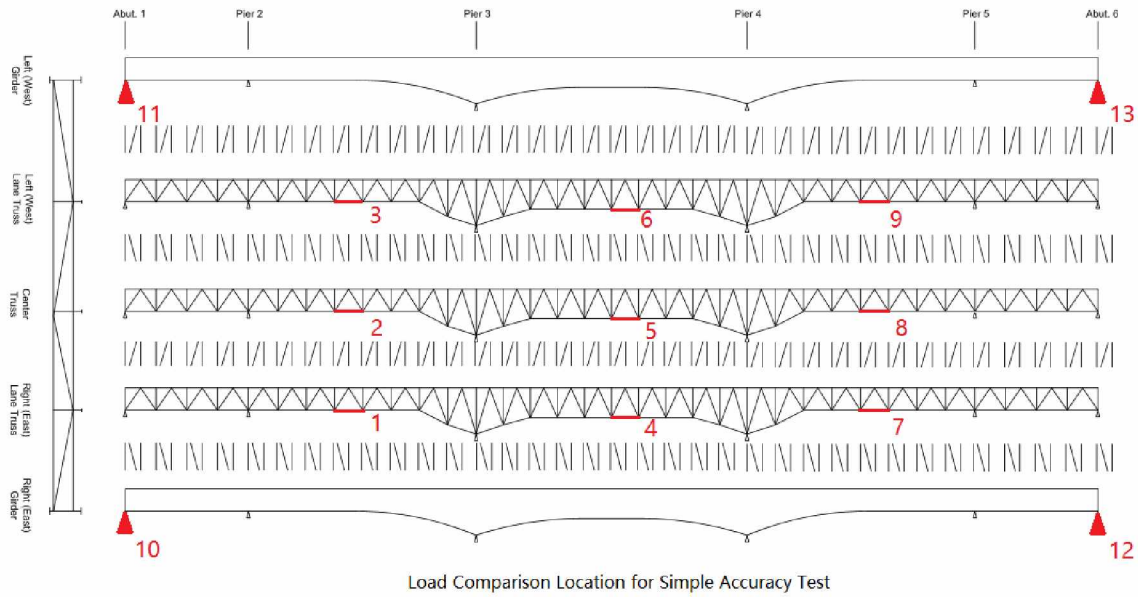

Figure 4.6: Locations Where the Influence of Mesh Refinement was Checked (see Table 4.1)

At this point, the results of this test simply prove that if this model represents the actual bridge structure, the model will provide sufficiently accurate strains, displacements, and forces for a given set of loads. The results of this test do not prove that the model represents the bridge structure that is being studied.

4.5.2 Group Directional Members and Select Objective Functions

The model updating was divided into two stages based on the longitudinal and the transversal directions. Girder, stringer, and concrete deck belong to the longitudinal member. The longitudinal objection function (J_1) is the difference between experimental data (Z_{e1}) and model analysis (Z_{m1}) in local-level longitudinal member and global-level natural frequencies. The number of selected variables is n_1.

$$J_1 = \sum_{i=1}^{n_1} \sqrt{\frac{(Z_{e1} - Z_{m1})^2}{{Z_{e1}}^2}} \tag{3.1}$$

The cross frames and roller supports are the transversal members. The objection function (J_2) is the difference between experimental data (Z_{e2}) and model analysis (Z_{m2}) in local-level transversal member and global-level natural frequencies. The number of variables is n_2.

$$J_2 = \sum_{i=1}^{n_2} \sqrt{\frac{(Z_{e2} - Z_{m2})^2}{{Z_{e2}}^2}} \tag{4.2}$$

In each model development stage, the direction members are changed in a reasonable range to make the objective functions converge. In order to show the overall behavior of model updating, the objective function (J) is the error between experimental data (Z_e) and model analysis (Z_m) in both longitudinal, transversal member and global natural frequencies. The number of variable is n which the sum of n1 and n2 is.

$$\mathrm{J} = \sum_{i=1}^{n} \sqrt{\frac{(Z_e - Z_m)^2}{{Z_e}^2}} \tag{4.3}$$

4.5.3 Bridge Longitudinal Direction Behavior

Thirteen fiber-optic strain sensors were installed in the middle of Span 3 longitudinal members including stringers and girder's flanges and lower chords (Figure 4.7). The strains in these sensors were used to evaluate the influence of the three ADOT&PF trucks driving side by side. Figures 4.8 show a comparison between stresses obtained from measured strain data and the "before

modification" original FEM calculated mid-span stresses. The results indicate that the FEM-calculated stresses carried by the composite trusses are higher than measured; that is, calculated lower chord stresses are higher than measured. This finding illustrates that the FEM does not properly represent the distribution of stiffness between the bridge composite stringers and the girders. In consideration of these problems, objective functions J_1 in longitudinal members were selected for the study. Modifications to the objective functions affected load distribution for the composite trusses and girders.

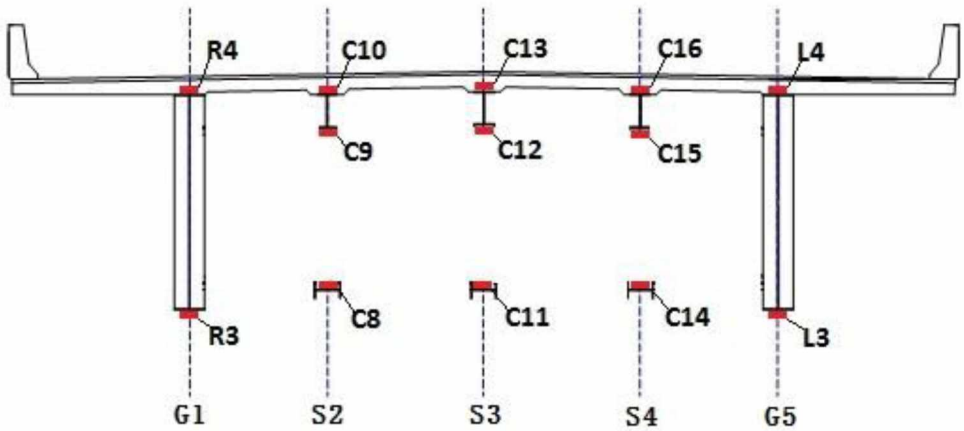

Figure 4.7: Strain Sensor at the Cross Section of Mid-span 3

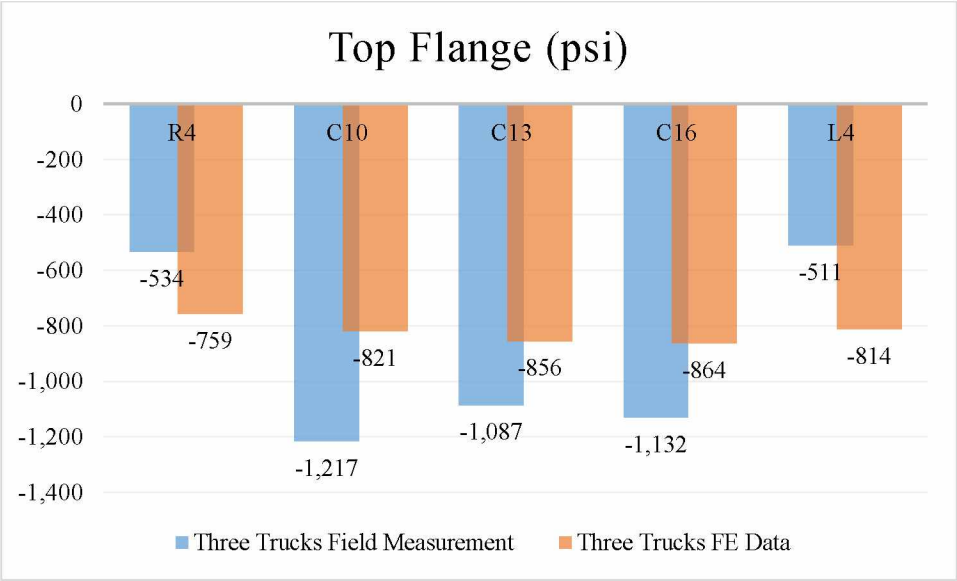

a. Top flange stress comparison between field measured and calculated values (psi)

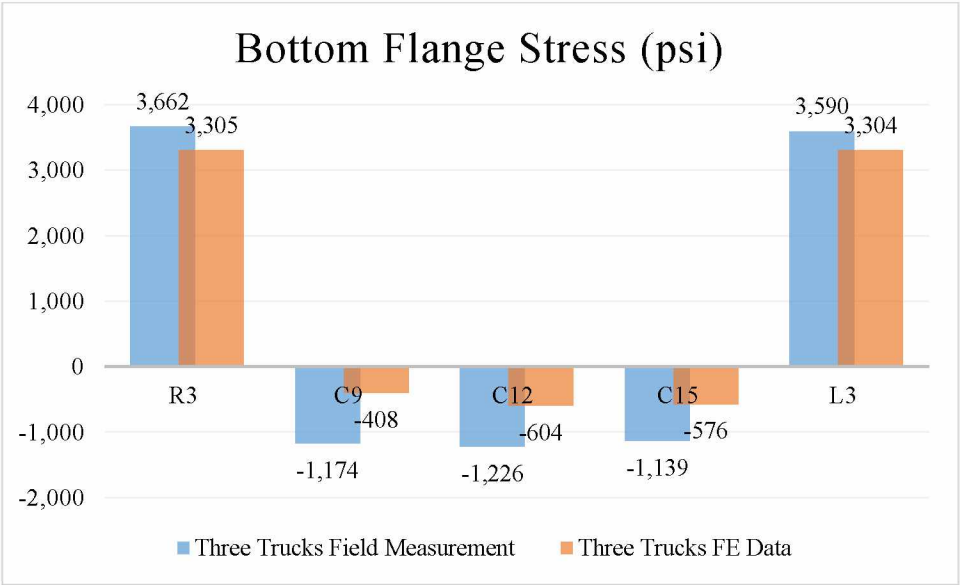

b. Bottom flange stress comparison between measured and calculated values (psi)

Figure 4.8: Stress Compression in Longitudinal Members before Modification

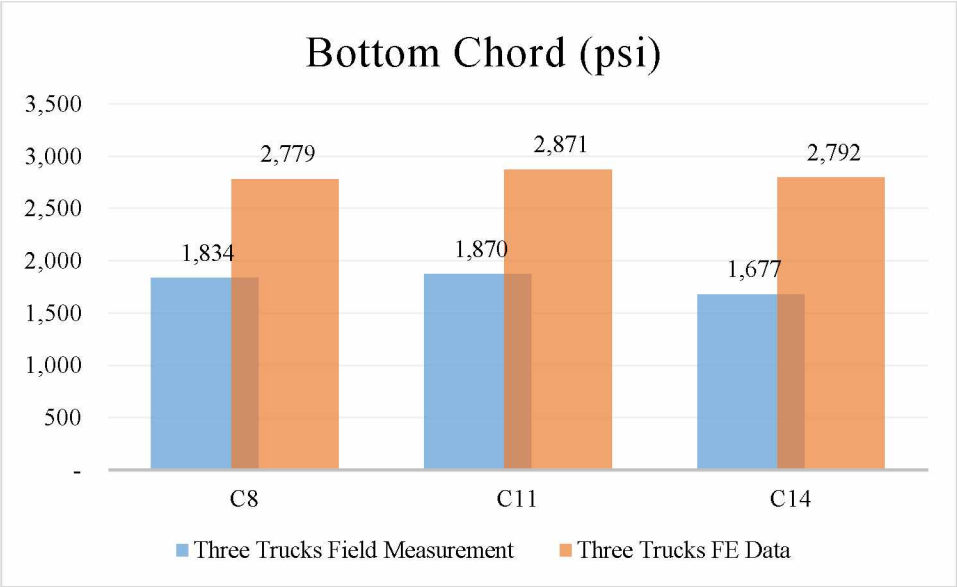

c. Lower chord stress comparison between measured and calculated values (psi)

Figure 4.8 Continued: Stress Compression in Longitudinal Members before Modification

4.5.4 Model Updating in Longitudinal Direction

Initially, we identified the members that were likely to affect structural response the most. In selecting objective functions for study, we adjusted member sectional data and member geometry to better reflect the 1993 as-is bridge condition. According to the longitudinal behavior described by the initial FEM, the largest error exists in a lower chord member. Modifications showed that if the cross-sectional area of the lower chord was reduced to 0.43, the resulting error in local strain dropped below 50%. This modification resulted in a change in behavior, and the largest error between measured and calculated stresses was now in the composite truss lower flange. We then investigated the bridge response to a change in stiffness for the concrete deck. Changing the elastic modulus of the concrete deck to 3,000 ksi improved structural response, and the error between the calculated and measured stresses were reduced to 5%. However, the difference between the global experimental frequency response and calculated values causes the percent error to increase to 15%.

The stiffness change went from too stiff to too flexible. In order to balance the difference in error between local and global values, the elastic modulus of the concrete deck was changed to 3,300 ksi and the stringer lower flange area was changed from 2.0 to 2.5. The change in the area represents the as-is bridge condition. Table 4.2 shows the influence of these modifications on structural response. Tables 4.3, 4.4, and 4.5 show the longitudinal difference between experimental and calculated stresses for both global and local values.

Ignoring signs, the largest error for the global values decreased from 10.2% to 8.8%, and the largest error for the local values decreased from 66.4% to 17.8% in the longitudinal direction.

Table 4.2: FEM Using Revised Variables

Bridge Sections	Locations	Property Modifiers	
Composite Trusses	3 Lower Chord	Area	0.43
Girders	2 Top Flange	Area	0.54
	2 Bottom Flange	Area	0.85
Stringer	3 Top Flange	Area	1.24
	2 Bottom Flange (No. 2,4)	Area	2.0
	Bottom Flange (No. 3)	Area	2.5
Concrete Deck	Throughout the deck	Elastic Modulus (ksi)	3,300

Table 4.3: Natural Frequency Differences after Model Revisions for Longitudinal Behavior

Mode	Field Measurement (Hz)	Long. Updated FEM (Hz)	Difference (%)
Longitudinal Mode 1	1.500	1.368	8.8
Longitudinal Mode 2	2.190	2.036	7.0
Vertical Mode 1	2.846	2.773	2.6
Vertical Mode 2	3.224	3.196	0.9
Vertical Mode 3	4.580	4.271	6.8
Transverse Mode 1	2.095	2.168	-3.5
Transverse Mode 2	2.346	2.325	0.9
Transverse Mode 3	2.782	2.683	3.6

Table 4.4: Difference in Flange Stress (%) after Model Revisions for Longitudinal Behavior

Location		G1	S2	S3	S4	G5
Sensor Number		R4	C9	C12	C15	L4
Top Flange	Field Measurement	-12.4	-12.0	-17.8	-17.4	-12.0
	FE Data					
Sensor Number		R3	C8	C11	C14	L3
Bottom Flange	Field Measurement	-6.7	1.2	11.7	5.7	-9.9
	FE Data					

Table 4.5: Difference in Lower Chord Stress (%) after Model Revisions for Longitudinal Behavior

Location		S2	S3	S4
Sensor Number		C8	C11	C14
Lower Chord	Field Measurement	-3.8	-6.8	-14.0
	FE Data			

4.5.5 Bridge Transversal Direction Behavior

The stiffness of the cross frame and the condition of the supports determined load distribution in the transversal direction. In the investigation by HDR, Inc., five roller bearings did not fully connect with the superstructure (Figure 4.9), and original model removed those supports (HDR, 2011).

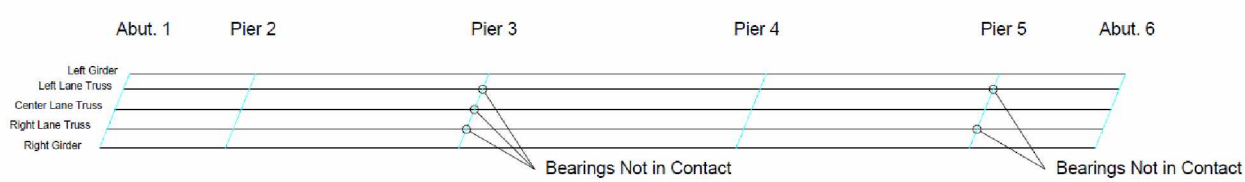

Figure 4.9: Plan View: Bearings that are Not Contact with Masonry Plates

In Fiber Optic SHMS, there are five displacement sensors are placed at those locations to measure the movement of the roller bearings in the vertical direction. In addition, we installed eight strain sensors in diagonal members in cross section of pier 3 (Fig. 4.10) and pier 5 (Fig. 4.11) to measure the reaction of the supports and the stresses in the cross frames.

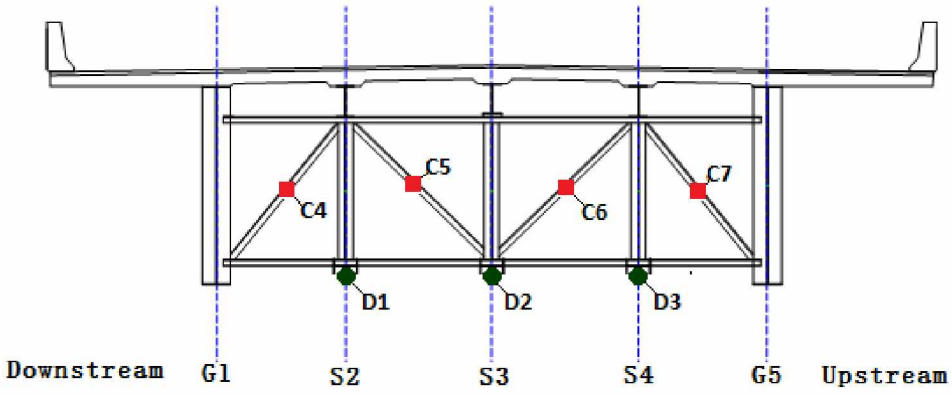

Figure 4.10: Strain Sensor (Red) and Displacement Sensor (Green) at the Cross Section of Pier 3

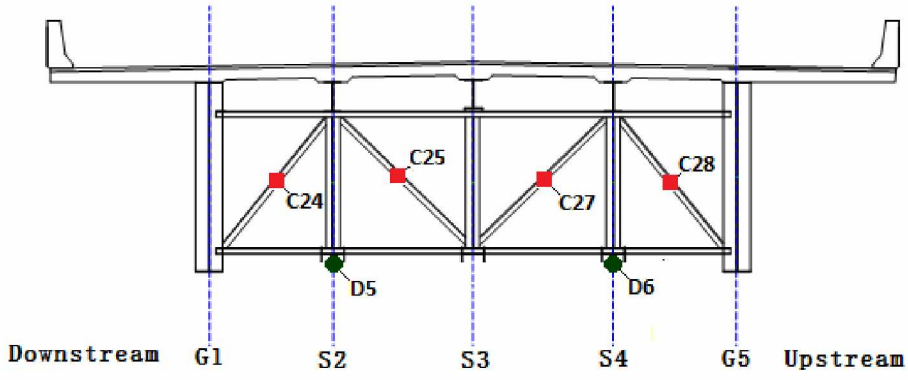

Figure 4.11: Strain Sensor (Red) and Displacement Sensor (Green) at the Cross Section of Pier 5

The load test cases conducted on September 10, 2012, three heavily loaded trucks traveling side by side crossed the bridge at low speed. The vertical movement of the five displacement sensors is shown in Figure 4.12 a–e. These graphs illustrate the response for an average of 50 data points over time for each of the five bearing locations.

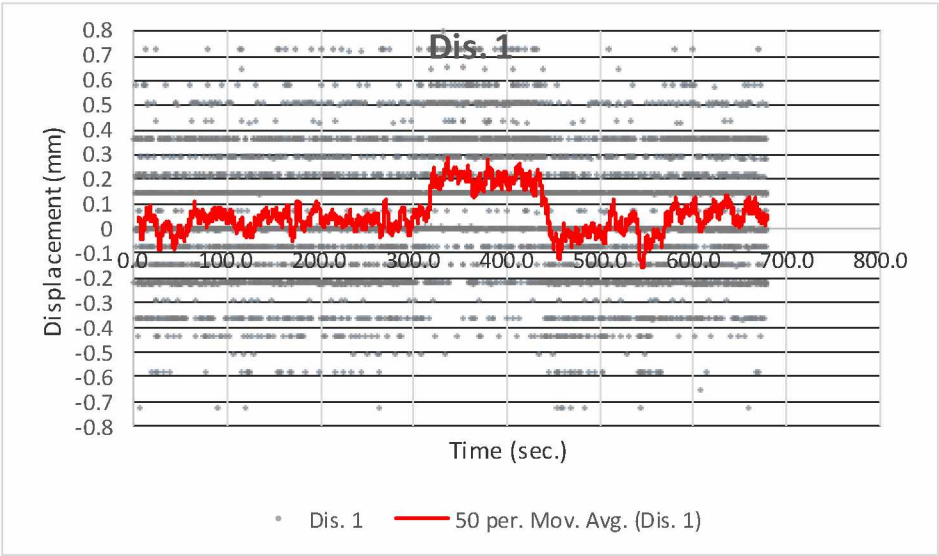

a. Vertical movement at displacement sensor 1

Figure 4.12: Vertical Movement at 5 Unconnected Bearing Supports

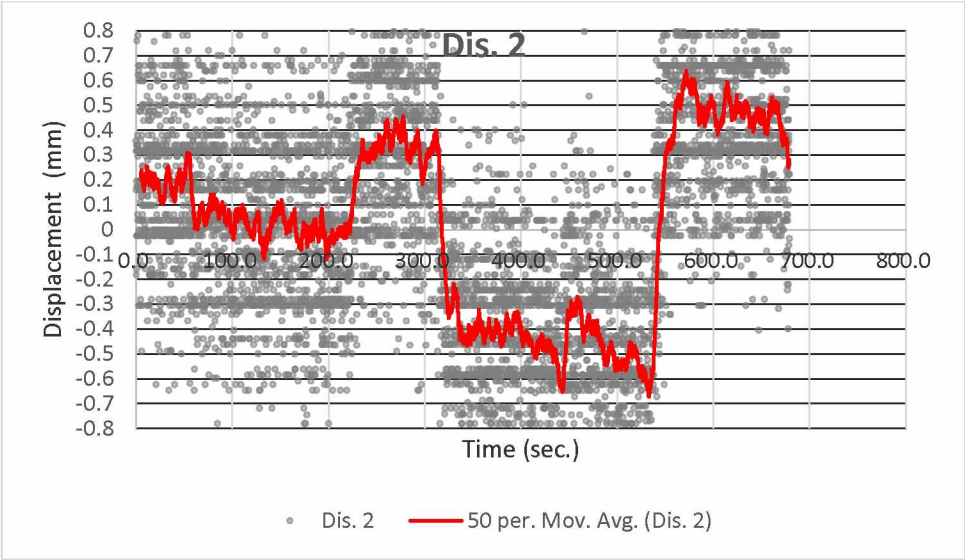

b. Vertical movement at displacement sensor 2

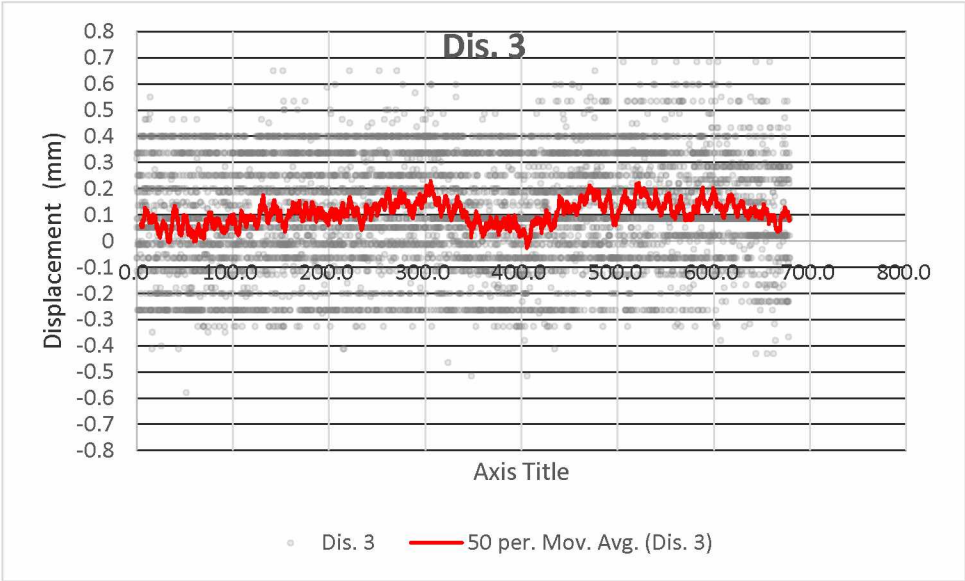

c. Vertical movement at displacement sensor 3

Figure 4.12 Continued: Vertical Movement at 5 Unconnected Bearing Supports

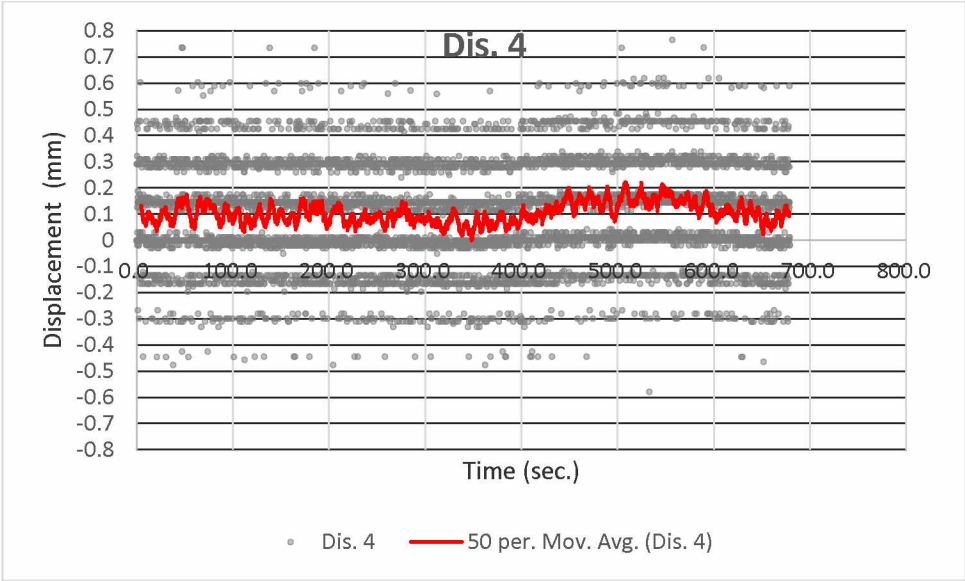

d. Vertical movement at displacement sensor 4

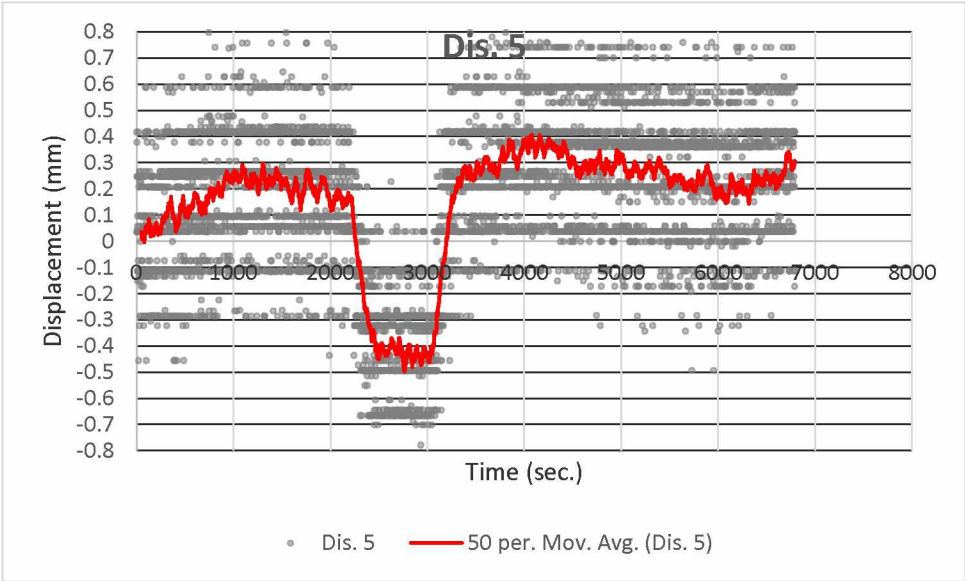

e. Vertical movement at displacement sensor 5

Figure 4.12 Continued: Vertical Movement at 5 Unconnected Bearing Supports

According to the displacement sensor results, roller bearings 1, 3, and 4 have limited movement in the vertical direction. When compared with the other roller bearings, bearings 2 and 5 are more flexible in the vertical direction than the others are.

In order to evaluate the distribution of reaction forces for a given load, eight strain sensors were installed on the cross frame at the five unconnected roller support locations (Figure 4.10, 4.11). Tables 4.6 and 4.7 and Figures 4.13 show the stress results of measured and FEM stress before the model was updated. Table 4.6 and Figure 4.13 (a) shows the stress results when two parallel trucks stop above Pier 3. Table 4.7 and Figure 4.13 (b) shows stress results when two parallel trucks stop over Pier 5.

Table 4.6: Two Trucks at Pier 3, before Transverse Modifications

Location	C7	C6	C5	C4
Measured Stress (psi)	-2,237	1,127	1,726	-2,021
HDR FEM Stress (psi)	-2,963	1,482	1,466	-2,898
Error (%)	-32.4	-31.5	15.1	-43.4

Table 4.7: Two Trucks at Pier 5 Stress Results before Transverse Updating

Location	C28	C27	C25	C24
Measured Stress (psi)	-2,171	-2,058	-376	-1,172
HDR FEM Stress (psi)	-2,184	-2,366	-2,305	-2,261
Error (%)	-0.6	-15.0	-512.3	-92.9

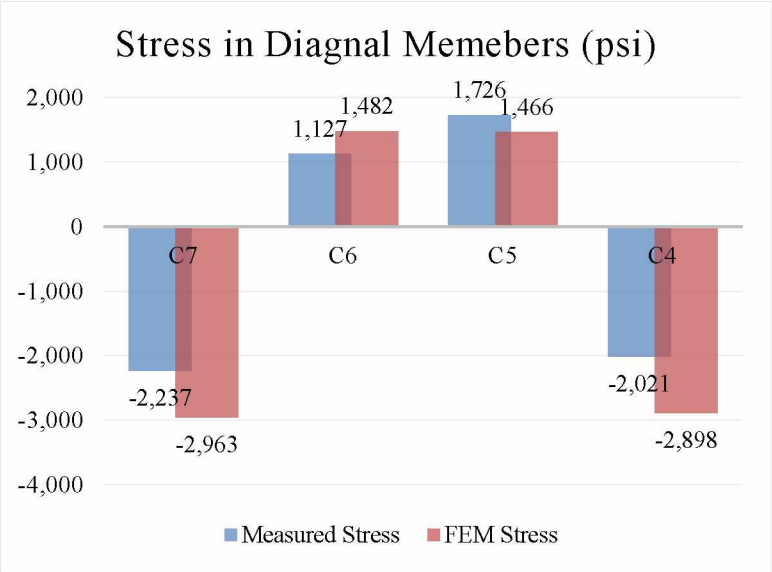

a. Two trucks at Pier 3 stress results before FEM transverse modifications

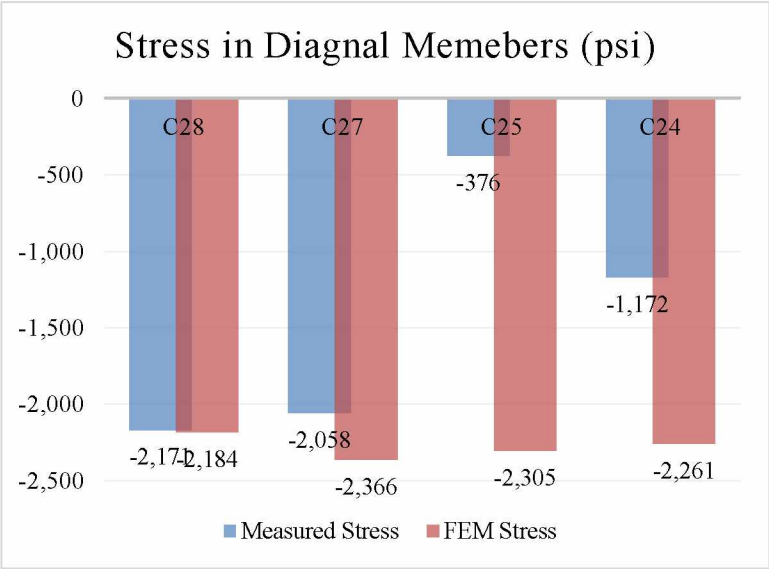

b. Two trucks at Pier 5 stress results before transverse updating

Figure 4.13: Stress Comparison in Cross-Frames before Model updating in Transversal Direction

4.5.6 Model Updating in Transversal Direction

Figures 4.13 shows for the 2012 load tests that large errors exist between measured and calculated stresses in the cross frame. At Pier 3, the largest error is -43.4% in the cross frame. At Pier 5, the largest error was -512.3%. Figure 4.12 indicates that bearings 1, 3, and 4 have limited movement. So the cross frame section may work as a semi-rigid support at those locations. As part of the model modifications, three spring supports were added at those locations. In order to reduce errors in the objective functions, we modified the support spring stiffness and sectional properties of the cross frame to more closely represent bridge as-is condition. Vertical spring support stiffness at locations 1, 3 and 4 are 1,200 kip/inch, 100 kip/inch, and 40,000 kip/inch, respectively. The cross frame truss section area was decreased to 0.8. The results for the modified FEM are shown in Tables 4.8 and 4.9 and Figures 4.14.

Table 4.8: Two Trucks at Pier 3 Stress Results after Model Modifications (psi)

	C7	C6	C5	C4
Measured Stress (psi)	-2,237	1,127	1,726	-2,021
FEM Stress (psi)	-2,419	1,002	1,560	-2,106
Error (%)	-8.1	11.1	9.6	-4.2

Table 4.9: Two Trucks at Pier 5 Stress Results after Model Modifications (psi)

	C28	C27	C25	C24
Measured Stress (psi)	-2,171	-2,058	-376	-1,172
FEM Stress (psi)	-1,8301	-1,0813	-2,027	-946
Error (%)	11.3	-17.0	-19.9	19.3

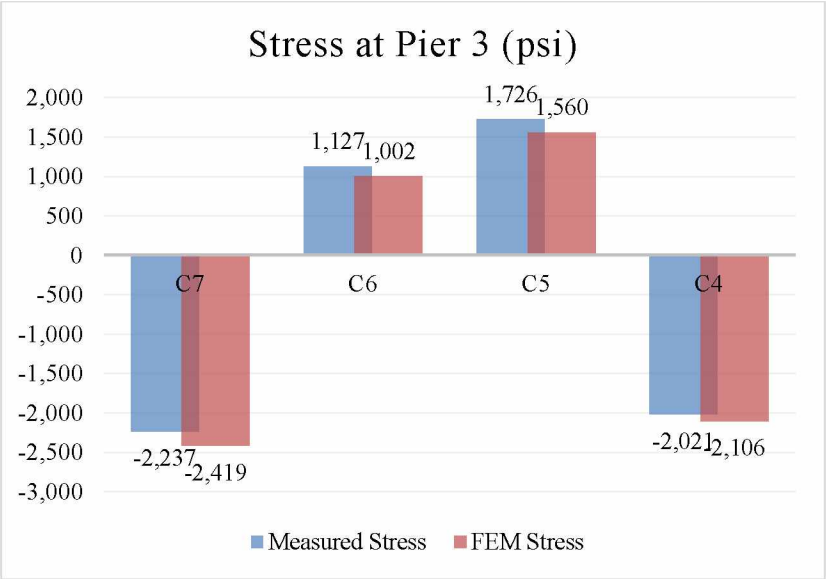

a: Two trucks at Pier 3 stress results after model modifications

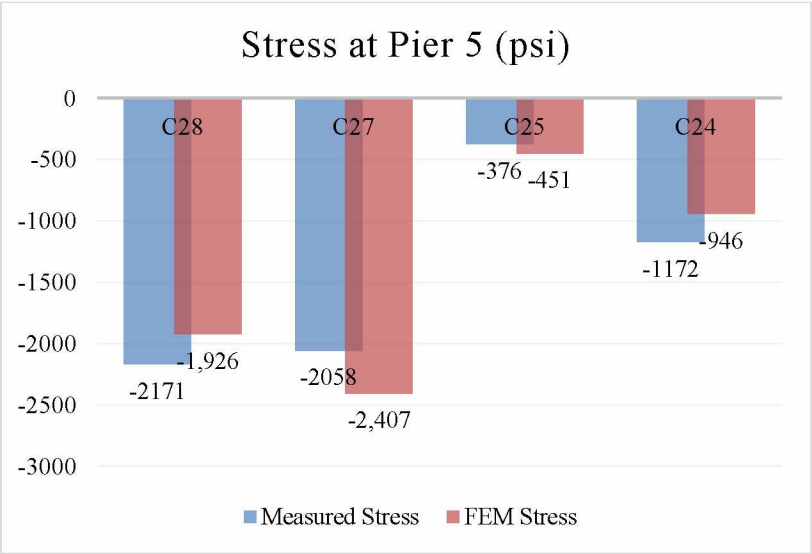

b. Two trucks at Pier 5 stress results after model modifications

Figure 4.14: Stress Comparison in Cross-Frames after Model Updating in Transversal Direction

Following modification of the model, the largest error in the transversal direction decreased from -512.3% to -19.9%. Initially, five support bearings did not support the bridge (i.e., the

superstructure was not in contact with the bearings). After the model was modified, we simulated the bridge response with two bearings (Bearings 2 and 4) that were not in contact with the structure. At the other three bearing locations, the superstructure is modeled with vertical springs between the bearing support and the structure. The cross frames were found to be too stiff compared with the bridge as-is condition.

After the FEM was modified to more accurately represent the transverse behavior of the bridge, a comparison between experimental and calculated stresses was made for the various load tests that were run on September 10, 2012. For example, Tables 4.10 and 4.11 show the difference in stresses between experimental and modified finite element values for the middle of the Span 3 girder flanges and the difference in stresses in the lower chord of the cross frame. These stresses are from a static load test in which three trucks side-by-side were on the bridge mid-span 3 (see Figure 4.15). The tables 4.10 and 4.11 show that the stiffness of the three spring supports and the cross frame had limited influence on the longitudinal distribution of load.

Table 4.10: Percent Difference between FEM and Experimental Flange Stresses Mid-Span 3

Location		G1	S2	S3	S4	G5
Sensor Number		R4	C9	C12	C15	L4
Top Flange	Field Measurement / FE Data	-13.10	-13.50	-16.48	-17.69	-9.19
Sensor Number		R3	C8	C11	C14	L3
Bottom Flange	Field Measurement / FE Data	-6.58	0.71	5.43	4.26	-8.64

Table 4.11: Percent Difference between FEM and Experimental Lower Chord Stresses Mid-Span 3

Location		S2	S3	S4
Sensor Number		C8	C11	C14
Lower Chord	Field Measurement / FE Data	-2.77	-5.24	-12.67

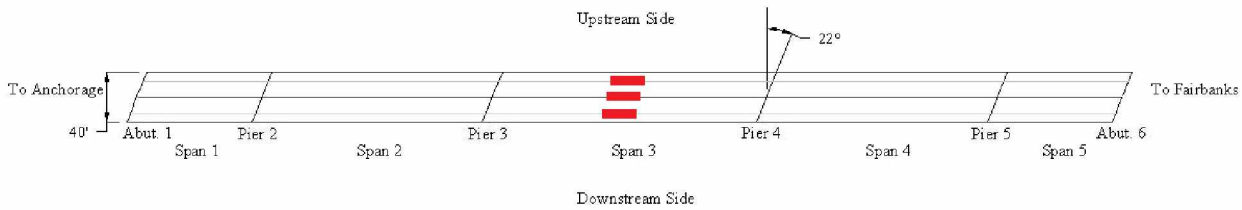

Figure 4.15: Three Trucks Positioned on Span 3, Southbound

The FEM that resulted from modifications to better predict transverse response was evaluated for both local and global data. Using the improved model, global natural frequencies were calculated and compared with those that were measured with the portable accelerometers. Natural frequencies were calculated in three directions (vertical, longitudinal, transverse) and compared with the measured values (Table 4.12). The largest error was 8.9% for the first mode in the longitudinal direction. Based on a comparison between test data and calculated values, it is clear that the modified FEM is sufficiently accurate.

Table 4.12: Year 2012 Natural Frequency Difference; Calibrated FEM

Mode	Field Measured (Hz)	FEM Results (Hz)	Difference (%)
Longitudinal Mode 1	1.500	1.367	8.9
Longitudinal Mode 2	2.190	2.044	6.7
Vertical Mode 1	2.846	2.756	3.2
Vertical Mode 2	3.224	3.348	-3.8
Vertical Mode 3	4.586	4.249	7.3
Transverse Mode 1	2.095	2.269	-8.3
Transverse Mode 2	2.346	2.542	-8.4
Transverse Mode 3	2.782	2.788	-0.2

4.5.7 Updated Finite Element Model

A simple accuracy test was conducted to refine the mesh to ensure that it converged to a reasonable estimation of the response. The simple accuracy test results showed that the original FEM had a mesh size that would provide an acceptable level of accuracy.

Next, we calibrated the FEM against structural response, which was done by modifying elements and structural properties to more accurately describe the as-is bridge structure. The modification process was divided into two stages: one is model updating in the longitudinal direction and another is in the transversal direction. In each stage, the accuracy of the modified FEM was checked against structural response as measured by the sensors at the local level in its direction (the structural health monitoring system) and global level frequency response as measured with 15 portable accelerometers placed on the bridge deck. Finally, to check the multi-direction updated FEM's accuracy was in the acceptable limit by using load test data (Fig. 4.16).

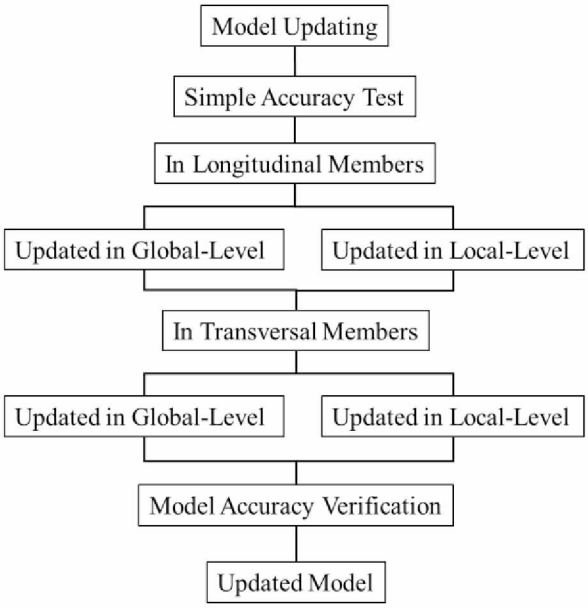

Figure 4.16: Multi-direction Model Updating Flowchart

Longitudinal members such as the girder flanges, stringer flanges, composite truss lower-chord cross area, and elastic modulus of the concrete deck were selected for study to determine if these items were accurately describing the as-is bridge structure. On September 10, 2012, three ADOT&PF dump trucks were used to load test the bridge. Static and dynamic strains, tilts, and displacements were measured for seventeen different combinations of truck positions. The measured local response data caused by these different load tests were compared with the FEM results; the differences between experimental and calculated data are the longitudinal objective functions. Longitudinal variables were selected and adjusted to match construction drawings so that response was within a reasonable range.

The purpose was to reduce the number of objective functions and variables. In addition to verifying that calculated local strains were sufficiently accurate, we checked calculated global (vertical, longitudinal, transverse) natural frequencies against measured values. This check ensured that element and material property corrections for the model would result in convergence between measured and calculated in global-level.

In the transverse direction, the unconnected roller bearings and cross frames were selected for the study. The transverse behavior was studied by evaluating load test response when two trucks were stopped at two critical cross sections. The difference between measured local strain values and calculated were evaluated and compared. The model was reviewed and modified to describe the as-is bridge condition. This process was continued until the model accurately described the behavior and the calculated values correlated well with the experimental values in multi-level.

After model modifications, both local and global values resulted in lower errors between measured and calculated. The longitudinal J_1, transversal J_2, and multi-direction objective functions show in Figure 4.17. Model updating in the longitudinal direction has limited influence

on the transversal member. According to the Figure 4.17, the longitudinal objective function enhanced 99% after updated in the longitudinal direction, however, transversal objective function only increased 1%. On the other hand, updating in transversal direction can result in 97% changed in transversal objective function, but only enhanced 3% in the longitudinal direction. This results firmly proved that the steel girder bridge model updated in one direction have limited influence on other direction and only updating steel girder bridge in longitudinal member couldn't get accurate bridge finite element model.

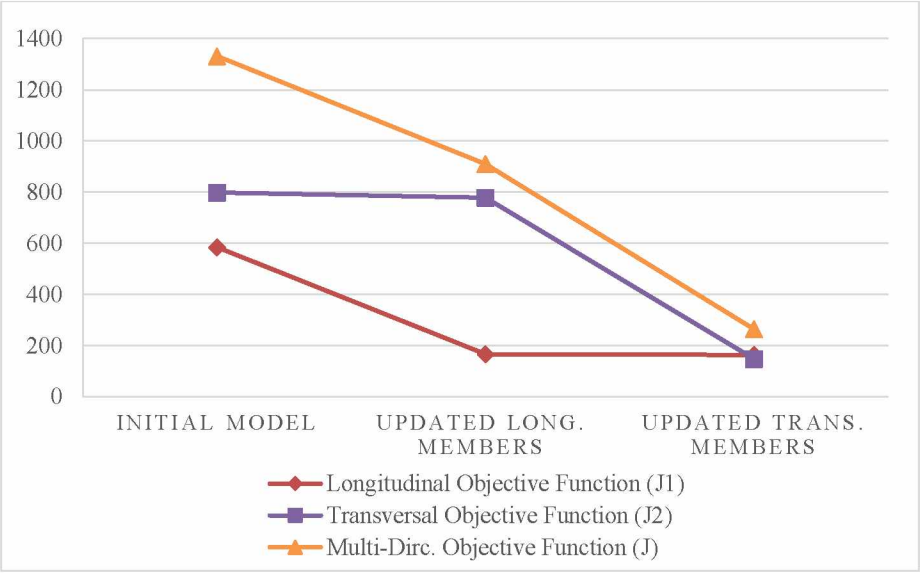

Figure 4.17: Objective with Model Development

For local values, the largest error decreased from -512.3% to -19.9%. For global values, the largest error decreased from -10.2% to 8.9%. The modified or refined (calibrated) FEM now provides calculated values with an accuracy that is within acceptable limits for both local and global values.

4.6 Conclusions

This research established a fiber optic structural health monitoring system for the Chulitna River Bridge. The system indicates the real-time local behavior of bridge. The ambient test identified the bridge global response. Combining the local-global test data to update bridge finite element model can eliminate the weakness of only rely on one type of test results to update the model. Multi-direction model updating approach separates the model updating into several stage which will help to reduce the number of objective functions and variables and make the function easy to coverage. From the updating results, this study shows only updating longitudinal members, such as girders, stringers and deck have a limited enhancement in the overall accuracy of the model. The updating uni-direction have every low influence on the accuracy of other directions. The overall accuracy is contributed by both longitudinal members and transversal members. It is necessary for steel girder bridge to be updated in the multi-direction.

4.7 References

Bedon, C., Morassi, A., (2014), Dynamic Testing a Parameter Identification of a base-isolated bridge, Engineering Structures 60 85-99.

Caglayan, O., Ozakgul, K., Tezer, O., (2012), Assessment of Existing Steel Railway Bridges", Journal of Constructional Steel Research 69 54-63.

Dan, D.H., Yang, T., Gong, J.X., (2014), Intelligent Platform for Model Updating in a Structural Health Monitoring System, Mathematical Problems in Engineering, Article ID 628619, 11 Pages.

Goulet, J. A., Michel, C., Smith, I.F.C., (2013), Hybrid probabilities and error-domain structural identification using ambient vibration monitoring, Mechanical Systems and Signal Processing 37 199-212.

HDR, Inc., (2011), Load Rating and Structural Assessment Load Rating Report – Bridge No. 255: Chulitna River Bridge.

Hulsey, J. L., Xiao, F., (2013), Structural Health Monitoring and Condition Assessment of Chulitna River Bridge: Mid-Span Loading Report, Alaska Department of Transportation Research, Development, and Technology Transfer, report, Fairbanks, Alaska.

Jung, D.S., Kim, C.Y., (2013), Finite Element Model Updating of a Simply Supported Skewed PSC I-girder Bridge Using Hybrid Genetic Algorithm, KSCE Journal of Civil Engineering 17(3):518-529.

Liu, Y., Li, Y., Wang, D.J., Zhang, S.Y., (2014), Model Updating of Complex Structures Using the Combination of Component Mode Synthesis and Kriging Predictor, The Scientific Word Journal, Article ID 476219, 13 pages.

Perea, R., Marin, R., Ruiz, A., (2013), Static-dynamic Multi-scale Structural Damage Identification in a Multi-objective Framework, Journal of Sound and Vibration 332 1484-1500.

Sanayei, M. Phelps, J.E., Sipple, J.D., Bell, E.S., Brenner, B.R., (2012), Instrumentation, Nondestructive Testing, and Finite-Element Model Updating for Bridge Evaluation Using Strain Measurements, Journal of Bridge Engineering ASCE, January/February.

Schlun, H. Plos, M., Gylltoft, K., (2009), Improved Bridge Evaluation through Finite Element Model Updating Using Static and Dynmic Measurements, Engineering Structures 31 1477-1485.

Xiao, F., Chen, G.S., Hulsey, J.L., (2014), Experimental Investigation of a Bridge under Traffic Loadings, Advanced Materials Research Vols. 875-877 pp 1989-1993.

Chapter 5 Optimal Static Strain Sensor Placement for Bridge Model Parameter Identification by using Numerical Optimization Method[4]

5.1 Abstract

A method to identify optimal strain sensor placement for examining structural response is presented. Based on applied static forces, and optimal placement to obtain measured strains enables the structural stiffness parameters can be identified. Change in a cross sectional area can be determined and used to minimize the difference between analytical and measured strains. These strain differences are evaluated by comparing measured with numerical. This approach (method) is used to identify the optimize sensor placement. The objective of this research is to identify the minimum number of static strain sensors and the optimal sensor layout needed to conduct a parameter model identification. This research includes automatic model parameter identification, optimal static strain sensor placement, damage detection, and method's application for a real bridge. Four numerical examples, including three trusses and the Klehini River Bridge are presented and the element stiffness is successfully and accurately evaluated by using the derived optimal sensor placement method.

Keyword: Optimal strain sensor, Model parameter identification, Numerical optimization, Bridge health monitoring, Damage detection, Static measurement

[4] This chapter will be submitted for publication as Xiao, F., Hulsey, J. L., Chen, S. G., Optimal Static Strain Sensor Placement for Bridge Model Parameter Identification by using Numerical Optimization Method.

5.2 Introduction

In Structural Health Monitoring, the engineer installs various kind of sensors in order to establish a real-time monitoring system for structural safety evaluation (Xiao et al., 2014; Xiao, 2015; Xiao et al., 2016). In order to evaluate the structure safety behavior, a numerical model needs to describe the "as-is" condition of the structure. The numerical model is prepared from the as-built construction drawings which present as "as-built" condition. It is expected that this model may not be used to accurately describe structural response for various loads as the structural properties will likely change with time. Subsequently, the "as-built" model needs to be updated according to measurement results.

There are two kinds of model updating methods to define an error function, and assess the quality of a match between the analytical and measured data. These are: a) manual model updating or b) using optimization techniques. A bridge model can be updated manually by using static loading based on measurement strain gage data (Sanayei et al., 2012). Multi-direction model updating (Xiao et al., 2015) was used to update the bridge model manually according to structural member's direction. The optimization algorithm is the technique to minimize the difference between analytical and measured data (Xu and Xiao, 2011). The Newton method can identify the change of structural cross section area for a simple structure (Sanayei and Saletnik, 1994) and lab test (Sanayei et al., 1997). Nelder-Mead simplex algorithm can also update the bridge successful by using measured static and dynamic measurements when using gradient based optimization algorithms has convergence problems (Schlune et al., 2009).

This research paper presented several examples that can be used for updating the structural response using numerical optimization method and the models have been updated automatically by using Newton Method and Steepest Descent Method (Nocedal and Wright, 2006). Sensors are

located on each truss member to measure strain. Numerical models are based on "as-built" conditions to examine the behavior. The cross sectional areas are selected as variables to be updated, because the most obvious problem for steel structures is the members' cross sectional areas that may be reduced because of corrosion and/or collision. The updated analytical strain results converge with the strain measurements. After using a sequence of search steps, the damaged cross section of each truss has been determined.

An objective function is used to measure the quality of a match between the analytical and measured data. A practical question that naturally arises is how to select a set with a minimum number of sensor locations from all possibilities, and the data collected can provide adequate information for the identification of the structural behavior by using numerical optimization method (Yi et al., 2012). Reducing the number of sensors will not only reduce the cost of equipment, but also saves installation time. Sensor layout optimization is essential for structural health monitoring. The sensor's number and location should be optimized when planning a Structural Health Monitoring system. A new sensor optimization method is presented in this study in order to assist the engineer to evaluate where and how many sensors should be used to evaluate the structural response. In previous research, the optimal dynamic sensor placement has been studied based on several kinds of bridges, and buildings by using dynamic measurement (You et al., 2013; Yi et al., 2011; Chang and Pakzad, 2014; Castro et al., 2013). However, there is few of study research on the static sensor placement optimization based on static measurement. This research established the optimal strain sensor placement method which including the study optimal strain sensor number and layout for model updating, damage detection based on the static measurement, and application in large-scale structure.

This study also established a method provide model updating for a large-scale problems. For a

large-scale complicated structure, whose finite element model may have thousands, tens of thousands, and even hundreds of thousands of DOFs., an exhaustive search would be extremely time consuming or even nearly impossible. Thus, a systematic and efficient approach is needed to solve such a computationally demanding problem (Yi et al., 2012). This study applied a numerical optimization method for damage identification for Klehini River Bridge (Xiao et al., 2015), this was done by using displacement sensor data to separate the large-scale problem into segments.

This study presented a new method to design a static strain sensor layout for automatically model updating, and it successfully was applied for a large-scale structure. By using the recommended numerical method to optimize the number of sensors and their layout during the planning stage in developing a structural health monitoring system; equipment costs and the labor costs related to the installation can be reduced. This application can solve the problem to use a limited number of static sensors to evaluate the large-scale bridge safety condition.

5.3 Numerical Optimization Method for Model Parameter Identification

5.3.1 Two Member Truss

Consider a two-dimensional two member truss (Figure 5.1). The objective is to present a method for modeling parametric identification using static strains. An example load of 2 kips was applied at location 2 in the downward direction. Initially, an x, y global coordinate system is established for the problem. Each member are defined by an arbitrary local coordinate system (an x-direction establishes the direction of the system forces for each member). Each joint will have two degrees of freedom (X, Y) in global coordinates. Using a numbering system for describing the appropriate degrees of freedom, the global stiffness of the structure was assembled, solved for joint displacements followed by member strains and stresses.

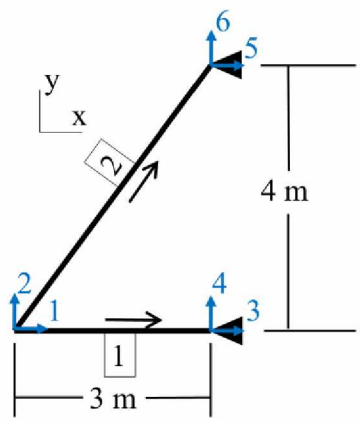

Figure 5.1: Two-member Truss with Notation

5.3.2 Structure Stiffness Matrix

The overall global structural stiffness matrix was assembled using the global stiffness matrices of each member (Hibbeler, 2009). This matrix has an order of 6×6; there are six designated degrees of freedom for the truss. E is the elastic modulus. A_1 is the cross section of member 1. A_2 is the cross section of member 2. Then equation 5.1 show as follows,

$$K = E \times \begin{bmatrix} 0.333\times A_1 + 0.072\times A_2 & 0.096\times A_2 & -0.333\times A_1 & 0 & -0.072\times A_2 & -0.096\times A_2 \\ 0.096\times A_2 & 0.128\times A_2 & 0 & 0 & -0.096\times A_2 & -0.128\times A_2 \\ -0.333\times A_1 & 0 & 0.333\times A_1 & 0 & 0 & 0 \\ 0 & 0 & 0 & 0 & 0 & 0 \\ -0.072\times A_2 & -0.096\times A_2 & 0 & 0 & 0.072\times A_2 & 0.096\times A_2 \\ -0.096\times A_2 & -0.128\times A_2 & 0 & 0 & 0.096\times A_2 & 0.128\times A_2 \end{bmatrix}$$

5.3.3 Displacement and Loads

From the problem, establish the displacement vector, D and the vector of external loads force, Q.

$$Q = \begin{bmatrix} 0 \\ -2 \\ Q_3 \\ Q_4 \\ Q_5 \\ Q_6 \end{bmatrix} \qquad D = \begin{bmatrix} D_1 \\ D_2 \\ 0 \\ 0 \\ 0 \\ 0 \end{bmatrix} \tag{5.2}$$

Q_3 to Q_6 are the unknown external force, D_1 and D_2 is the unknown displacements. According to Q = KD, for the truss, we have equation 5.3 show as follows,

$$\begin{bmatrix} 0 \\ -2 \\ Q_3 \\ Q_4 \\ Q_5 \\ Q_6 \end{bmatrix} = E \times \begin{bmatrix} 0.333\times A_1 + 0.072\times A_2 & 0.096\times A_2 & -0.333\times A_1 & 0 & -0.072\times A_2 & -0.096\times A_2 \\ 0.096\times A_2 & 0.128\times A_2 & 0 & 0 & -0.096\times A_2 & -0.128\times A_2 \\ -0.333\times A_1 & 0 & 0.333\times A_1 & 0 & 0 & 0 \\ 0 & 0 & 0 & 0 & 0 & 0 \\ -0.072\times A_2 & -0.096\times A_2 & 0 & 0 & 0.072\times A_2 & 0.096\times A_2 \\ -0.096\times A_2 & -0.128\times A_2 & 0 & 0 & 0.096\times A_2 & 0.128\times A_2 \end{bmatrix} \begin{bmatrix} D_1 \\ D_2 \\ 0 \\ 0 \\ 0 \\ 0 \end{bmatrix}$$

From this equation, we can now express displacement D_1 and D_2 by using A_1 and A_2.The internal member forces are calculated from the global joint displacements. The applied to internal force equation to calculate q_1 and q_2 are given by,

$$q_1 = \frac{A_1 E}{3}\begin{bmatrix} -1 & 0 & 1 & 0 \end{bmatrix}\begin{bmatrix} D_1 \\ D_2 \\ 0 \\ 0 \end{bmatrix} \tag{5.4}$$

$$q_2 = \frac{A_2 E}{5}\begin{bmatrix} -0.6 & -0.8 & 0.6 & 0.8 \end{bmatrix}\begin{bmatrix} D_1 \\ D_2 \\ 0 \\ 0 \end{bmatrix} \tag{5.5}$$

q_1 and q_2 are the internal force in member 1 and 2. According to the strain-internal force relationship, we have analytical strain s_1 and s_2,

$$s = \frac{q}{EA} \tag{5.6}$$

Finally, we set the objective function as follows,

$$f = (T_1 - s_1)^2 + (T_2 - s_2)^2 \tag{5.7}$$

f is the error between measured strain results T_1, T_2 and analytical strain results. The analytical strain results content the variable A_1 and A_2. In this condition, minimizing the difference between measured and analytical strain can determine the cross sectional area which stands for structural "as-is" condition.

5.3.4 Model Updating by Using Numerical Optimization

Assuming the two-member truss "as-built" condition has cross sectional area A_1=1 and A_2=1. Because of corrosion, the "as-built" cross section areas change to A_1=0.8, A_2=0.7. The static strain model parameter identification is based on the applied forces and measured strains to determine the change of structural member's cross section area. The measured strain at member 1 is -625 / (333 × E) and member 2 is 25 / (7 × E).

In order to use numerical optimization to update the mathematical model. The initial guess A_1 = 1 and A_2 = 1. The objective function f is the difference between the measured and analytical strain results. The selected variable to be updated is the cross sectional area A_1 and A_2.

Backtracking Line Search

The backtracking line search algorithm chooses step lengths appropriately (Nocedal et al., 2012).

Choose $\overline{\alpha} > 0, \rho \in (0,1), c \in (0,1)$; Set $\alpha \leftarrow \overline{\alpha}$;

Repeat until $f(x_k + \alpha p_k) \leq f(x_k) + c\alpha \nabla f_k^T p_k$

$\alpha \leftarrow \beta\alpha$;
End (repeat)

Terminate with $\alpha_k = \alpha$.

In this procedure, the initial step length $\overline{\alpha}$ is chosen to be 1. An acceptable step length will be found after a finite number of trials. The backtracking approach ensures either that the selected step length is some fixed value, or else that it is short enough to satisfy the sufficient decrease condition but not too short and too long (Nocedal and Wright, 2006).

Newton Method

p_k is the search direction in order to make sure the optimization function is to converge. The Newton iteration is given by

$$p_k^N = -\nabla^2 f_k^{-1} \nabla f_k \tag{5.8}$$

Table 5.1 shows the detail of calculation results in each step. Figure 5.2 plots of A_1, A_2 as functions of iteration horizontal coordination shows iteration steps, vertical coordination shows the value of A_1 and A_2.

Table 5.1: Newton Method with the Backtracking Line Search

step	α	A_1	A_2	f (A1, A2) × 10^{-15}
0	0.000	1.000	1.000	1532540
1	0.125	0.938	0.625	308502
2	1.000	0.692	0.680	115026
3	1.000	0.766	0.698	8567
4	1.000	0.796	0.700	111
5	1.000	0.800	0.700	0
6	1.000	0.800	0.700	0

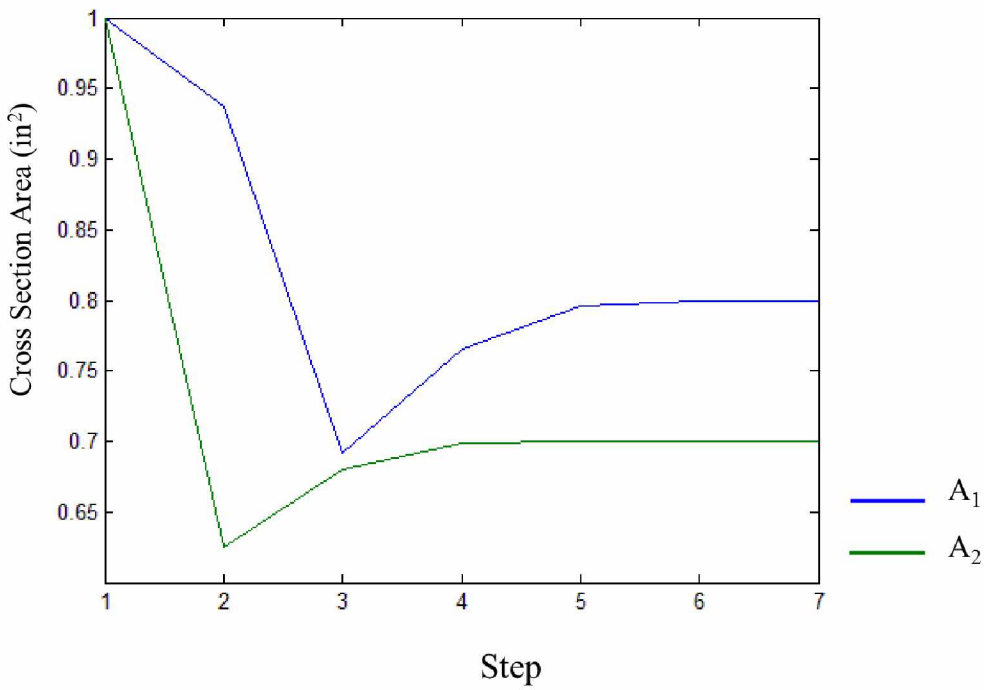

Figure 5.2: Functions of Iteration for Newton Method

Steepest Descent Method

The steepest descent method is another method for designing the search direction. The search direction p_k at every step (Nocedal and Wright, 2006).

$$p_k = -\nabla f_k \tag{5.9}$$

It can choose the step length α_k in a variety of ways. In this study $\alpha_k = 2000$. It is excruciatingly slow on this problem. It takes 154,890 steps to research the objective value of 3.9723×10^{-13}.

Figure 5.3 plots of A_1, A_2 which are the cross sectional areas of member 1 and 2 as functions of iteration horizontal coordination shows iteration steps, vertical coordination shows the value of A_1 and A_2, Blue line is the cross section of A_1 and the green line is the cross section of A_2.

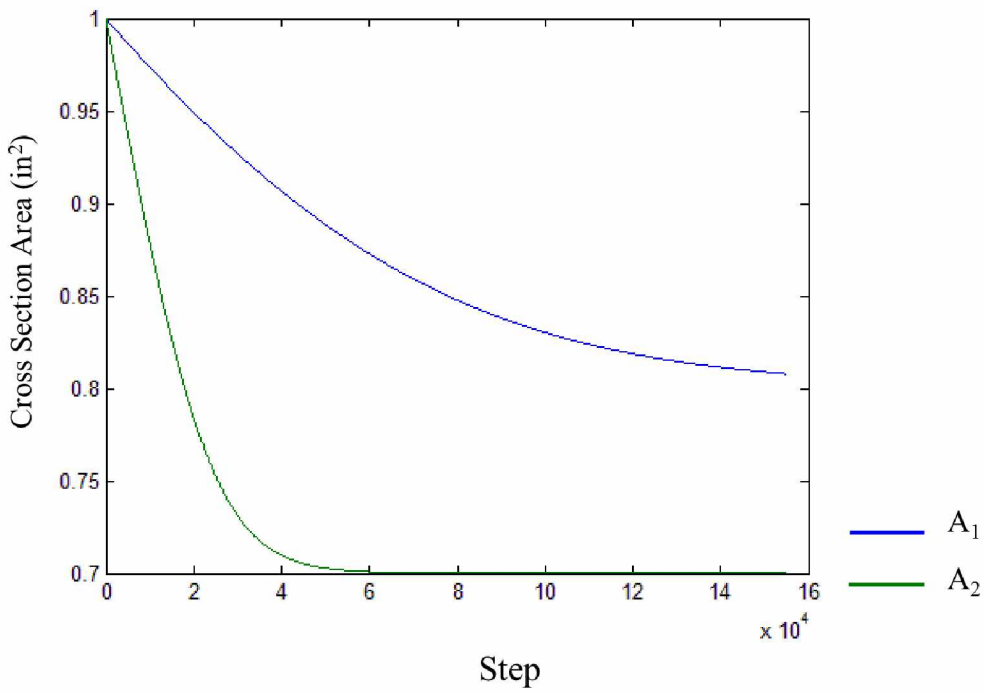

Figure 5.3: Functions of Iteration by Steepest Decent Method

5.4 Optimal Sensor Placement based on Numerical Optimization

The previous example has used a strain sensor on every truss member. In the real application, sensor placement will be divided into three aspects (Udwadia, 1994). Firstly, what is the least number of sensors required to be installed in a structure for a successful dynamic testing? Secondly,

where should a sensor be installed? Lastly, the effectiveness of different sensor placement methods are to be evaluated? This study shows the process of sensor placement optimization and answers to those questions.

5.4.1 Eight Member Truss

The "as-built" condition cross sectional area for an eight-member truss member is 10 inch^2. The structural layout shows in Figure 5.4. Consider that some existing damage is located in member 1 and 5 which can be qualified based on the numerical optimization method. This study is used to determine the minimal number and optimal strain sensor layout that can be successful used to conduct accurate model updating.

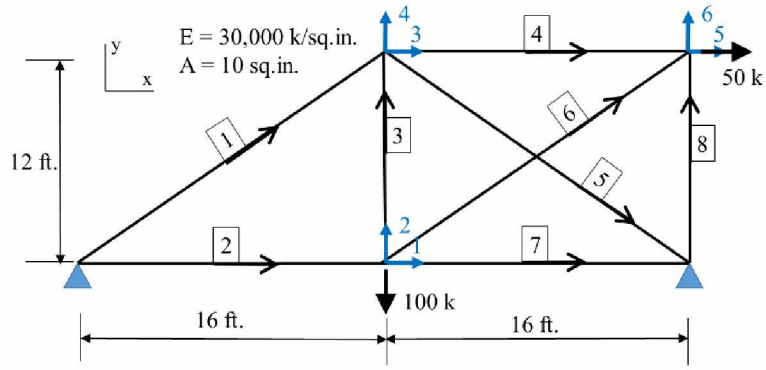

Figure 5.4: Eight-member Truss with Notation

5.4.2 Sensor Number and Layout Optimization

The sensor placement issue is important in cases where the properties of a structure, described in terms of continuous function, needs to be identified using discrete sensor information. Thus, sensor placement optimization is a kind of combinatorial optimization problem that can be

generalized as "given a set of n locations, find m locations, where m < n, which may provide the best possible performance." The number of all distinct sensor configurations involving m sensors is given by the expression (Yi et al., 2012),

$$C_n^m = \frac{n!}{m!(n-m)!} \tag{5.10}$$

Thus firstly start with C_8^1, using one strain sensor put on each truss member which including 8 different sensor layout, and the calculation shows fail to converge by using Newton Method. Then test on two sensor conditions C_8^2 which including 28 cases, and there are 7 cases coverage. Table 5.2 shows only $f = (T_1 - s_1)^2 + (T_i - s_i)^2$ can give a valid result. The minimal sensor number for this structure is two, and one of the sensors must be located on member 1.

Table 5.2: Sensor Layout with Numerical Optimization

Sensor Number	Sensor Layout (Objective Function)	i	Number of Cases	Optimization
One	$f = (T_i - s_i)^2$	1 to 8	8	Fail
Two	$f = (T_1 - s_1)^2 + (T_i - s_i)^2$	2 to 8	7	Success
	$f = (T_2 - s_2)^2 + (T_i - s_i)^2$	3 to 8	6	Fail
	$f = (T_3 - s_3)^2 + (T_i - s_i)^2$	4 to 8	5	Fail
	$f = (T_4 - s_4)^2 + (T_i - s_i)^2$	5 to 8	4	Fail
	$f = (T_5 - s_5)^2 + (T_i - s_i)^2$	6 to 8	3	Fail
	$f = (T_6 - s_6)^2 + (T_i - s_i)^2$	7 to 8	2	Fail
	$Y = (T_7 - s_7)^2 + (T_i - s_i)^2$	8	1	Fail

5.4.3 Sensor Number Influence on the Speed of Numerical Optimization

The sensor placement optimization could find the minimal sensor number and optimized layout.

Figure 5.5 and 5.6 show eight-member model parameter identification by using Newton Method in two (Figure 5.5) and eight (Figure 5.6) sensor conditions. Two sensor layout objective function is $f = (T_1 - s_1)^2 + (T_5 - s_5)^2$, and eight sensor layout objective function is $f = (T_1 - s_1)^2 + (T_2 - s_2)^2 + \ldots + (T_5 - s_5)^2$.

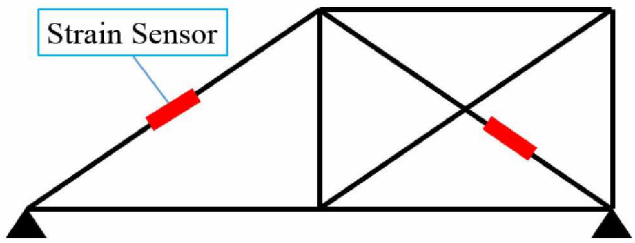

a. Two Sensor Layout

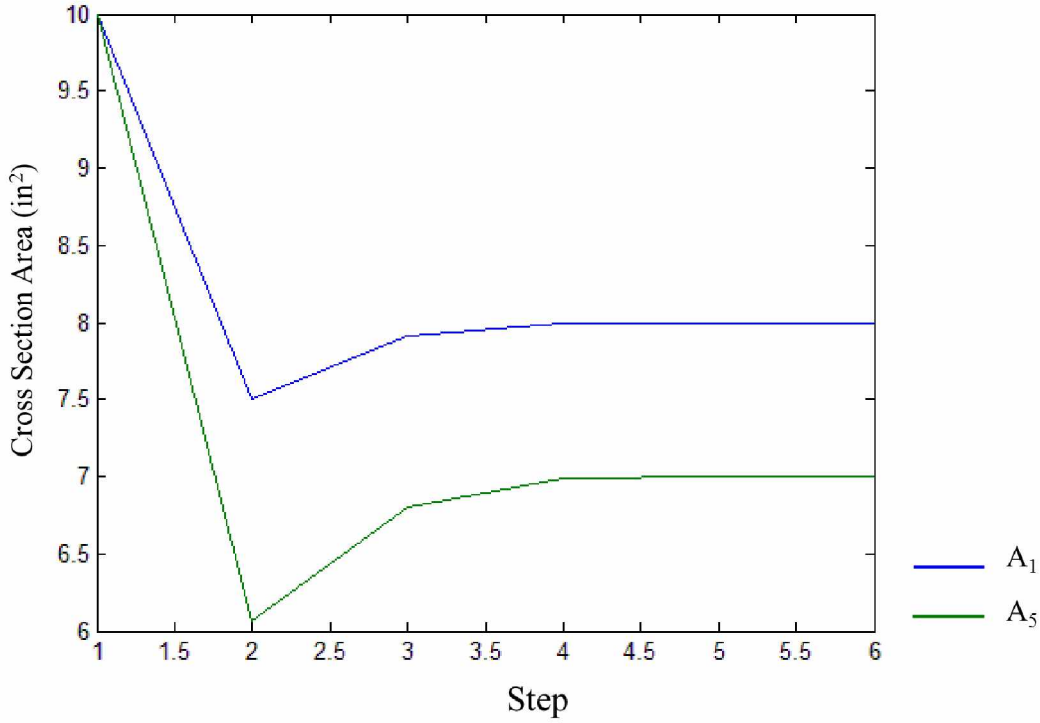

b. Functions of Iteration

Figure 5.5: Two Sensors Model Parameter Identification

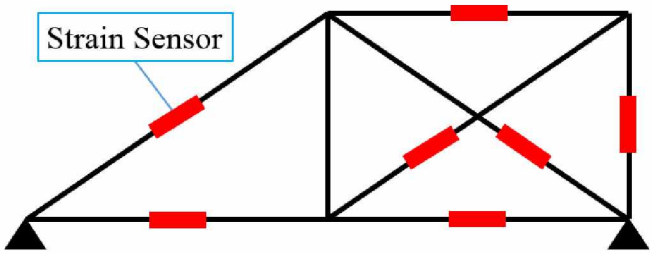

a. Eight Sensor Layout

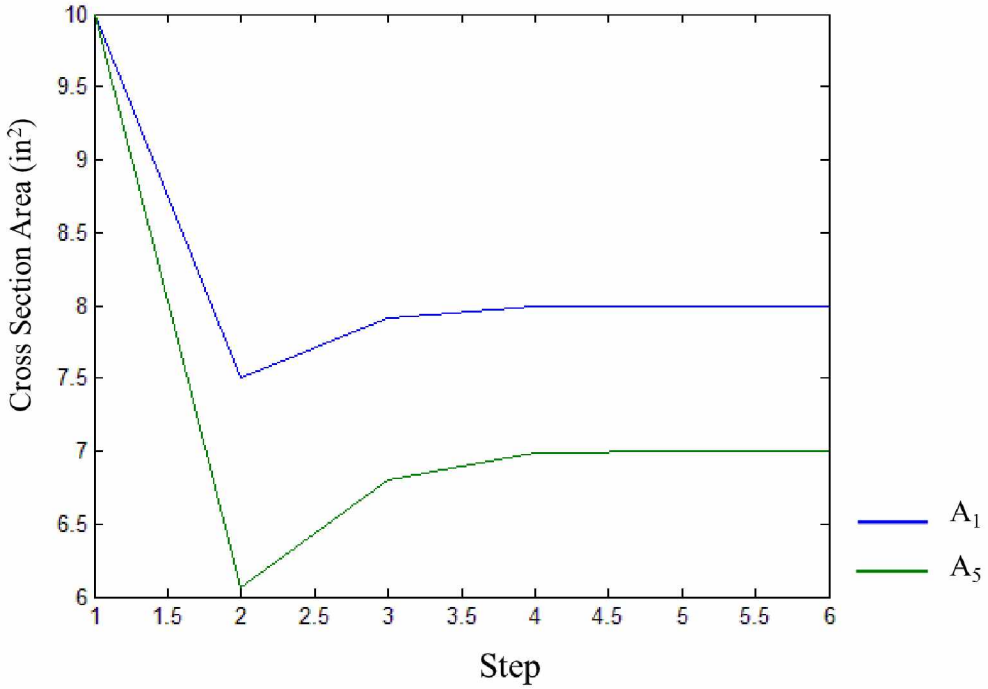

b. Functions of Iteration

Figure 5.6: Eight Sensors Model Parameter Identification

According to the results show in Figure 5.5 and 5.6, the study proves that increasing sensor number will not enhance the speed of model parameter identification. Both two sensor layouts and eight sensor layouts take 6 steps to identify the "as-is" cross section at location 1 and 5. The sensor's number should be optimized at the beginning of structural health monitoring, redundancy sensors can only increase the cost of a project. There exist optimal sensor number and layout of

certain problems.

5.5 Numerical Optimization in Damage Detection

The numerical optimization method can also apply for damage detection. It can distinguish damaged sections with non-damaged. Figure 5.7 shows a truss structure with 13 members, and the "as-built" cross section areas are 10 iches^2. Consider that damages exist in members 1 to 5. Strain sensors are placed on those locations. The "as-is" cross sectional area of member 1, 2, 3, 4 and 5 are unknown which are A_1, A_2, A_3, A_4, and A_5.

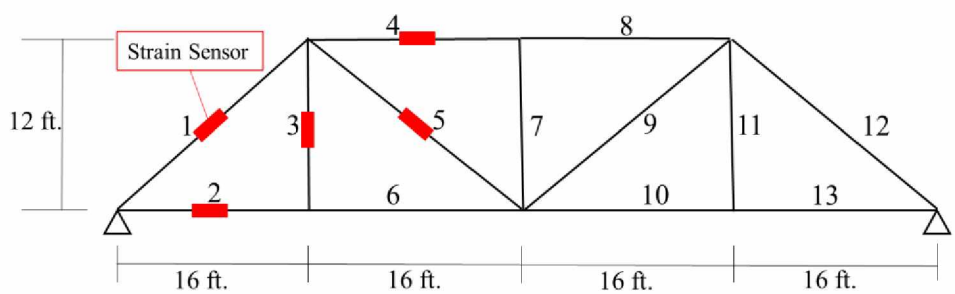

Figure 5.7: Truss Structure Sensor Layout

Analytical strains at those 5 locations can be expressed by using the stiffness method which are s_1, s_2, s_3, s_4, and s_5. The objective function is $f = (T_1 - s_1)^2 + (T_2 - s_2)^2 + \cdots + (T_5 - s_5)^2$. T_1 to T_5 are measured strains. Figure 5.8 shows the steps of damage detection by using Newton Method. The initial guess of cross sectional area A_1 to A_5 is 10 inches^2. The "as-is" cross section area of A_1 to A_5 are calculated by minimal the objective function. Figure 5.8 shows the "as-is" cross section area of A_1 is 9 inces^2 and A_5 is 8 inches^2. There is no change in other member's cross section area.

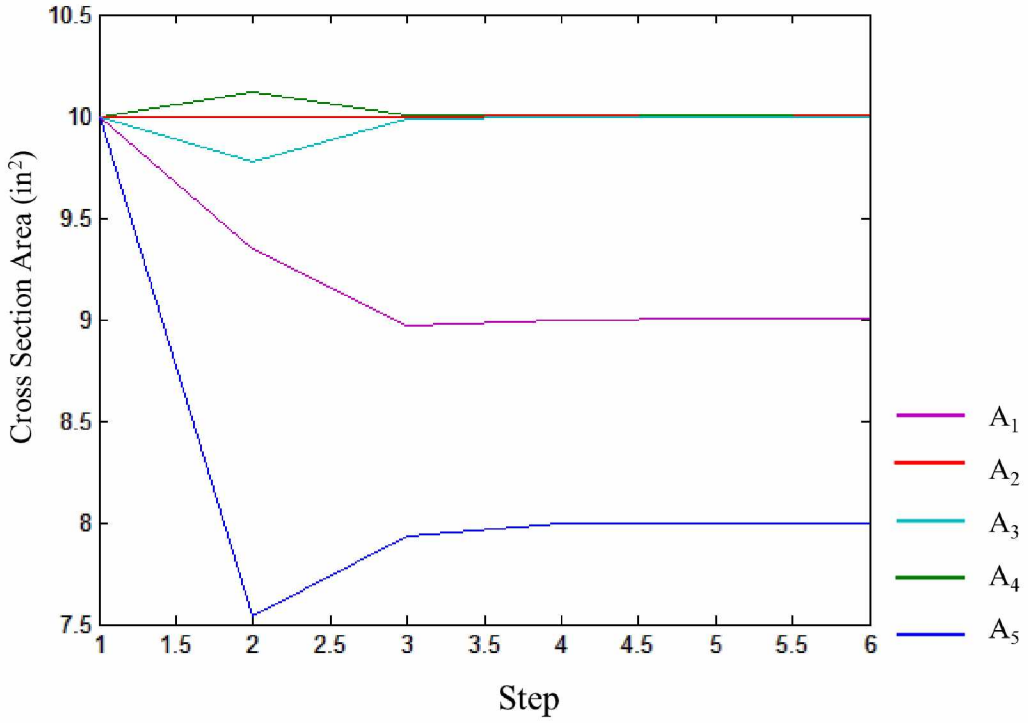

Figure 5.8: Functions of Iteration for Damage Detection

5.6 Numerical Optimization Model Updating for Large Scale Structure

Numerical Optimization for large scale structures is challenging as there are several difficulties. For example, first, the stiffness matrix will become large with increasing degrees of freedom, it takes a longer time to calculate the displacement. Secondly, the objective function will be complicated and it will be hard for the numerical optimization function to provide coverage. In order to solve this type of problem, this study used a displacement sensor to control the boundary condition. The size of stiffness matrix can be scaled to a limited size. By using this method, the large-scale structural problem can be transferred into a simple structural problem.

5.6.1 Klehini River Bridge

The Klehini River Bridge is located on the Porcupine Crossing Road accessed at mile point 26.3 of the Haines Highway. The bridge structure is made of a two-span riveted steel parker truss (see Figure 5.9). The total length of this bridge is 74 meters (243 feet). The superstructure consists of various box sections with inverted channel sections riveted to two steel plates. The timber deck is supported by a series of timber girders connected to transverse I-beams. Both spans rest on a central concrete abutment and the side banks.

Figure 5.9: Klehini River Bridge

ADOT&PF inspections (AKDOT, 2008; AKDOT 2010) reported the current damage in a variety of structural members which included torn gusset plates, cracking at rivet holes, damaged or missing lateral bracing, damaged sway bracing, and etc. Examples of one damage member (Figure 5.10) and its location are shown in Figure 5.11.

Figure 5.10: Crack on Truss Member

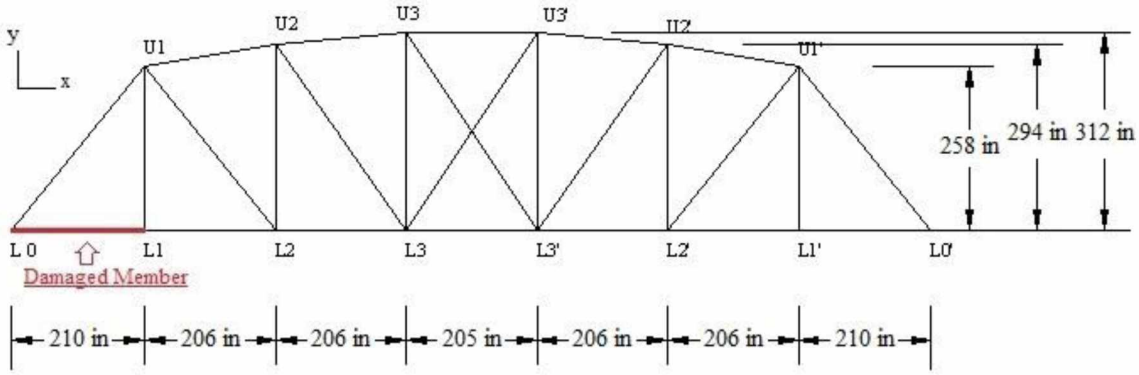

Figure 5.11: Location of Damaged Member

5.6.2 Model Parameter Identification for Klehini River Bridge

In order to identify the "as-is" cross sectional area of damaged section L0-L1. This study used displacement sensor located at U2 and L2 to separate the structure into a small section (Figure 5.12), and the large-scale problem then was transferred into a simple problem.

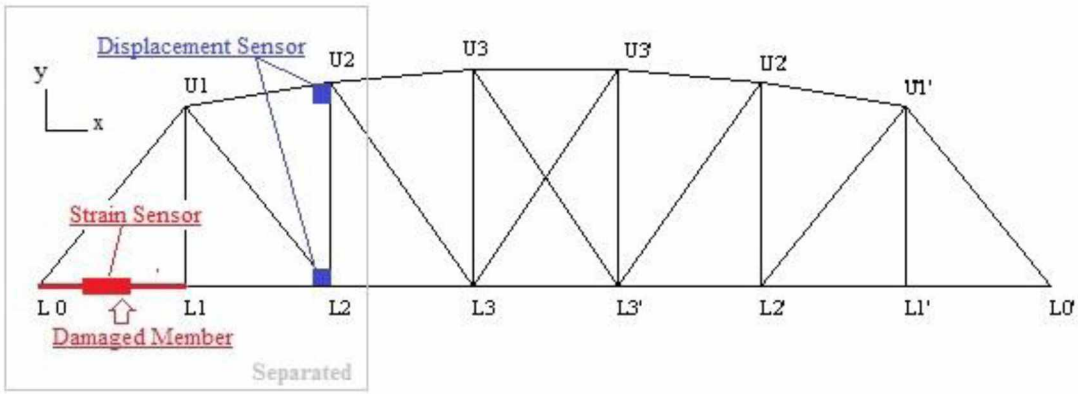

Figure 5.12: Separated Structure by Using Displacement Sensor

There are 6 members in the separated structure (Figure 5.13), these are member 1 (L0-U1), member 2 (L0-L1), member 3 (L1-U1), member 4 (U1-U2), member 5 (U1-L2) and member 6 (L1-L2). The "as-built" cross sectional areas are 12, 8, 7, 12, 6 and 8 inches^2 correspondingly. Damage existed in member L0-L1, so a strain sensor is located on the problem member.

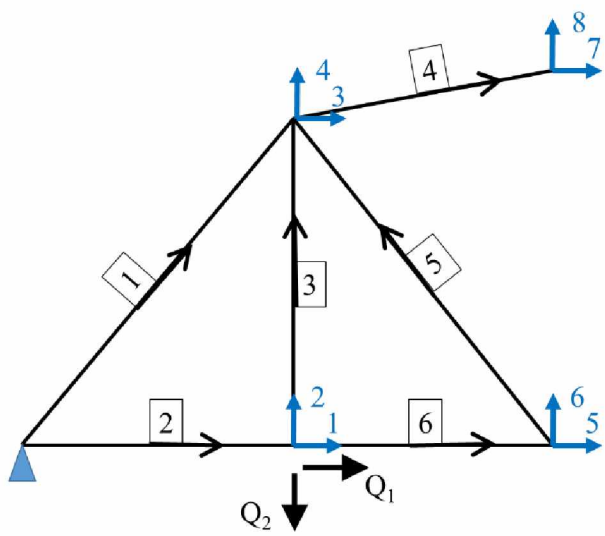

Figure 5.13: Separated Structure

Applied Q_1 is 1000 kips and Q_2 is 1000 kips. Displacements at D_5, D_6, D_7, and D8 are 1.3962,

-2.3543, 1.3402 and -2.0268 inches. The "as-is" cross section at member 2 is unknown which is A_2. The displacements D_1, D_2, D_3, and D_4 can be determined by using stiffness method. The relationship between separated structural stiffness, applied loads and displacements can be expressed by using stiffness method, equation 5.11.

$$\begin{bmatrix} 1000 \\ -1000 \\ 0 \\ 0 \end{bmatrix} = E \times \begin{bmatrix} 142.86 \times A_2 + 1165.0 & 0 & 0 & 0 & -1165.05 & 0 & 0 & 0 \\ 0 & 813.95 & 0 & -813.95 & 0 & 0 & 0 & 0 \\ 0 & 0 & 2314.0 & 555.91 & -212.26 & 265.84 & -167.47 & -291.93 \\ 0 & -813.95 & 555.91 & 1848.8 & 265.84 & -332.94 & -291.93 & -51.02 \end{bmatrix} \begin{bmatrix} D_1 \\ D_2 \\ D_3 \\ D_4 \\ 1.3962 \\ -2.3543 \\ 1.3402 \\ -2.0268 \end{bmatrix}$$

The analytical strain at member 2 (s_2) determined by using calculated D_1 to D_4. The measured strain at member 2 is calculated based on global truss bridge stiffness which is known and is 0.0062. The objective function is $f = (T_2 - s_2)^2$. The extreme minimal result of function f was calculated by using Newton Method. The original guess of the member 2 cross section is 8 inches^2. The "as-is" A_2 was 6 inches^2 after 6 steps of calculation (Figure 5.14).

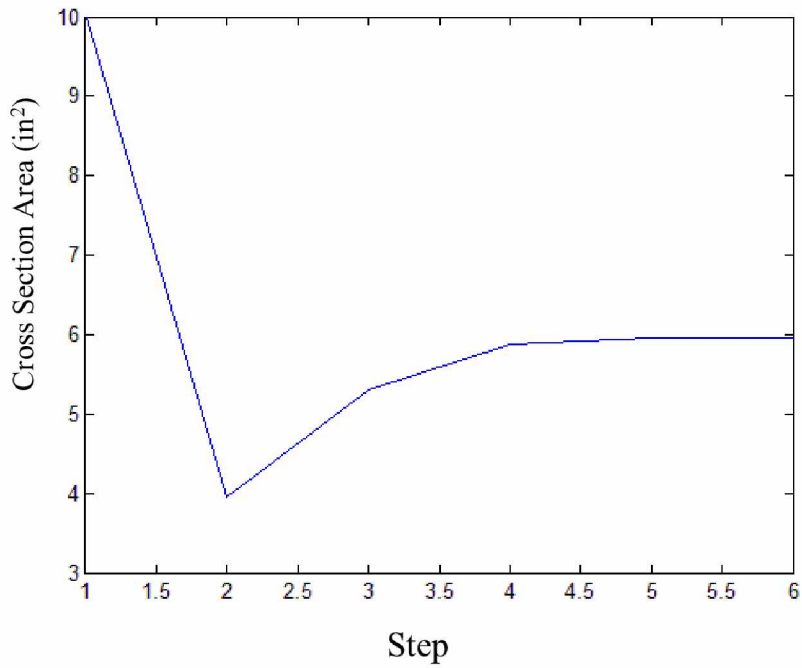

Figure 5.14: Member 2 Cross Section Area Identification by Using Newton Method

5.7 Conclusions

In this study, both simple structures and the Klehini River Bridge model were successfully updated by using the optimal static measurement method. The established objective function is the difference between measured and analytical strain results which can be used to detect the change in the structural cross sectional areas.

There exists an optimal number of sensors and their layout for certain model parameter identification problem. The four examples illustrates that the number of measurements must be greater than or equal to the number of unknown parameters, as a necessary condition for a solution to exist (Sanayei and Saletnik, 1994). Including the redundancy strain measurements in the objective function cannot enhance the speed of optimization. The strain sensor placement should

be evaluated prior to selecting a structural health monitoring system. This is needed to reduce equipment costs, reduce installation (labor) costs and provide a more logical method for evaluating experimental response.

Static measurements may be used to conduct model parameter identification and but also detect damage and located the position of problem. The numerical optimization calculation time becomes every long or not sufficient coverage can be obtained with increases in the number of DOFs and number of members to be identified. Therefore, a displacement sensor can be used to separate large scale structure into simple problems. The large-scale problem can be transferred to simple problem successfully.

The numerical optimization is a great tool for structural health monitoring. In practical engineering, load tests are always conducted in order to evaluate the structural safety condition and various kinds of sensor are installed on the structure to evaluate whether the measured parameters are in the safety range. However, there are only limited numbers to be checked and the other members safety condition are calculated by the structural mathematical model. Checking static measurement parameter identification ability and Optimized the sensor layout at the beginning stages can be used evaluate the structural health monitoring system capability for bridge evaluation. By using optimal static measurements; this approach can be used to identify the bridge "as-is" condition and it can be used to help evaluate the structural safety.

5.8 References

Chang, M., Pakzad, S. N., (2014), Optimal Sensor Placement for Modal Identification of Bridge Systems Consider Number of Sensing Nodes, Journal of Bridge Engineering, ASCE, 19.

Hibbeler, R. C., (2009), Structural Analysis, Pearson Prentice Hall Pearson Hall, New Jersey.

Meo, M., Zhumpano, G., (2005), On the Optimal Sensor Placement Techniques for Bridge Structure, Engineering Structure, 27, pp. 1488-1497.

Nocedal, J., Wright, S., (2006), Numerical Optimization, Springer Series Operations Research Financial Engineering, Springer.

Sanayei, M., Saletnik, M. J., (1994), Parameter Estimation of Structures From Static Strain Measurements I: Formulation.

Sanayei, M., Imbaro, G. R. McClain, J. A. S., Brown, L. C., (1997), Structural Model Updating Using Experimental Static Measurements, Journal of Structural Engineering, Vol. 123, No. 6.

Sanayei, M., Phelips, J. E., Sipple, J. D., Bell, E. S., and Brenner, B. R. (2012), Instrumentation, Nondestructive Testing and Finite-Element Model Updating for Bridge Evaluation using Strain Measurements, Journal of bridge engineering, Vol 17, No.1, ASCE.

Schlune, H., Plos, M., Gylltoft, K., (2009), Improved bridge evaluation through finite element model updating using static and dynamic measurement, Engineering Structure, 31, 1477-1485.

Udwadia, F. E., (1994), Methodology for optimum sensor locations for parameter identification in dynamic system, Journal of Engineering Mechanics, vol. 120, no. 2, pp. 368-390.

Xiao, F., Chen, G. S., Hulsey, J. L., (2014), Experimental Investigation of a Bridge under Traffic Loadings, Advanced Materials Research, Vols. 875-877, 1989-1993, Trans Tech Publication.

Xiao, F., (2015), Structural Health Monitoring Alaska Bridge Research in Cold Remote Area, Lambert Academic Publishing.

Xiao, F., Hulsey, J. L., Cheng, G. S., (2015), Multi-direction Bridge Model Updating using Static and Dynamic Measurement, Applied Physics Research, Vol. 7, No. 1.

Xiao, F., Hulsey, J. L., Chen, G. S., (2016), Structural Health Monitoring of the Klehini River Bridge, Journal of Vibration Engineering and Technologies, Vol 4, No 4.

Xu, Y. L., Xiao, Y., (2011), Structural Health Monitoring of Long-Span Suspension Bridges, CRC Press.

Yi, T. H., Li, H. N., Gu, M., (2011), Optimal Sensor Placement for Structural Health Monitoring Based on Multiple Optimization Strategies, the structural design of tall and special buildings, 20, 881-900.

Yi, T. H., Li, H. N., (2012), Methodology Developments in Sensor Placement for Health Monitoring of Civil Infrastructures, International Journal of Distributed Sensor Networks, Hindawi Publishing Corporation.

You, T., Jin, H., Li, P., (2013), Optimal Placement of Wireless Sensor Nodes for Bridge Dynamic Monitoring Based on Improved Particle Swarm Algorithm, International Journal of Distributed Sensor Networks, Hindawi Publishing Corporation.

Chapter 6 Conclusions and Future Work

This study contributes to the field of structural health monitoring mainly in developing new approaches for structural identification, optimal sensor placement, and application in large-scale structures.

Firstly, this dissertation has presented the design method for developing a structural health monitoring system that can be used in cold, remote areas. A fiber-optic sensor system was selected for use in an extremely cold climate. A SAP2000 global finite element model was prepared based on as-built conditions. From the modal analysis, the lowest mode shapes and natural periods in vertical, transverse, longitudinal, and rotational direction were found based on the mass participation factor. The mode shapes indicated the best position to place the accelerometers. After field measurement of mode shapes and natural periods, the field dynamic results will be calibrated with the finite element results to identify the accuracy of the finite element model. A local finite model (substructure) was developed using ABAQUS to determine the rotational stiffness of one connection.

Secondly, this dissertation investigated the dynamic behavior of the Chulitna River Bridge by using ambient free-decay response. By using frequency spectrum analyzes, several modes of vibration were characterized. A finite element model was developed to simulate the virtual response of the bridge. Calculated frequency values using this model compared well with the measured results. Based on portable accelerometer data, empirical mode decomposition, and the Hilbert transform were used to identify the modal parameters including the damping coefficients of the steel girder Chulitna Bridge under ambient free-decay truck loading. This approach was first examined by using the portable accelerometer data of a long steel girder bridge under ambient

free-decay truck loading. Compared with conventional approaches, the Hilbert-Huang method was found to be effective and suitable for modal parameter identification of Chulitna River Bridge. This research firstly identified the bridge nonlinear damping behavior based on the nonlinear slope of amplitude-time by using Empirical mode decomposition and the Hilbert transform method. The nonlinear amplitude-time slope demonstrated the nonlinear behavior exist in this bridge. The identified damping is a sensitive index for structural health monitoring. We demonstrated that multiple sensors are required to comprehensively record modal frequencies and damping. Multiple sensors are necessary to efficiently and effectively identify pertinent information about the bridge prior to conducting field testing so that the sensor locations can be optimized into groups to provide measurements of significant value. Improperly located sensors or an insufficient number of sensors may result in the loss of significant information due to weak instrument signals.

Thirdly, the research established a fiber optic structural health monitoring system for the Chulitna River Bridge. The system indicates the real-time local behavior of bridge. The ambient test identified the bridge global response. Combining the local-global test data to update bridge finite element model can eliminate the weakness of only relying on one type of test results to update the model. The multi-direction model updating approach separates the model updating into several stage which will help to reduce the number of objective functions and variables and make the function easy to coverage. From the updating results, this study shows only updating longitudinal members, such as girders, stringers, and deck have a limited enhancement in the overall accuracy of the model. The updating uni-direction has a low influence on the accuracy of every other direction. The overall accuracy is contributed by both longitudinal members and transversal members. It is necessary for steel girder bridge to be updated in the multi-direction.

Finally, both simple structures and the Klehini River Bridge model were successfully updated by using the optimal static measurement method. The established objective function is the difference between measured and analytical strain results which can be used to detect the change in the structural cross sectional areas. There exists an optimal number of sensors and their layout for certain model parameter identification problem. Including the redundancy strain measurements in the objective function cannot enhance the speed of optimization. The strain sensor placement should be evaluated prior to selecting a structural health monitoring system. This is needed to reduce equipment costs, reduce installation (labor) costs, and provide a more logical method for evaluating experimental response. Static measurements may be used to conduct model parameter identification and but also detect damage and located the position of problems. The numerical optimization calculation time can take every long time or not sufficient coverage with increases in the number of DOFs and number of members to be identified. Therefore, a displacement sensor can be used to separate large-scale structure into simple problems. The large-scale problem can be transferred to a simple problem successfully. The numerical optimization is a great tool for structural health monitoring. In practical engineering, load tests are always conducted in order to evaluate the structural safety condition and various kinds of sensors are installed on the structure to evaluate whether the measured parameters are in the safety range. However, there are only limited numbers to be checked and the other members safety condition are calculated by the structural mathematical model. Checking static measurement parameter identification ability and optimized the sensor layout at the beginning stages can be used evaluate the structural health monitoring system capability for bridge evaluation. By using optimal static measurements; this approach can be used to identify the bridge “as-is” condition and it can be used to help evaluate the structural safety.

This research is focused on vibration techniques, structural identification and model calibration, and optimal sensor placement. Other topics, such as sensors and instrumentation, signal processing and data management, structural health evaluation, structural safety and prognosis, vibration control and damping, and practical applications need to be further studied in structural health monitoring research.